SLAC-PUB-2650
November 1980
(T/E)

LEPTON PAIR PRODUCTION IN HADRON COLLISIONS*

Ryszard Stroynowski†

Stanford Linear Accelerator Center

Stanford University, Stanford, California 94305

Submitted to Physics Reports

---

* Work supported by the Department of Energy under contract number DE-AC03 76SF00515.

† Present Address: California Institute of Technology, Pasadena California, 91125.

TABLE OF CONTENTS

1. Introduction

2. Sources of Leptons

   2.1 Decays and Conversions

   2.2 Vector Mesons

   2.3 Drell-Yan Mechanism

      2.3.1 Definitions and Variables

      2.3.2 Differential Cross Sections

      2.3.3 Consequences of the Point-Like Approach

   2.4 Sources of Low Mass Lepton Pairs

      2.4.1 Dalitz Decays

      2.4.2 Decays of Charmed Particles

      2.4.3 Models

3. Review of the Data

   3.1 Target Dependence

   3.2 Beam Dependence

   3.3 Mass Spectra

   3.4 Transverse Momentum Distributions

   3.5 Longitudinal Momentum Distributions

4. Drell-Yan Process in QCD

   4.1 Perturbative Approach

   4.2 QCD Corrections to the Drell-Yan Process

5. QCD Phenomenology of High Mass Data

   5.1 Scaling Violations

   5.2 Angular Distributions

   5.3 Transverse Momentum Distributions in QCD

   5.4 Normalization

6. Structure Functions and Quark Distributions

6.1 General Remarks

6.2 Extraction of the Proton Sea

6.3 Structure Functions of Unstable Particles

6.3.1 Pion

6.3.2 Kaon

6.3.3 Antiproton

7. Review of Low Mass Data

8. Outlook

1. Introduction

The interest in the lepton pair production in hadronic collisions can be traced back to the experiments searching for the intermediate vector boson. In 1969, in one of the first experiments of its type, the Columbia-Brookhaven group observed[1] the production of direct $\mu^+\mu^-$ pairs in proton nucleus collisions at 29.5 GeV. Their dimuon mass spectrum extended up to about 5 GeV and was not compatible with the estimates of experimental background. The explanation of the production process in terms of the quark-parton model was proposed in 1970 by Drell and Yan[2], as the annihilation of the quark-antiquark pair into the virtual photon which subsequently decays into pair of leptons. This approach has been, in general successful and it is now customary to call the high mass dileptons the Drell-Yan continuum.

The high yield of single leptons observed during the period of 1972-1974 in a number of experiments renewed the interest in lepton pair production. At that time it was speculated that the production and decay of some new particles, like for example charmed mesons, may result in the emission of single lepton in the final state. It was important, therefore, to learn how much of the observed signal is due to the pair production. This motivation, together with the continuous research for the W boson, led to a series of high precision experiments. They culminated in unexpected and spectacular discoveries of the families of new vector mesons. In 1974 the MIT-Brookhaven group observed[3] the J/ψ (3.1) in its $\mu^+\mu^-$ decay mode and in 1977 the Columbia-Fermilab-Stony Brook Collaboration discovered[4] the upsilon family. Today the knowledge of the dimuon mass spectrum in proton interactions extends from threshold to about 20 GeV. Similar good quality data are also becoming available for the pion, kaon and antiproton induced reaction

The continuous improvement of the quality of the data had a stimulating influence on the theory. The quark parton model developed around 1969 by Feynman, Bjorken and others[5-7] was remarkably successful in describing the gross

features of such different processes as deep inelastic lepton scattering, e^+e^- annihilations into hadrons, massive lepton pair production and large p_T processes. In the recent years, however, it was found that certain aspects of the data, like scaling violation in deep inelastic electron and muon scattering, narrow width of the ψ meson or large average values of the transverse momentum of muon pairs were not compatible with the simple picture. Such observations justified the necessity of the extension of the quark parton model to more formal but also more complicated theory of Quantum Chromodynamics (QCD). Most of the successful predictions of the quark parton model have been rederived in QCD, which is at present the leading candidate for the theory of strong interactions. Precise calculations in the QCD framework are still, however, difficult. The high accuracy dilepton data represent, therefore, an excellent testing ground of the theory. Furthermore, the measurements of the lepton pair production in pion, kaon and antiproton interactions, which became available recently, provide the unique opportunity to study the structure functions of π, K and $\bar{p}$ which are inaccessible by any other method.

Both theoretically and experimentally the dilepton data are traditionally divided into two domains. The high mass data are thought to be entirely due to the Drell-Yan mechanism and are discussed in terms of the parton model or QCD, while at low mass, where also most of the cross section lies, many different effects contribute. The division, though somewhat artificial, will be kept in the following for the simplicity of presentation.

This report represents a sequel to two previous articles which appeared in Physics Reports on this subject, by L. Lederman[8] in 1976 and N. S. Craigie[9] in 1978. These articles contain excellent reviews of earlier data; I will concentrate, therefore, on more recent results. Specific aspects of the theory and the data not mentioned here may be found in other reviews[10-13].

2. Sources of leptons

2.1 Decays and conversions

Most of the muons and electrons observed in hadronic processes come from the well understood "trivial" sources and represent a background to the interesting signal. For the muon experiments these are predominantly the decays of pions, kaons, hyperons, etc. The electron experiments on the other hand are plagued by the conversions of photons originating from the π^0, η and ω decays. Both types of the backgrounds occur characteristically at some distance from the interaction vertex and the experimental set-ups are usually designed to minimize their influence on the trigger rates. Muon experiments typically have large amount of dense material situated close to the interaction point. Fast muons penetrate the absorber while most of the hadrons interact before they have a chance to decay. In contrast, for the electron experiments the amount of material in the path of produced photons is required to be very small in order to minimize the probability of conversion of $\gamma \rightarrow e^+e^-$.

In both types of experiments the requirements of direct lepton pairs, i.e., pairs originating at the interaction vertex eliminates usually most of the above problems. The remaining background due to decays close to the interaction point or decays of short-lived particles, e.g., charmed mesons, is in general charge independent and can be estimated from the observed number of pairs of leptons with the same charge. In case of electron pair experiments, the additional background of direct electrons produced in Dalitz decays of π^0, ω and η mesons is usually eliminated by cuts on the effective mass of e^+e^-.

2.2 Vector mesons

The main source of the direct lepton pairs are the decay of vector mesons. Such decays proceed through the electromagnetic coupling to the virtual photon which then decays into either e^+e^- or $\mu^+\mu^-$ pair. The peaks of high mass mesons,

in particular of ϕ, ψ and Υ are usually clearly visible above the dilepton continuum and their branching ratios are well measured in the e^+e^- storage rings experiments. The knowledge of the branching fractions of most common ρ^0 and ω mesons come, however, from the early experiments and is burdened with rather large uncertainties. This poses serious problems in the study of low mass lepton pairs which are dominated by the ρ and ω production and have large contribution from the ω Dalitz decays.

2.3 Drell-Yan mechanism

2.3.1 Definitions and variables

After substraction of the known sources of direct dileptons the experiments measuring $\mu^+\mu^-$ or e^+e^- spectra observe[1,8] sharply falling with mass and rather featureless high mass continuum. This continuum is usually described in terms of the Drell-Yan mechanism[2] depicted in fig. 1. In this model a quark from one of the incoming hadrons annihilates with the corresponding antiquark from the second hadron. The produced virtual photon of mass M then decays into a pair of leptons. For simplicity one usually neglects the transverse momenta of quarks inside the hadrons and the masses involved. The cross section is then described in the simple parton model by:

$$\sigma = \int dx_1 dx_2 \sum_{\substack{\text{all} \\ \text{flavours}}} \left[G_{q_{i/A}}(x_1)\, G_{\bar{q}_{i/B}}(x_2) + G_{\bar{q}_{i/A}}(x_1)\, G_{q_{i/B}}(x_2) \right] \cdot \sigma_i(q_i\bar{q}_i \to \gamma^*)\, \delta(M^2 - (k_a + k_b)^2)\, dM^2 \qquad (1)$$

Functions G(x) represent here the probabilities of finding the quark or antiquark with momentum k being the fraction x of the parent particle momentum

$$k = xP.$$

The variables describing the virtual photon are related to the center of mass energy squared s and the fractional momenta of the quarks by:

$$M^2 = (k_a + k_b)^2 = s x_1 x_2 \qquad (2)$$

$$x_F = 2p_L/\sqrt{s} = x_1 - x_2 \qquad (3)$$

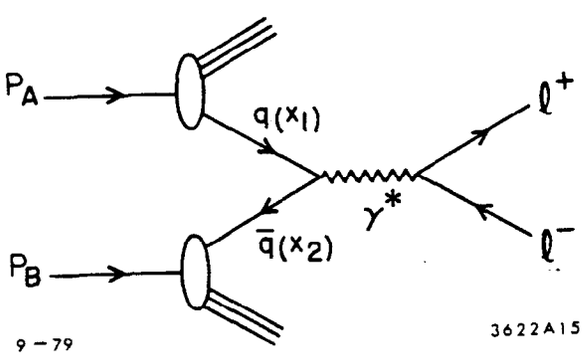

1. The Drell-Yan diagram.

It is often convenient to introduce the scaling variable τ,

$$\tau = M^2/s = x_1 x_2 \tag{4}$$

representing the fraction of the total c.m. energy used in the formation of the virtual photon. The quark variables may then be expressed in terms of the lepton pair quantities by the following set of relations:

$$x_1 + x_2 = \sqrt{x_F^2 + 4\tau},$$
$$x_{1,2} = \frac{1}{2}\sqrt{x_F^2 + 4\tau} \pm x_F \tag{5a}$$

Sometimes another definitions of x_1 and x_2 are used:

$$x_1 = \sqrt{\tau}\, e^{y}$$
$$x_2 = \sqrt{\tau}\, e^{-y}\ , \tag{5b}$$

where y is the rapidity of the virtual photon. These are equivalent to the relations (5a) only when the lepton pair is produced with zero transverse momentum.

Detailed studies of scaling often require comparison of longitudinal momentum distributions of different lepton pairs masses. The kinematic factor is then correctly taken into account when using the variable

$$x_F' = \frac{x_F}{1-\tau}\ .$$

2.3.2 Differential Cross Sections

The point-like cross section for the subprocess of the quark-antiquark annihilation may be written in analogy to the electron-positron annihilation

$$\sigma_i(q_i\bar{q}_i \to \gamma^*) = \frac{4\pi\alpha^2}{3M^2} e_i^2 \frac{1}{n}, \tag{6}$$

where α is the electromagnetic coupling constant, e_i represents the quark charge and n is the number of colours.

The differential form of Equation (1) may be then written as:

$$\frac{d\sigma}{dM^2} = \frac{4\pi\alpha^2}{3nM^4} \sum_i e_i^2 \frac{M^2}{s} \int dx_1 dx_2 \left[Gq_{i/A}(x_1)\, G\bar{q}_{i/B}(x_2) + (q_i \leftrightarrow \bar{q}_i) \right] \delta(M^2/s - x_1x_2) \tag{7}$$

or with number of colours set to three:

$$\frac{d\sigma}{dM^2} = \frac{4\pi\alpha^2}{9M^4} F(\tau). \tag{8}$$

Similarly, the double-differential form of Equation (1) may be written as:

$$\frac{d^2\sigma}{dM^2 dx_F} = \frac{4\pi\alpha^2}{9M^4} F(\tau, x_F) \tag{9}$$

where

$$F(\tau, x_F) = \frac{\tau}{\sqrt{x_F^2 + 4\tau}} \sum_i e_i^2 \left[Gq_{i/A}(x_1)\, G\bar{q}_{i/B}(x_2) + (q_i \leftrightarrow \bar{q}_i) \right] \delta(\tau - x_1x_2)\, \delta(x_F - (x_1 - x_2)). \tag{10}$$

The scaling functions $F(\tau)$ and $F(\tau, x_F)$ are formed entirely from the dimensionless variables. In the case of, e.g., proton-proton collisions, one can write them explicitly, neglecting charmed and heavier quarks:

$$F(\tau) = \tau \int dx_1 dx_2\, \delta(\tau - x_1x_2) \left\{ \frac{4}{9} \left[u_A(x_1)\bar{u}_B(x_2) + \bar{u}_A(x_1)u_B(x_2) \right] + \frac{1}{9} \left[d_A(x_1)\bar{d}_B(x_2) + \bar{d}_A(x_1)d_B(x_2) \right] + \frac{1}{9} \left[s_A(x_1)\bar{s}_B(x_2) + \bar{s}_A(x_1)s_B(x_2) \right] \right\},$$

where u (x), d(x) and s(x) are the probability distributions for finding the up, down, and strange quark respectively with fraction x of the parent proton momentum. It is the premise of the parton model that these functions are the same as measured in deep inelastic lepton interactions. In contrast, however, to electron proton scattering they appear in these formulae in quadratic form.

2.3.3 Consequences of the Point-like Approach

The attractively simple model explained above became widely accepted during the past few years since it formulates the description of the data in the same language as that for the deep inelastic lepton scattering, e^+e^- annihilations and large transverse momentum phenomena. It has several both qualitative and quantitative predictions following from the $q\bar{q}$ annihilation picture of the process. These are:

1) The differential distributions $M^3 \frac{d\sigma}{dM}$ and $M^3 \frac{d^2\sigma}{dMdx_F}$ should scale,

2) The cross section depends on the number of colors n since only quarks of the same color can annihilate,

3) The shapes of the distributions are determined by quark distribution fuctions measured, e.g., in deep inelastic lepton scattering experiments,

4) The relative yields of lepton pairs produced in different reactions depends on the quark content of the interacting particles,

5) Due to the point-like coupling of the quarks to the photon one expects the angular distribution in the dilepton rest frame to have the form: $W(\theta) = 1 + \cos^2\theta$,

6) The transverse momentum of the lepton pair is due to the transverse momentum of the annihilating quarks only. Therefore, it is expected to be small and independent of the overall c.m. energy.

Many of the above properties have been seen in the lepton pair production experiments. However, the observation of large and increasing with energy values of $< p_T >$ of the $\mu^+\mu^-$ pairs indicated the need to go beyond this naive picture. Together with scaling violations seen in the deep inelastic electron scattering the $\mu^+\mu^-$ data justified the extension of the simple parton model to Quantum Chromodynamics discussed in more detail in chapter 4.

2.4 Sources of low mass lepton pairs

2.4. 1 Dalitz decays

In addition to the previously mentioned vector meson decays, there are also other known sources of the low mass direct lepton pairs. The main contribution to the very small masses is due to the Dalitz decays of the η and ω mesons:

$$\eta \longrightarrow \mu^+\mu^-\gamma \ ,$$

$$\omega \longrightarrow \mu^+\mu^-\pi^0 .$$

Also the tensor mesons are expected[14] to have measurable branching ratios into the radiative channels, e.g.,

$$A_2 \longrightarrow \rho\mu^+\mu^- \ ,$$

$$A_2 \longrightarrow \omega\mu^+\mu^- \ ,$$

$$f \longrightarrow \omega\mu^+\mu^- \ .$$

The branching ratios for such decay modes have been calculated in Quantum Electrodynamics and the corresponding mass distribution functions can be obtained from the calculations of Kroll and Wada[16]. Recent measurements[17] of the $\eta\rightarrow\mu^+\mu^-\gamma$ and $\omega\rightarrow\pi^0\mu^+\mu^-$ channels confirm the accuracy of theoretical calculations. Due to the μ-e mass difference, the e^+e^- pairs are expected to dominate the final state decays near the 2μ mass threshold. In practice, one encounters serious difficulties in the quantitative estimates of the contribution of these decays to the observed dilepton mass spectra. This is mainly due to the fact that neither the production cross sections of

ω, η, f, etc. nor their momentum distributions needed for the usual acceptance calculations are sufficiently well known. In various experiments these uncertainties lead to contradictory answers at low mass. In any case the contribution of these decays is negligible in the mass range above the ρ.

2.4.2 Decays of charmed particles

Another source of the direct dileptons widely discussed in the literature[18] is the semileptonic decay of charmed particles. In general the problem here is similar to that of the semileptonic π or K decays. The lifetime of charmed particles of less than 10^{-11} sec results, however, in very short decay length unmeasurable in the standard experiments. The final state leptons appear thus as directly produced in the interaction. The semileptonic branching ratio of charmed particles is of the order of 10% and since in hadronic collisions they are produced in pairs of opposite charm quantum numbers, one may expect that about 1% of the charm production cross section will result in the direct pairs of leptons of opposite charge. Included here are also $e^+\mu^-$ and $e^-\mu^+$ final states. The shape of the resulting dilepton mass spectrum depends on the dynamics of the charmed particles production and the acceptance of individual experiments. In general, however, the kinematics of the decays favours the observation of low mass pairs at rather large transverse momentum.

2.4.3 Models

The contribution from the charmed particles and Dalitz decays to the low mass spectrum is subject to many uncertainties, mainly due to the poorly known production cross sections and the kinematic distributions of the parent particles. It is, nevertheless, generally agreed that these sources contribute little to the dilepton mass above 1 GeV, where the substantial cross section has been

observed[1,3] at lower energies (see figure 2). On the other hand, the impulse approximation used in the derivation of the formula (1) is not valid for the low dilepton mass which is related through equation (2) to the low values of x of the annihilating quarks. Naive extrapolations of the domain of applicability of the Drell-Yan process to the low mass region results in the predicted cross section too low by almost two orders of magnitude [9,19]. Studies of the target mass dependence discussed in chapter 3 also indicate the existence of other than Drell-Yan sources of the dileptons below M $\approx$ 3 GeV.

There are two main classes of models proposed to explain this mass region. These are a) the enhanced Drell-Yan mechanism by soft parton-antiparton, quark-pion and pion-pion annihilations and b) internal conversion of virtual photons.

The general idea of the soft annihilation picture was originally proposed by Bjorken and Weisberg[20] who noticed that in the Drell-Yan mechanism the annihilation occurs only among the partons initially present in the beam and target particles. They proposed that the many soft partons produced in the collisions may also form virtual photons. The effect enhances the hard Drell-Yan process by a factor of about 25 in the low mass range. This picture has been further extended by Černy, Lichard and Pišut[21] who had used the concept of the space-time evolution of the collisions to suggest that the quarks and antiquarks produced in different rapidity regions are created in different times and therefore do not annihilate. This restricts the additional annihilations to pairs of partons created close-by in rapidity and as a result to the low masses of produced dileptons. Such picture provides a smooth transition from the low mass region to the large mass hard annihilation regime.

Along similar lines other theoretical suggestions have been made of possible low mass enhancements from parton-pion and pion-pion annihilations using the framework set up by Sachrajda and Blankenbecler[22] (fig. 3). In particular

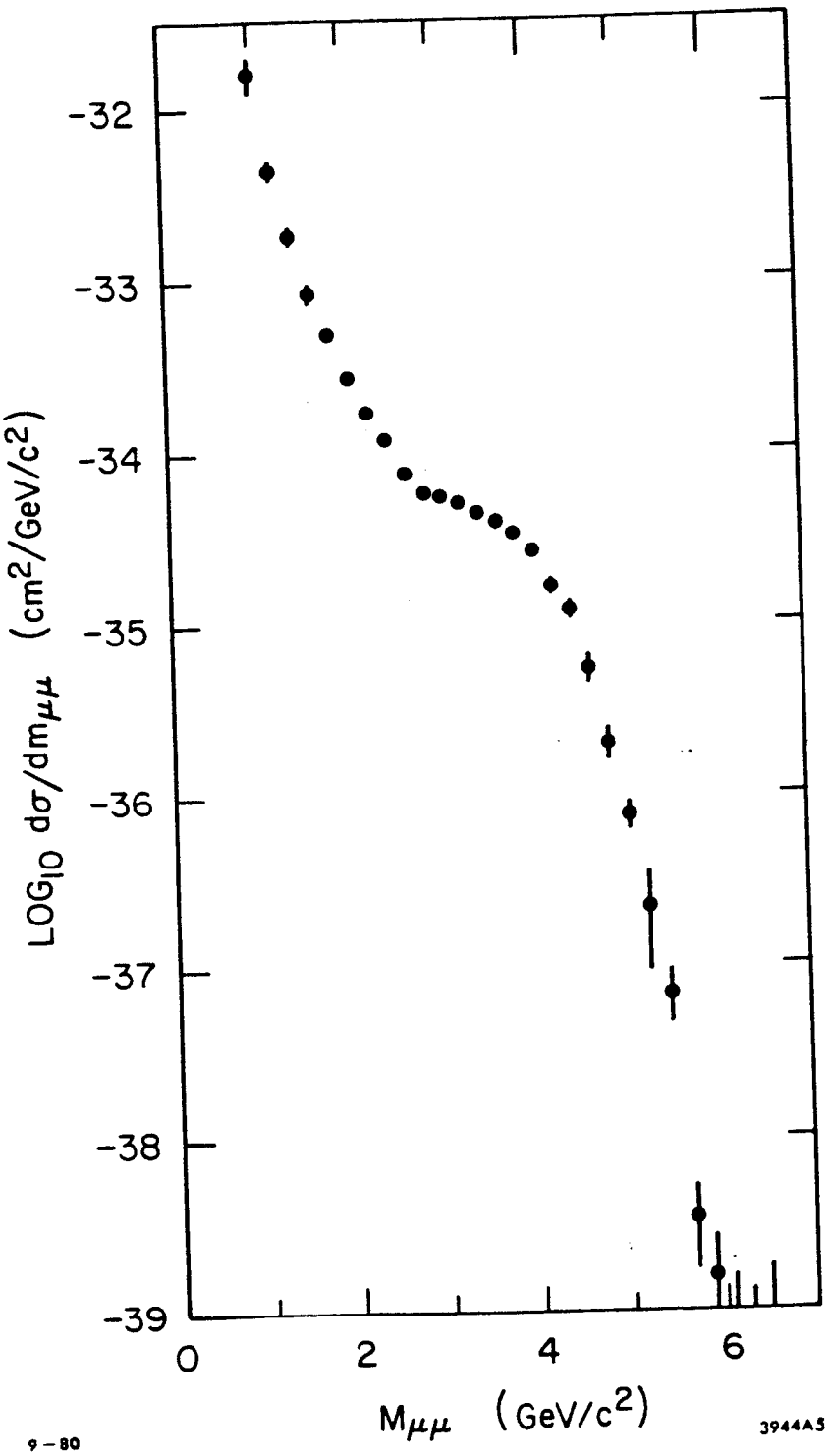

2. The dimuon mass spectrum produced by 29.5 GeV/c protons (ref. 1).

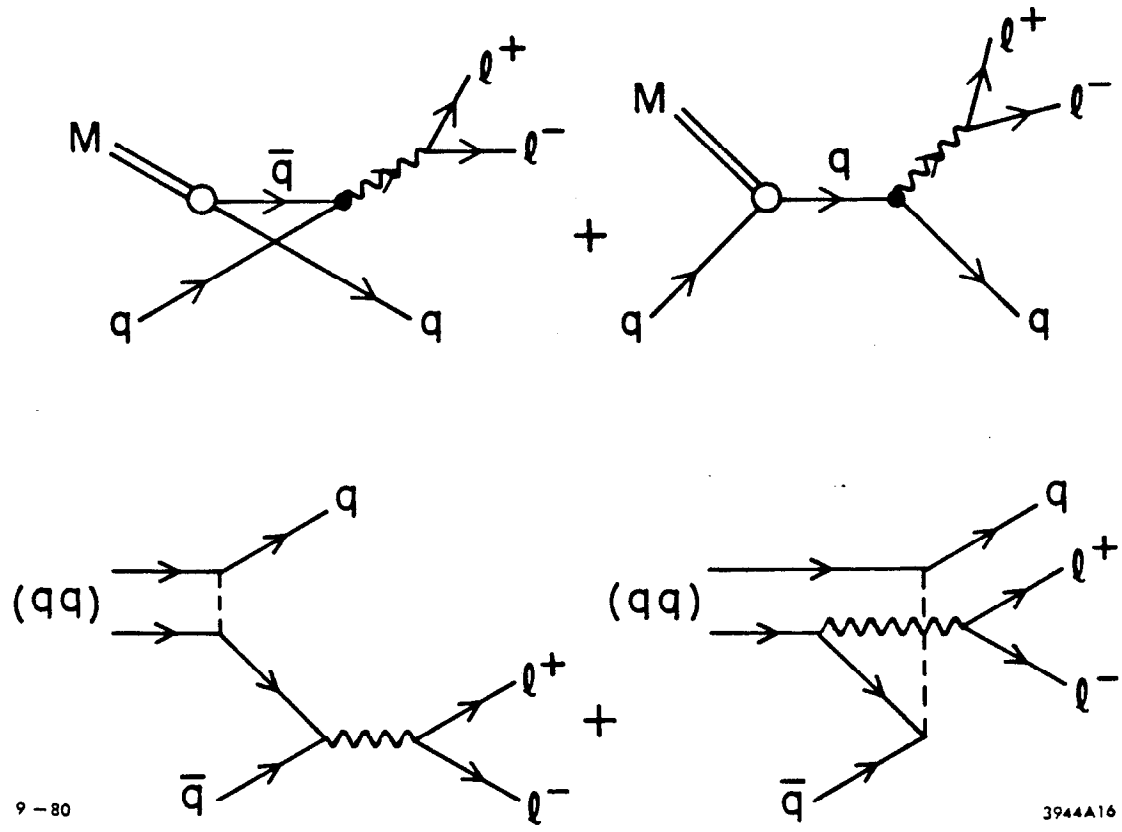

3. Meson-quark and diquark-quark annihilation diagrams.

calculations of Goldman, Duong-van and Blankenbecler[23] of the meson-meson annihilation process satisfactorily describe the low mass data[24].

The second class of models is based on the idea of the internal conversion of virtual photons produced by the bremsstrahlung of charged particles created in the collisions. The production of such slightly off-shell virtual photons is electromagnetic in nature and analogous[25] to the production of real photons. The expected rate of an electromagnetic type process is proportional to α^2 and is comparable with the observed rate of dileptons, thus suggesting that such mechanism may play an important role.

The mass distribution of the produced dileptons is related to the cross section for production of virtual photons σ_{γ^*} by[19]:

$$\frac{d\sigma}{dM^2} = \frac{\alpha}{3\pi} \frac{1}{M^2} \sqrt{1 - \frac{4m^2}{M^2}} \left(1 + \frac{2m^2}{M^2}\right) \sigma_{\gamma^*} \qquad (12)$$

Various authors had used different approaches to calculate σ_{γ^*}. Craigie and Schildknecht[26] had used vector dominance arguments, other authors[27-30] created models for real photon production and then continued them off-shell by various means. The general features of all these bremsstrahlung models are evident from the formula (12): The mass spectrum is expected to have 1/M behaviour, while the yield is proportional to the real photon cross section and may vary with x, p_T and s. The most characteristic is, however, a prediction that the yield of e^+e^- pairs will be higher than that of $\mu^+\mu^-$:

$\sigma(e^+e^-) / \sigma(\mu^+\mu^-) \geq 3$. It is a consequence of the 1/M mass dependence and the difference of the e^+e^- and $\mu^+\mu^-$ mass thresholds; the yields are expected to be the same for large dilepton mass.

3. Review of the Data

There was a great number of experiments performed during the last few years which addressed the problem of direct lepton production. In the following text data are usually referred to according to the collaboration by which they were obtained. The major experiments and corresponding references are listed in the following tables. Some earlier results superseded by better quality measurements are omitted.

Table 1. High Mass Lepton Pair Experiments at the ISR

COLLABORATION	EXPERIMENT NUMBER	MASS RANGE, GeV	$\sqrt{s}$, GeV		REFERENCES
CERN-Columbia-Oxford-Rockefeller (CCOR)	R108	$6 < M(e^+e^-) < 14$	62.4	Solenoid spectrometer with two lead glass arrays	31
Athens-Athens-Brookhaven-CERN-Syracuse-Yale (A^2BCSY)	R806	$M(e^+e^-) < 12$	28,52,62	Transition radiation detectors and liquid argon colonmeters	32,33
CERN-Harvard-Frascati-MIT-Naples-Pisa (CHFMNP)	R209	$3 < M(\mu^+\mu^-) < 25$	62	Iron toroids spectrometer	34,35

Table 2. High Mass Lepton Pair Experiments at Fixed Target Machines

COLLABORATION	EXPERIMENT CODE	BEAM, GeV/c	MASS RANGE, GeV		REFERENCES
Columbia-Fermilab-Stony Brook	CFS	p : 200,300,400	M $(\mu^+\mu^-)$ < 20 M (e^+e^-) < 14	Two arms spectrometer	36,37,38 39,40
CERN-College de France-Ecole Polytechnique-Orsay-Saclay	NA3	π,K,p : 150,200,280	M $(\mu^+\mu^-)$ < 12	Large acceptance superconducting dipole spectrometer	41,42
Chicago-Princeton	CPI	p : 200,300,400	7<M $(\mu^+\mu^-)$<11	Magnetic spectrometer	43,44
Chicago-Illinois-Princeton	CPII/CIP	π,K,p : 150,200,225	M $(\mu^+\mu^-)$ < 11	Chicago cyclotron magnet	45,46,47
Saclay-Imperial College-Southampton-Indiana	GOLIATH	π^- : 150,175	M $(\mu^+\mu^-)$ < 9	Large aperture magnetic spectrometer	48,49
Seattle-Northeastern-Michigan-Tufts	SNMT	p : 400	M $(\mu^+\mu^-)$ < 12	Spectrometer	50
Birmingham-CERN-Ecole Polytechnique	OMEGA	π,K,p : 39.5	M $(\mu^+\mu^-)$ < 7	Omega spectrometer	60

Table 3. Low mass muon pair experiments.

COLLABORATION	BEAMS AND TARGET		REFERENCES
BNL-FNAL-NSF-Rochester	$\pi^{\pm}$ Cu, plab = 16,22 GeV/c	Wide aperture magnetic spectrometer	51,52,53
SLAC-Vanderbilt-Santa Cruz-MIT	$\pi^{\pm}$ p, plab = 15.5 GeV/c	Streamer chamber with hydrogen target	54,55
Chicago-Princeton (CPII)	π, p Be, plab = 150,225 GeV/c	Chicago cyclotron magnet spectrometer	56,57
BNL-Yale	pW, plab = 28 GeV/c	Beam dump; $0.2 < x\ (\mu^{+}\mu^{-}) < 0.7$	58,59
Birmingham-CERN-Munich-Neuchatel-Ecole Polytechnique-Rutherford	π, K, p Cu, plab = 39.5 GeV/c	Omega spectrometer, $M(\mu^{+}\mu^{-}) < 5.7$	60
SLAC-Stanford-Irvine	K^{o}_{L} Cu, $4 < P_{LAB} < 20$ GeV/c	Spectrometer	61

Table 4. Low Mass electron pair experiments

COLLABORATION	BEAMS AND TARGET		REFERENCES
CERN-Saclay-Zurich	pp at $\sqrt{s}$ = 53,63 GeV	ISR experiment R702, Double arm spectrometer with Cerenkov and lead glass counters	62,63
BNL-CERN-Syracuse-Yale	pp at $\sqrt{s}$ = 55 GeV	ISR experiment R806, Transition radiation detectors and liquid argon colorimeters	64
SLAC-Johns Hopkins-Caltech	$\pi^- p$, p_{LAB} = 16 GeV/c	LASS spectrometer	65
Kyoto-KEK-Osaka-Tokyo-Saitame-KEK	pBe, p_{LAB} = 9, 13 GeV/c	Double arm spectrometer	66
Bologna-Glasgow-Rutherford-Saclay-Turin	$\pi^- p$, p_{LAB} = 70 GeV/c	Big European Bubble Chamber with Track Sensitive Target	67
SLAC-Duke-Imperial College	$\pi^{\pm} p$, p_{LAB} = 18 GeV/c	Bubble chamber with plates	68
Tohoku-Golkuin-Nara-KEK	pp, p_{LAB} = 8 GeV/c	Bubble chamber	69
BNL-Pennsylvania-Stony Brook	$\pi^- p$, p_{LAB} = 17 GeV/c	Multiparticle Spectrometer	112

3.1 Target Dependence

Since the density of a heavy nuclear target is much higher than that of the hydrogen, nuclear targets are often used to study the low cross section processes. It is then an experimental problem of how to extract the cross section of a given process on single nucleon from the measurements involving heavy nuclei. It has been observed in several different experiments that the cross section has, to a good approximation, a power law behaviour as function of the nuclear number A:

$$\sigma = \sigma_o A^{\alpha} \quad . \tag{13}$$

In coherent processes, e.g., diffractive production, where one expects the shadowing effects to exist, the value of $\alpha = 2/3$ is both observed experimentally and expected from the Glauber theory. On the other hand, for hard scattering processes involving partons, one does not expect the shadowing to play an important role. The incoming set of partons inside the projectile should see the target as an ensemble of point-like constituents with their members proportional to the number of nucleons, i.e., $\alpha = 1$. In the kinematical regions where both shadowing and hard processes occur the value of α reflects presumably the relative contributions of these processes to the measured quantity.

The dependence of the parameter α on the mass of the $\mu^+\mu^-$ pairs produced in pN collisions is shown[40,45,57] in fig. 4. At low mass the value of α is close to $\alpha = 2/3$. It rises with increasing mass and attains plateau consistent with $\alpha = 1$ for $M > 3$ GeV. The high mass data obtained by the Columbia-FNAL-Stony Brook Collaboration give the average value of $\langle\alpha\rangle = 1.007 \pm 0.018 \pm 0.028$ for $5 < M < 11$ GeV, where the errors describe statistical and systematic uncertainties respectively. As can be seen in fig. 5 the value of α is also independent of the transverse momentum of the pair. Similar qualitative behavior can be seen in fig. 6 which summarizes the values of α for the pion induced reactions[41,56,57,70]. Also here the parameter α has no obvious $p_\perp$ or x_F dependence (see fig. 6b and 6c).

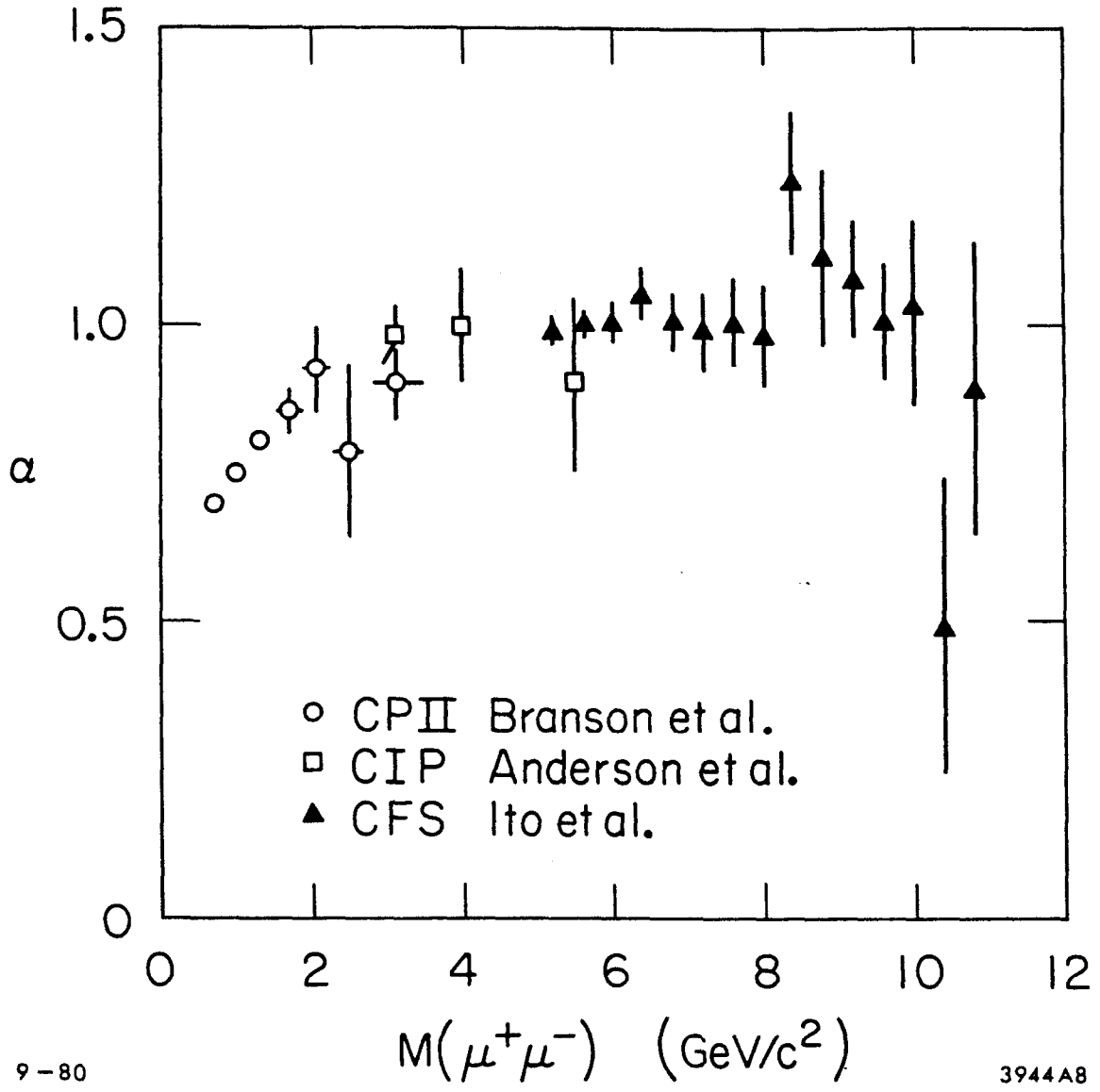

4. The atomic mass number dependence A^{α} for dimuons produced by protons.

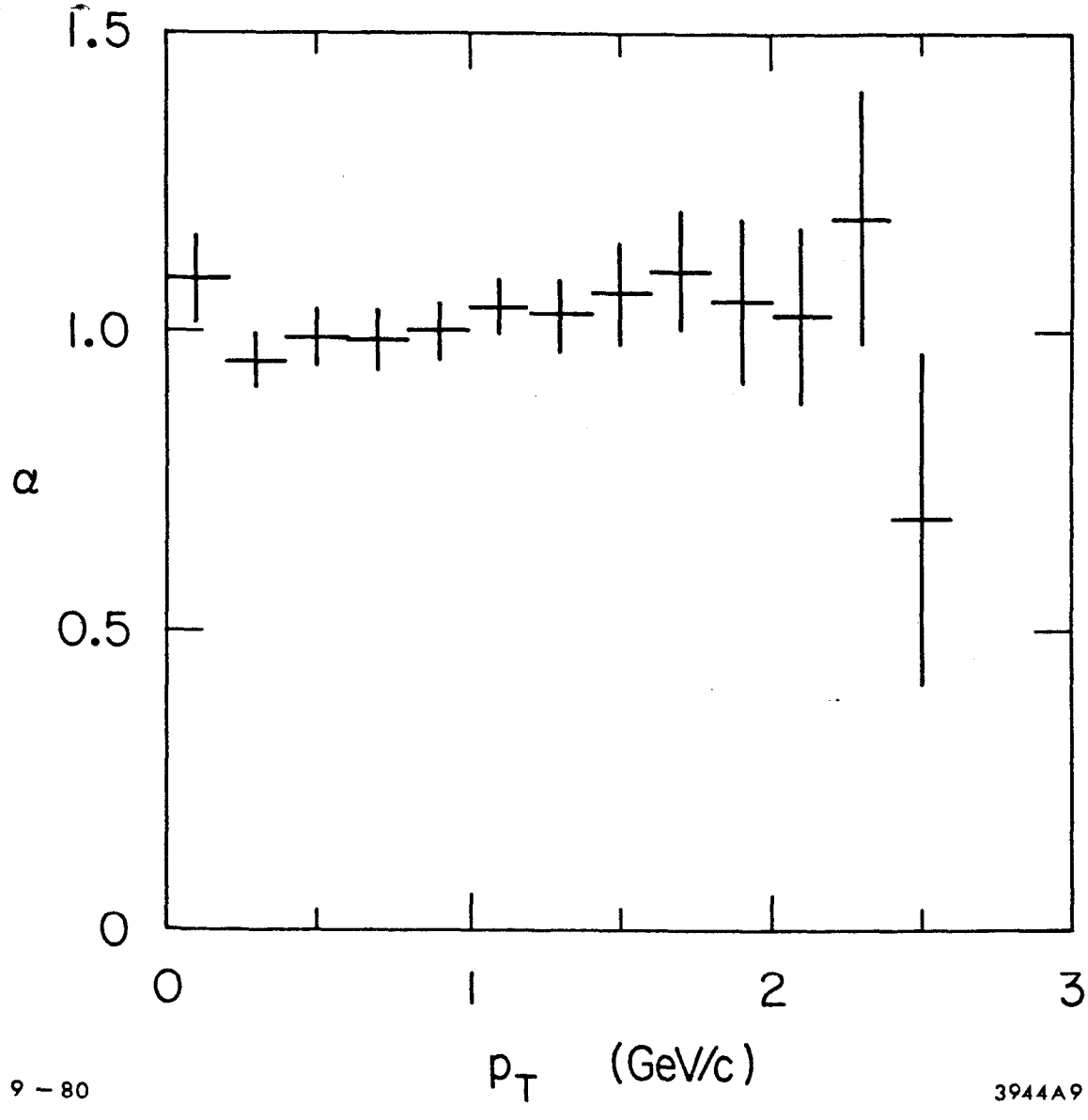

5. The dependence of the parameter α on transverse momentum of muon pairs produced by proton beam.

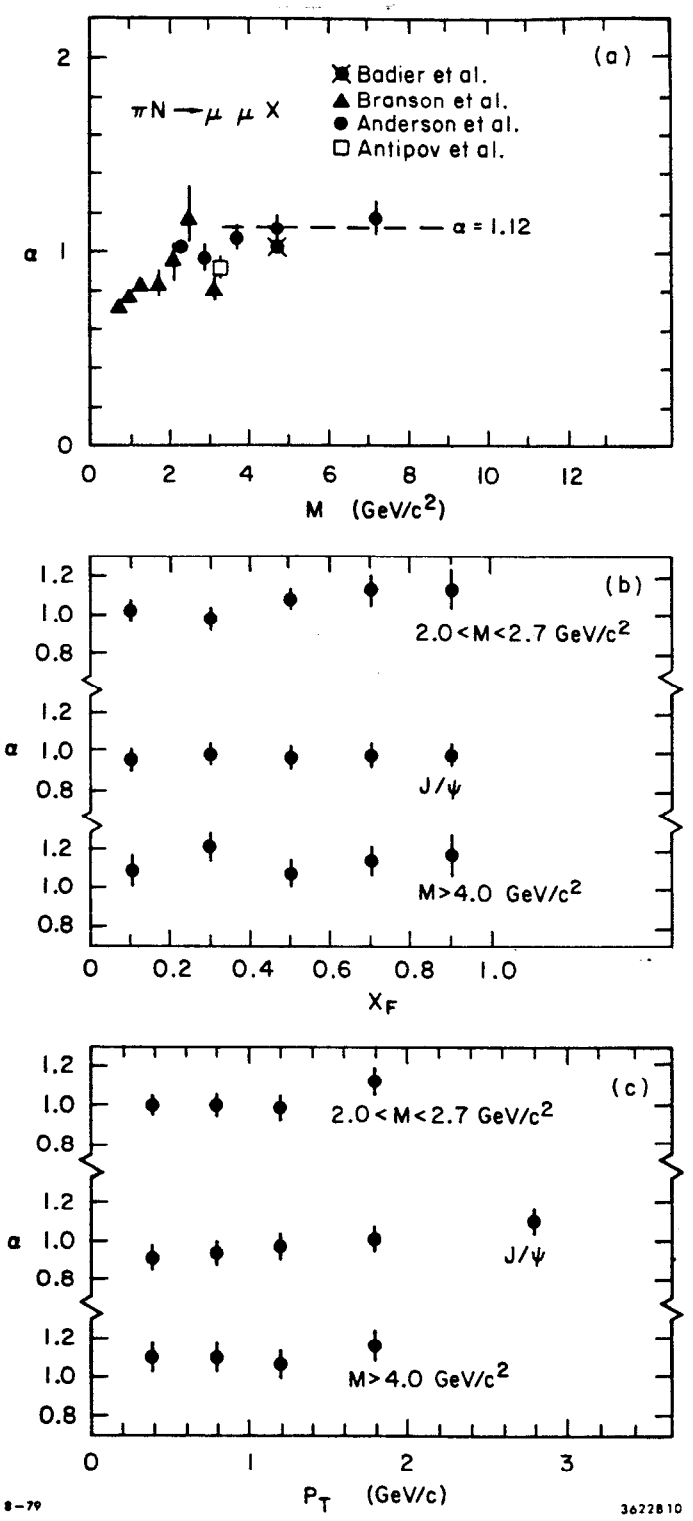

6. The dependence of the parameter α on: a) mass, b) Feynman x, c) transverse momentum of muon pairs produced by pion beams.

for high $\mu^+\mu^-$ mass indicating that the normalisation of the cross section is independent of the kinematics.

The value of the parameter α at the plateau has generated recently some controversy. The Chicago-Illinois-Princeton group had obtained the value of $\alpha = 1.12\pm0.05$ for the π^- interactions on Cu, C and W targets. On the other hand the NA3 experiment at CERN measured $\mu^+\mu^-$ production on hydrogen and platinum targets using both π^+ and π^- beams. In the framework of the Drell-Yan model and with additional assumptions concerning the quark structure functions the authors obtained the value of $\alpha = 1.03\pm0.03$ at 200 GeV/c and $\alpha = 0.994\pm0.015$ at 150 GeV/c. Although the difference between the two sets of values of α is only about $\alpha \sim 0.10$, it is important to remember that it corresponds to the difference of $\sim 70\%$ in the absolute cross section on single nucleon extracted from the measurement on a tungsten target. New measurements now underway in both FNAL and CERN are expected to clarify the experimental situation soon. From the phenomenological standpoint it is unclear what kind of mechanism could be responsible for the value of α greater than 1. As will be discussed in chapter 5, the nucleon structure function extracted from the high mass dimuon data by the NA3 experiment is easier to understand in terms of the present QCD phenomenology, thus motivating the general use of $\alpha = 1$.

There is a natural interpretation of the observed effects. At low lepton pair mass the Drell-Yan process represents only a small fraction of the total cross section. Other coherent mechanisms and absorptive effects contribute substantially to the measured cross section, thus masking the characteristic features of the hard process. At higher mass, however, those other processes may be assumed to be negligible and the Drell-Yan mechanism dominates. The study of the target mass dependence defines, therefore, the region of applicability of the Drell-Yan description of massive lepton pair production. Only the region where $\alpha = 1$, i.e., for $M > 4$ GeV, can be used for tests of the

parton model and QCD calculations of the Drell-Yan process. At lower masses other processes have to be taken into account in the phenomenological description of the data.

3.2 Beam Dependence

One of the first qualitative successes of the Drell-Yan picture of massive lepton pair production was the observation of the effects expected for the quark-antiquark annihilations. For the isoscalar nuclear targets and high dilepton masses one may in first approximation neglect the contribution of the sea component to the annihilation process. With such assumption the relative yield of lepton pairs depends only on the quark content of the beam (see eq. (1)). Figure 7 shows the ratio R_1 of muon pair production in π^+N and π^-N interactions as function of mass of the $\mu^+\mu^-$ pair. In the region where the sea of the pion may be neglected, i.e., at large values of x corresponding to large mass, the value of R_1, should approach the ratio of the charges squared of the annihilating antiquarks:

$$R_1 = \frac{\sigma\ (\pi^+N \to \mu^+\mu^-\ X)}{\sigma\ (\pi^-N \to \mu^+\mu^-\ X)} \xrightarrow[\text{at high } x]{} \frac{e^2_{\bar{d}}}{e^2_{\bar{u}}} = \frac{1}{4}$$

The data in figure 7 show a clear trend confirming such expectations. The value of R_1, expected from the contribution of hadronic processes and of the sea contamination to be close to 1 at low x, decreases with increasing mass and is compatible with 1/4 at large x. The energy dependence of the decrease reflects variations of the range of x contributing to the fixed value of mass. The asymptotic value of R_1 depends also on the isospin composition of the target. For example, for the hydrogen target with the number of up quarks twice the number of down quarks, the limiting value of R_1 is:

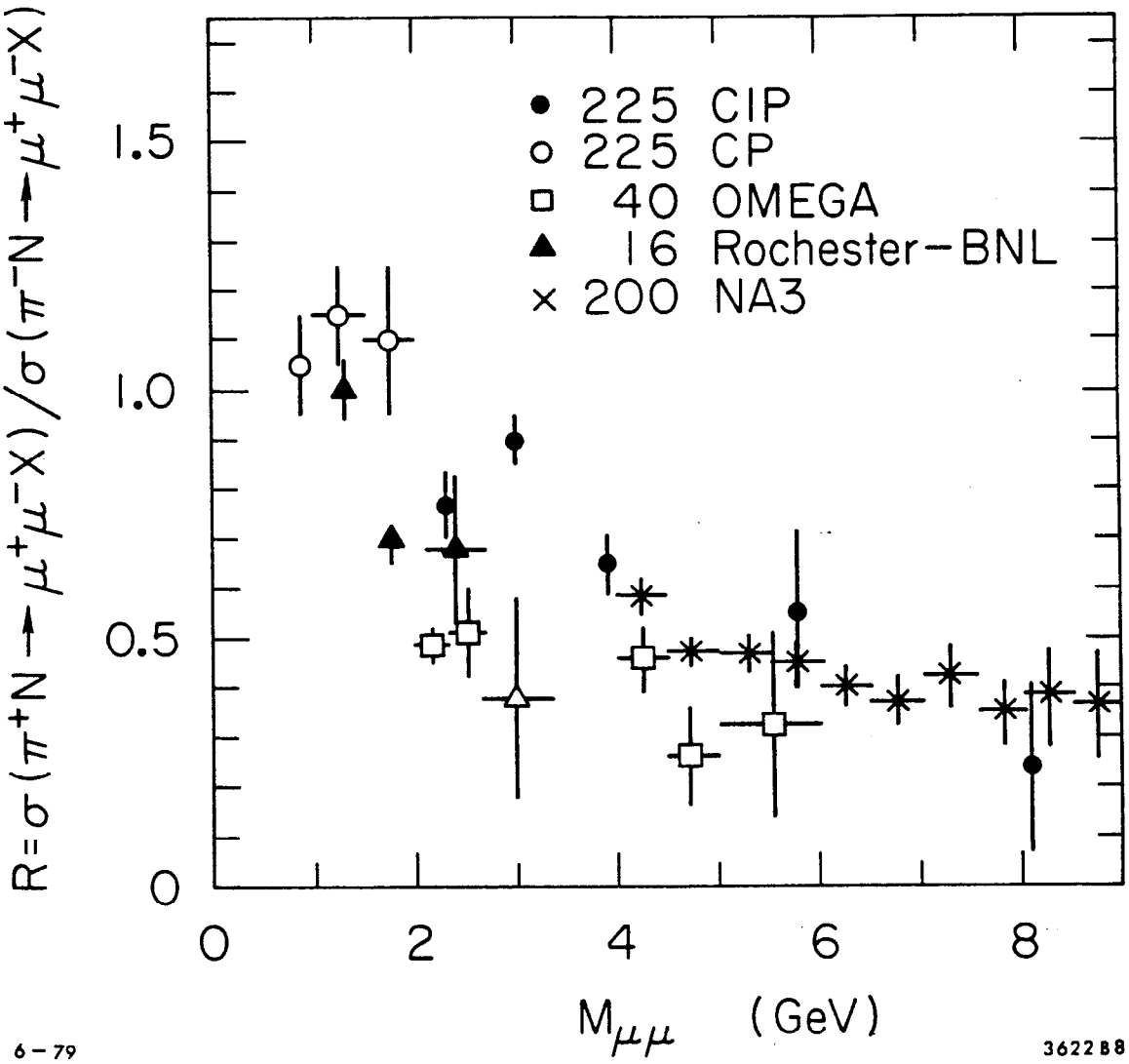

7. Ratio of the dimuon production cross section in π^+N and π^-N interactions versus $M(\mu^+\mu^-)$.

$$R_1 = \frac{\sigma\,(\pi^+ p \to \mu^+\mu^- X)}{\sigma\,(\pi^- p \to \mu^+\mu^- X)} \longrightarrow \frac{e_{\bar{d}}^2}{2e_{\bar{u}}^2} = \frac{1}{8}$$

The experimental data of the NA3 Collaboration shown in fig. 8 reproduce well this parton picture prediction.

More dramatic effects are expected for the ratio of pion and proton interactions producing lepton pairs. In pN collisions the annihilating antiquarks originate from the sea and are confined to small values of x. The cross section, therefore, is expected to decrease sharply with increasing mass. On the other hand, the incoming pion has a valence antiquark thus providing a larger x (or mass) range for the Drell-Yan process. The ratio of the muon pair production by the pion and proton beams is shown in fig. 9. It exceeds the value of 100 for masses above 10 GeV reflecting the difference of the antiquark x distributions.

Similar stricking effects are expected also for the antiproton beam in which case all valence quarks can annihilate. The mass dependence and the limiting value of the $\bar{p}p/pp$ ratio will depend here on the shapes of the quark distributions.

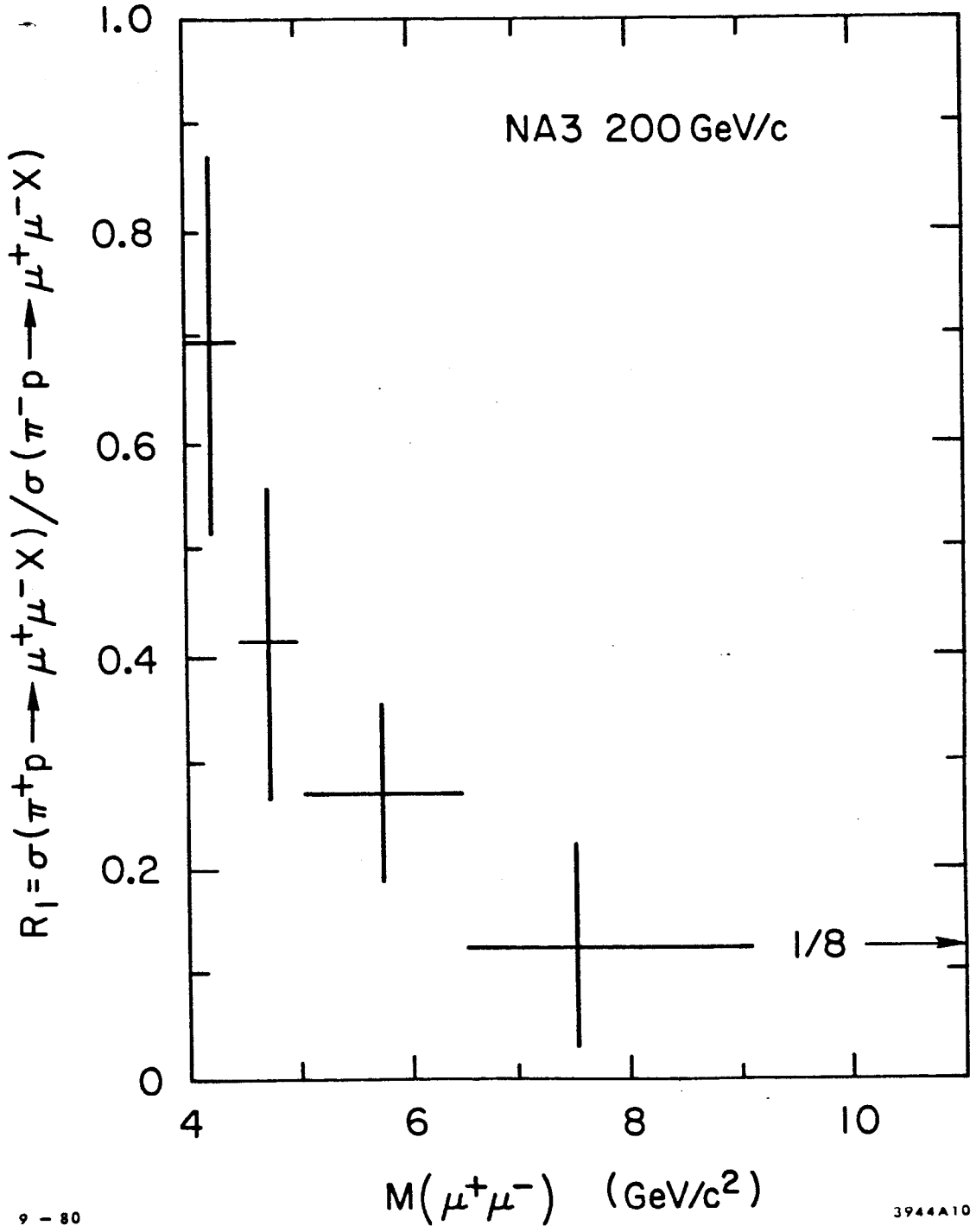

8. Ratio of the dimuon production cross section in π^+ and π^- interactions on protons versus $M(\mu^+\mu^-)$.

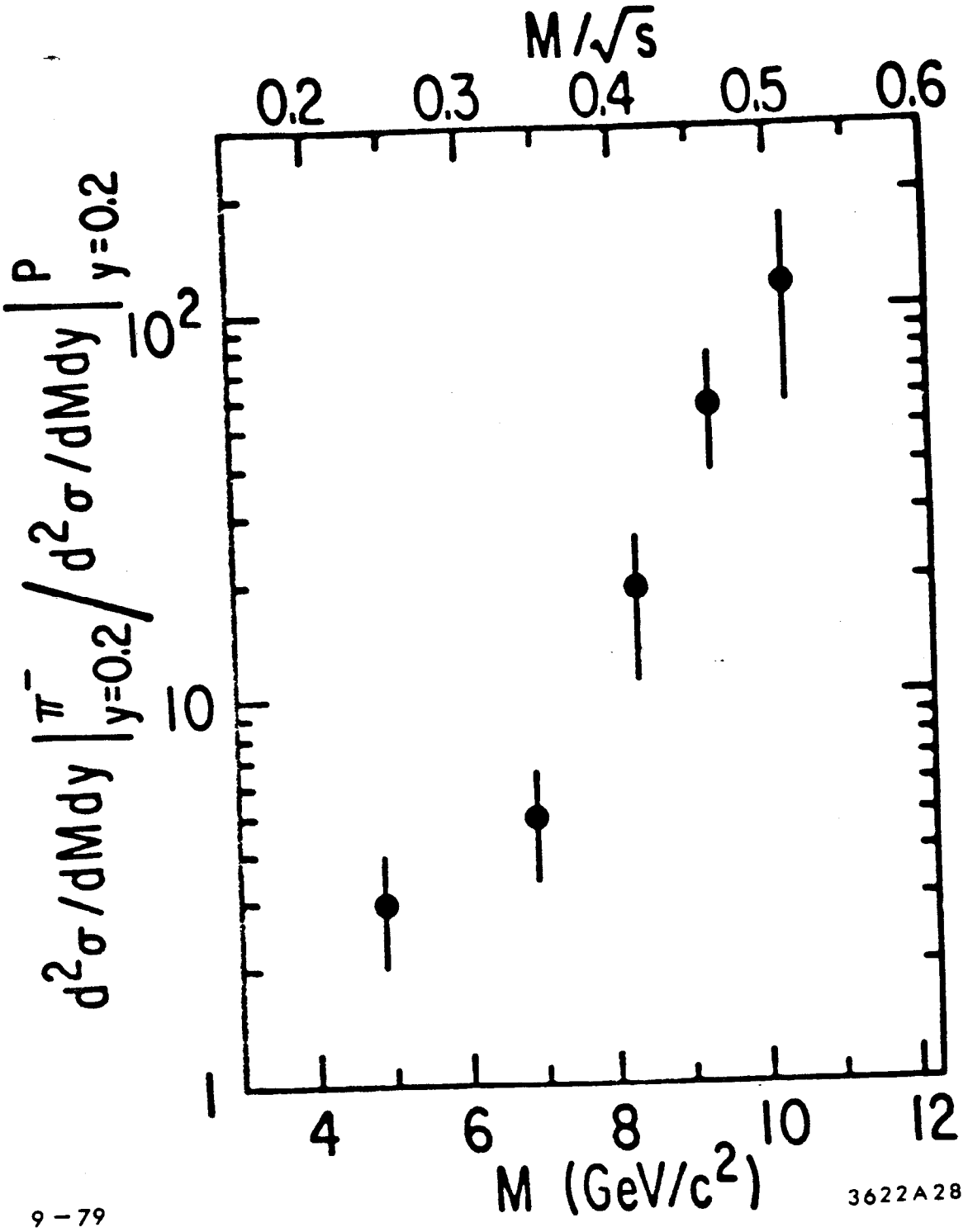

9. The ratio of π^- induced to proton induced $\mu^+\mu^-$ pair cross sections at $y_{cm} = 0.2$ as function of mass.

3.3 Mass Spectra

The proton induced dilepton mass spectra, shown in fig. 10, represent some of the most impressive measurements made during the last few years. Both dimuon and electron pairs distributions extend to mass of about 20 GeV and in the case of the Columbia-Fermilab-Stony Brook results span almost 10 orders of magnitude of the cross section. In both cases good mass resolution allows for clear separation of vector mesons from the dilepton continuum.

Above the dimuon mass threshold no difference is expected nor observed for the $\mu^+\mu^-$ and e^+e^- mass spectra at the same energy. The much higher cross section for the continuum measured in the ISR experiment is due to the energy dependence of the Drell-Yan mechanism. Simple parton model approach, described in section 2.3, predicts scaling in terms of the dimensionless variable $\tau = M^2/s$. The compilation of the dilepton mass distributions measured in proton-proton and proton-nucleon interactions is shown in fig. 11 as function of $\sqrt{\tau}$. It is evident that tests of scaling over larger energy range are extremely difficult. Low energy data, which could reach high values of τ, are limited to the low mass region where other than Drell-Yan processes contribute. On the other hand, the high energy ISR experiments are concentrated at small values of τ. The present practical limit of mass $M \lesssim 20$ GeV corresponds to $\tau \approx 0.3$ at highest ISR energies. The largest range of τ is covered, therefore by the Fermilab experiments.

The best test of scaling existing so far is shown in fig. 12, where the 200, 300 and 400 GeV/c pN results of the CFS group are presented. The agreement with scaling, to within $\sim(10\div20)$ % precision of the data, is not in contra-

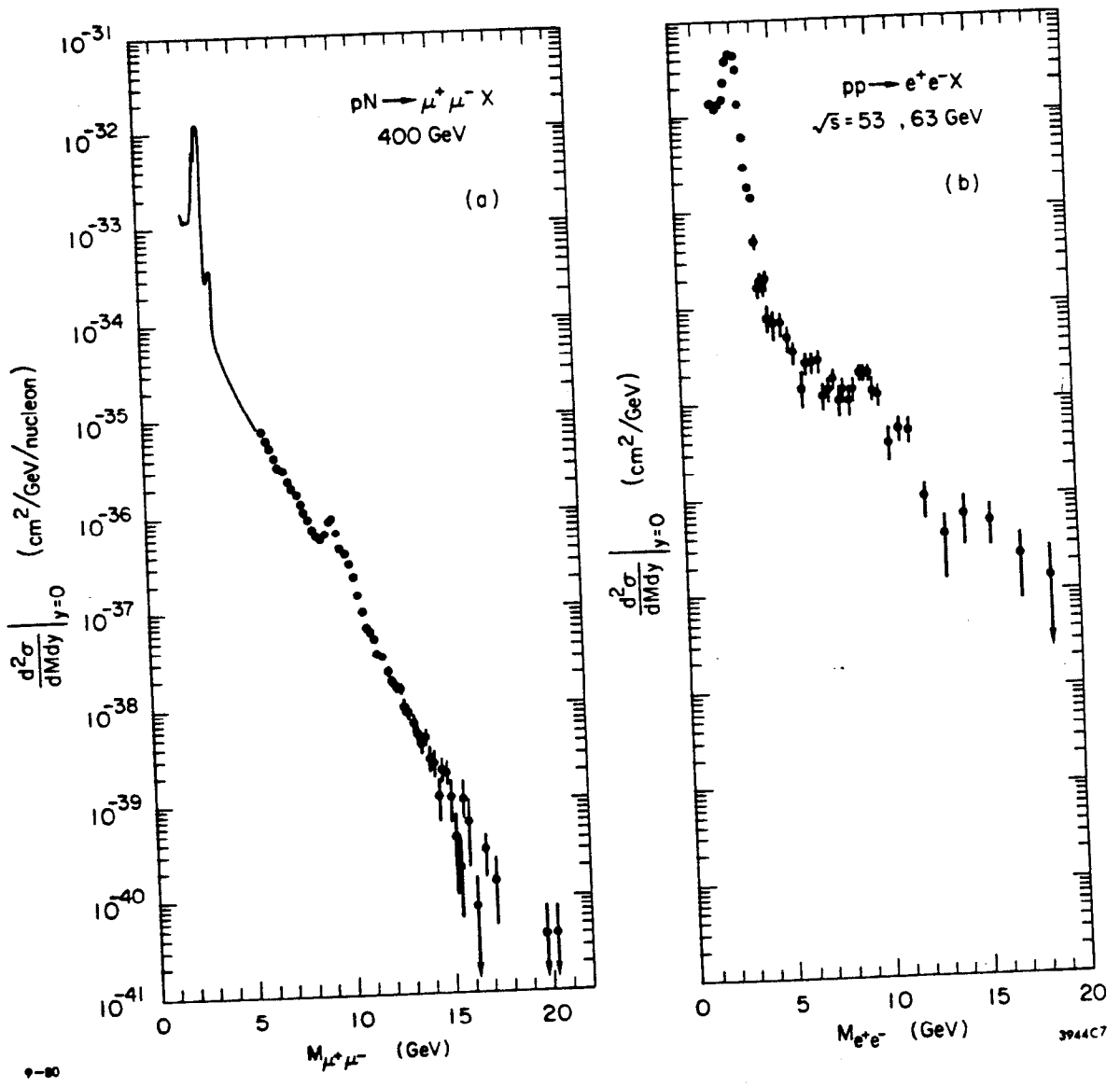

10. a) Dimuon spectrum measured by the CFS Collaboration. Solid line describes 1976 results. b) Dielectron spectrum measured by the A^2BCS Collaboration.

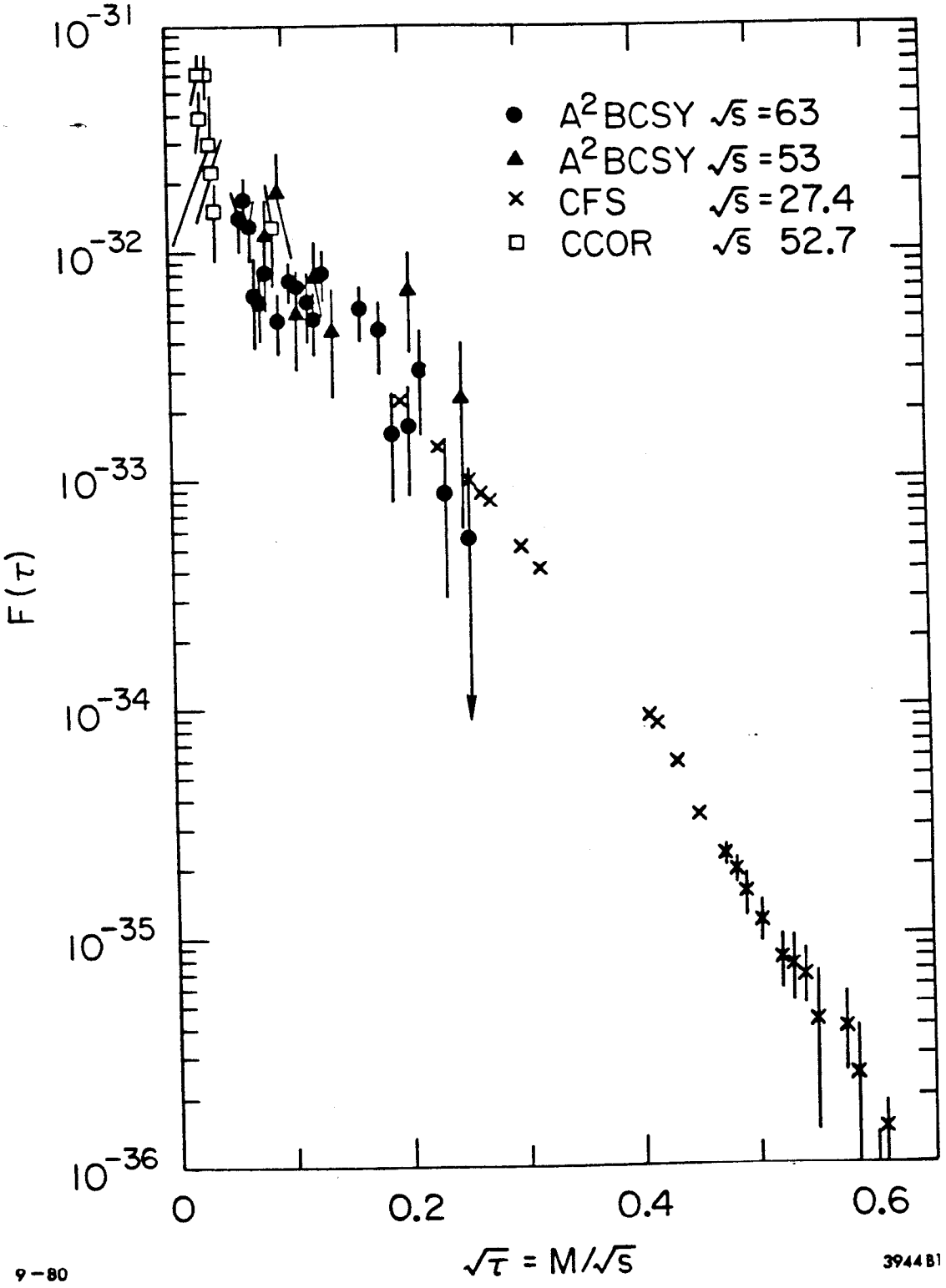

11. The experimental function F(τ) versus $\sqrt{\tau}$ for the dileptons produced by protons.

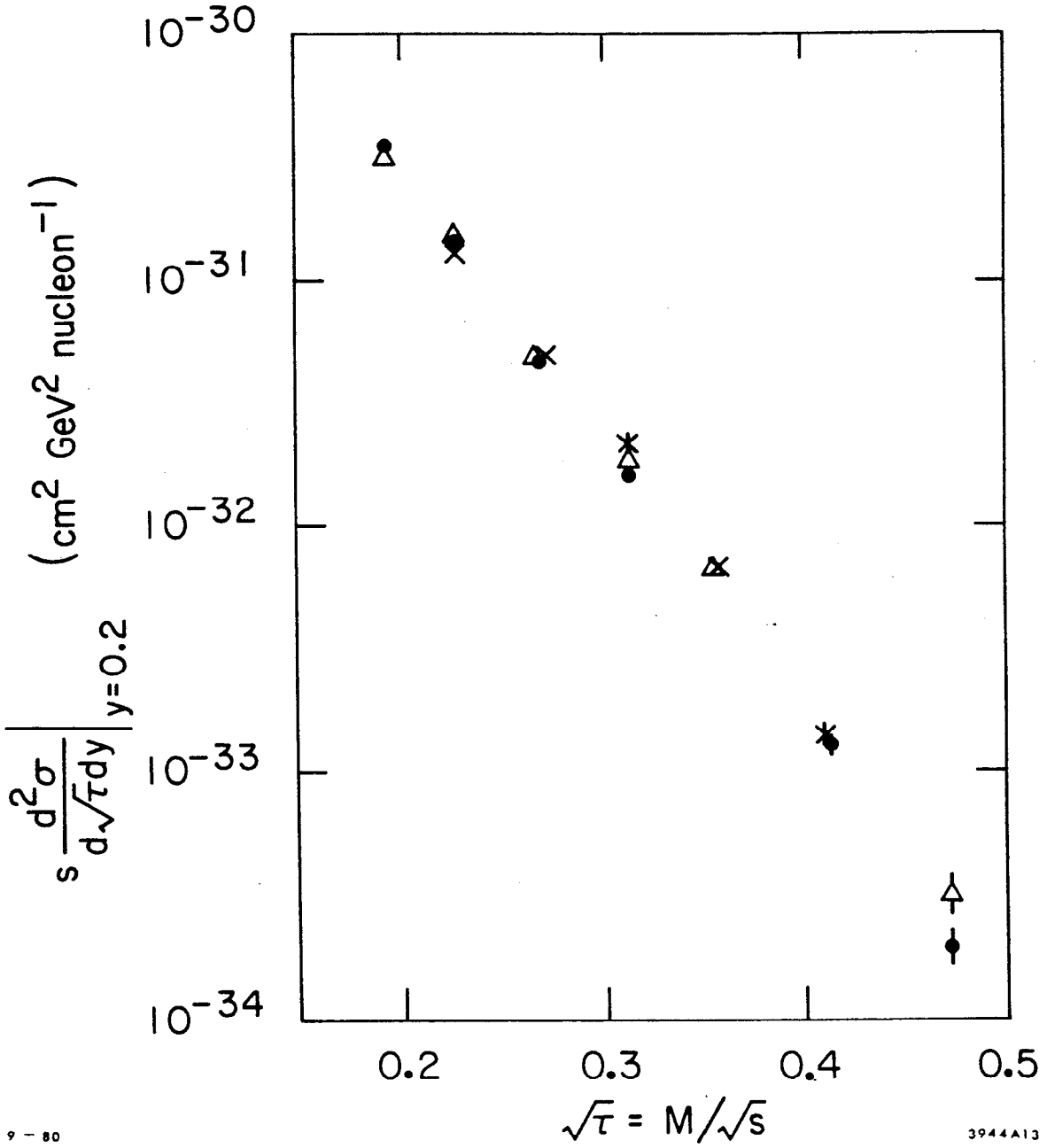

12. Test of scaling of the CFS Collaboration measurements.

diction with the expectations of QCD, that scale breaking should occur. This problem will be further described in chapter five. In spite of the lack of sufficient overlap of the data over the wider energy range, the data from different experiments, shown in fig. 11, seem to be in agreement with each other. The Fermilab measurements are well parametrized by the formula;

$$s \left.\frac{d^2\sigma}{d\sqrt{\tau}\,dy}\right|_{y=0.2} = (42.\pm.2\pm11.)e^{-(25.1\pm.1\pm.6)\sqrt{\tau}} \ \mu b\ GeV^2, \qquad (14)$$

while the CHFMNP group at the ISR obtained the best fit to the data with:

$$M^3 \left.\frac{d^2\sigma}{dMdx}\right|_{x=0} = (1.04\pm0.16)\cdot10^{-32}\ \frac{(1-\sqrt{\tau})^{10}}{\sqrt{\tau}}\ cm^2\ GeV^2, \qquad (15)$$

and the A^2BCSY group also at the ISR has described their e^+e^- spectrum as:

$$M^3 \left.\frac{d^2\sigma}{dMdy}\right|_{y=0} = (2.60\pm0.13)\cdot10^{-32}\ e^{-(2.0\pm0.7)\tau}\ (1-\tau)^{9.7\pm0.4}\ cm^2\ GeV^2, \qquad (16)$$

All these parametrizations are compatible with each other in the region of the overlap of the data, i.e., around $\tau=0.2$. Their extrapolations into the region of other experiments shows, however, deviations (see fig. 13) indicating that simple scaling functions may be incompatible with the data and that the scaling violations of the QCD type (see chapter 4) are necessary to describe the results.

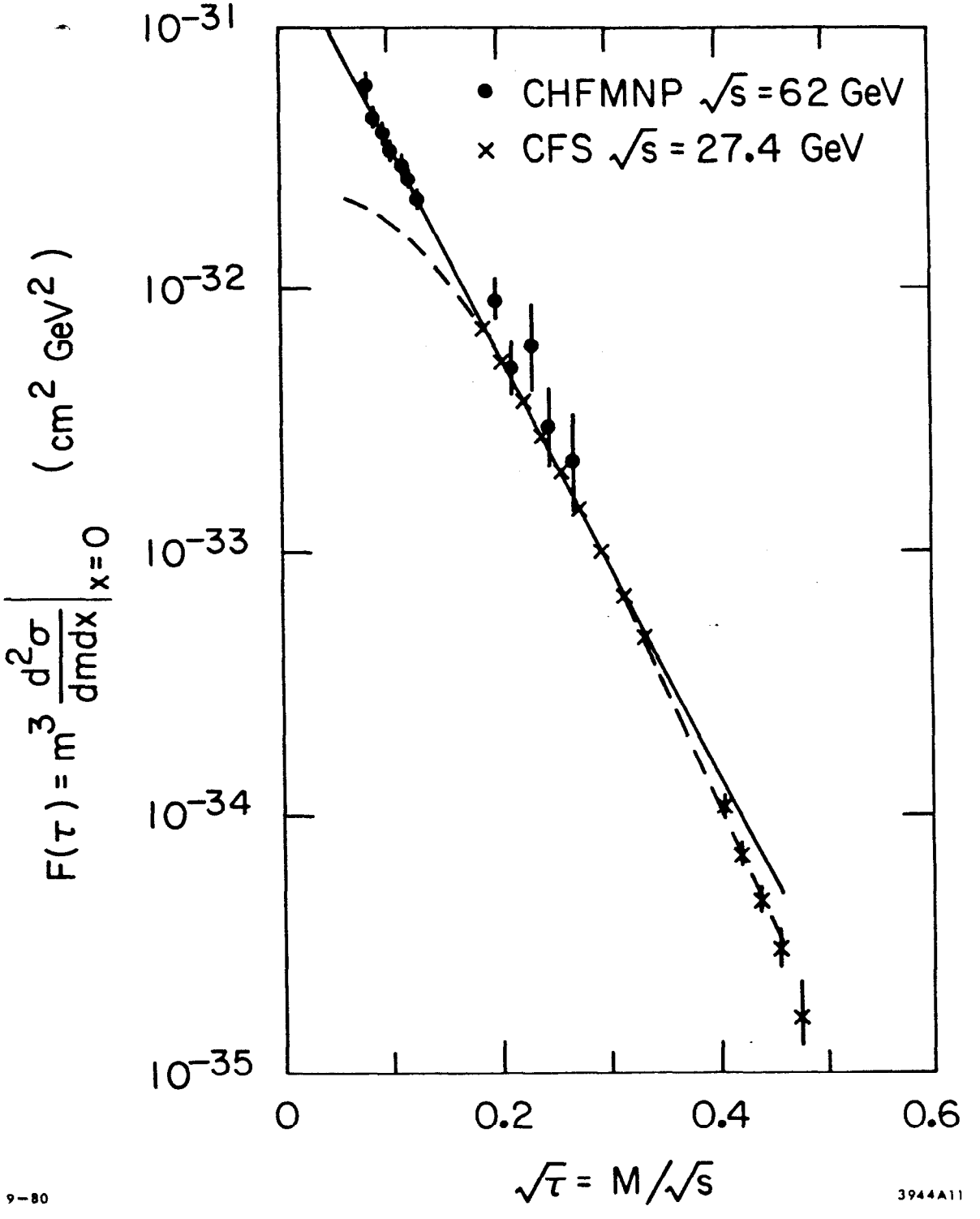

13. The scaling function $F(\tau)$ plotted as a function of $\sqrt{\tau}$. The dashed line represents the phenomenological fit to the CFS Collaboration data (eq. 14). Solid line describes the CHFMNP results (eq. 15).

The knowledge of the dilepton mass spectra produced by incident particles other than proton is not as yet very good. The spectrum obtained in π^-N collisions is at present best known but here again, the energy range covered by high mass experiments is relatively small. The measurements of the NA3 and Omega experiments at CERN shown in fig. 14 as function of $\sqrt{\tau}$ have the contribution of the Υ resonance already removed. The data show an approximate scaling between 40 and 280 GeV within about 15 % precision of the measurements.

The low energy data correspond at lower τ values to the dilepton mass range where other than Drell-Yan processes may contribute. It is, therefore, not surprising that the Omega results are substantially above those of NA3 experiment for $\sqrt{\tau} < 0.4$. The 39.5 GeV/c data are parametrised by

$$\frac{d\sigma}{dM} = (6.80 \pm .54)e^{-(1.75 \pm .03)} \quad \mu b/GeV/W \text{ nucleus.}$$

The parametrisation with similar function describes well also the NA3 data.

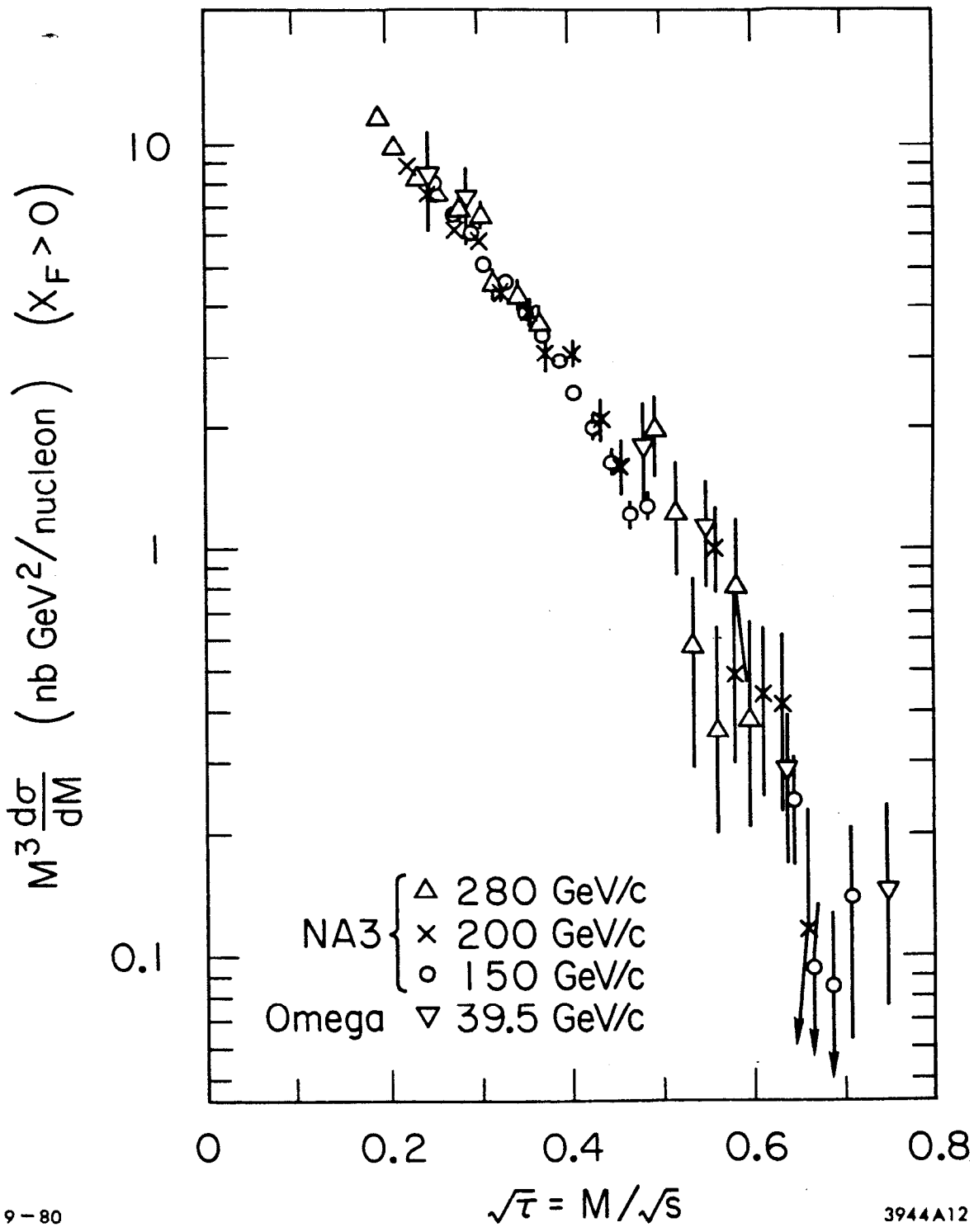

14. Compilation of the $F(\tau)$ versus $\sqrt{\tau}$ for pion produced dimuons.

3.4 Transverse Momentum Distributions

In the simple Drell-Yan mechanism the transverse momentum of the virtual photon is related to the transverse momentum of the annihilating quarks. In the parton model such momentum is related through the uncertainty principle to the size of the parent hadron and is expected to be of the order of 300 MeV/c. It was, therefore, a surprise when the observed transverse momentum of the lepton pairs was found to be large for large masses and to increase with s.

An example of the p_T distribution of the muon pairs produced in pN collisions is shown[40] in fig. 15. The data of both Columbia-Fermilab-Stony Brook and Michigan-Northwestern-Seattle-Tufts groups [39,50] at 400 GeV/c are not compatible with the exponential behavior. They are well parametrized by the formula:

$$E\frac{d^3\sigma}{dp^3} = c\left[1+\left(\frac{p_T}{p_o}\right)^2\right]^{-6}, \qquad (17)$$

where the parameter p_o depends little on mass and x_F but does depend on the incoming energy. The typical value of p_o is $p_o \sim 2.8$.

At higher energies the flattening of the distributions for small p_T values is less visible, and e.g., the CHFMNP group has succesfully fitted their $\sqrt{s}=62$ GeV data[34] with the single exponential form:

$$\frac{1}{p_T}\frac{d\sigma}{dp_T} \sim e^{-bp_T}. \qquad (18)$$

Above $p_T > 500$ MeV/c they found $b = 1.20\pm.11$ GeV^{-1} for $6 \leq M \leq 8$ GeV and $b = 0.37 \pm 0.17$ GeV^{-1} for $11 \leq M \leq 20$ GeV.

The changes of the shape of the p_T distributions are probably best

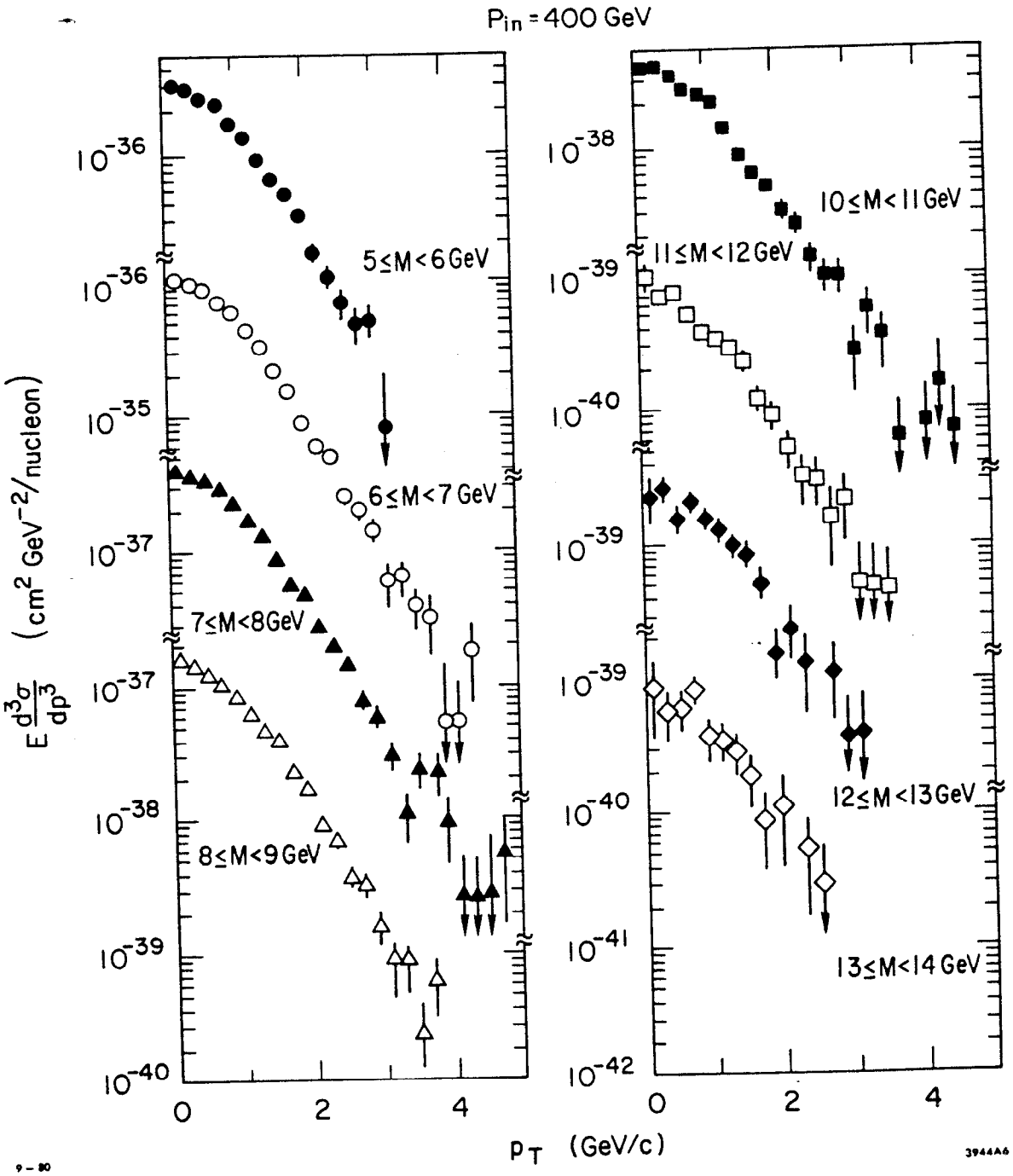

15. Invariant yield of dimuons as function of the transverse momentum of the muon pair for 400 GeV/c incident protons.

visible in plots of the average transverse momentum $\langle p_T \rangle$ versus the mass of the lepton pair. The compilation of the available data for the proton beams is shown in fig. 16. The data points rise from about 600 MeV/c at low dilepton mass to values exceeding 1.0 GeV/c at higher masses. For M > 4 GeV the average transverse momentum seem to saturate. There is, however quite strong energy dependence of the developed plateau.

The increase of the average transverse momentum with rising energy is visible in fig. 16. The high energy data, available so far, have rather large errors which may hide any mass dependence of the results. The $\langle p_T \rangle$ values at the highest measured masses are nevertheless substantially higher than those at lower masses. Special care has to be exercised, therefore, when discussing the energy dependence. The theoretical calculations based on QCD[71,72,73] predict the linear s dependence at fixed value of τ. The data of fig.16 replotted in fig. 17a as function of $\sqrt{\tau}$ show again that the high energy ISR results cover different $\sqrt{\tau}$ region than the CFS measurements. They overlap only at $\sqrt{\tau} \approx 0.2$ which for the Fermilab data corresponds to the beginning of the plateau. At this point the energy dependence of $\langle p_T \rangle$ (fig. 18) exhibits linear rise well described by the form:

$$\langle p_T \rangle = a + b \sqrt{s} \quad . \tag{19}$$

Fit to the data points in fig. 18 gave $a = 0.44 \pm 0.10$ and $b = 0.026 \pm 0.004$.

The behavior of the transverse momentum distribution of dileptons produced in πN collisions is similar to those from proton interactions. Also here the $\langle p_T \rangle$ depends very little on mass above M > 4 GeV but rises with increasing energy (see fig. 17b). Fit to the form (19) at $\sqrt{\tau} = 0.275$

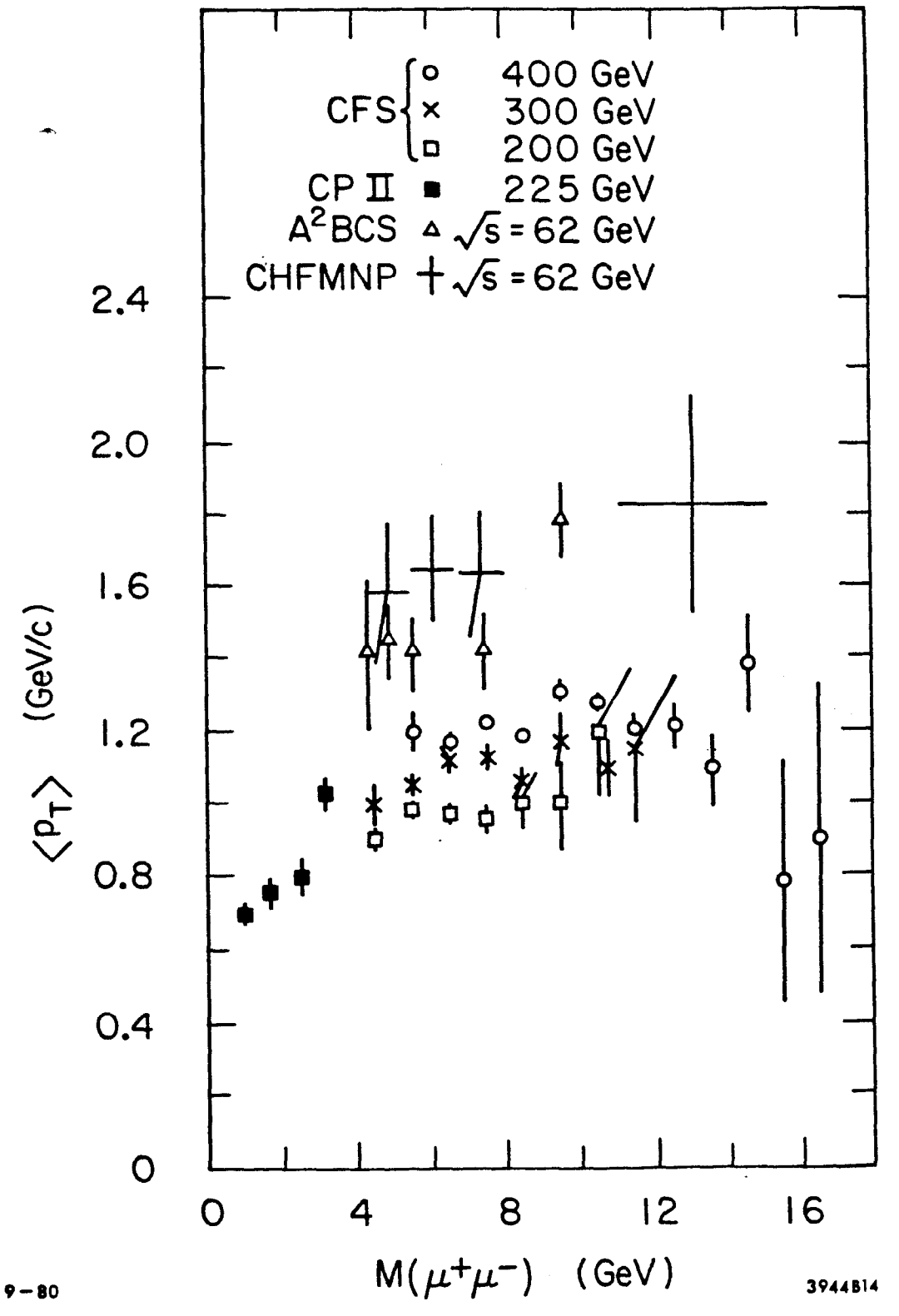

16. Average transverse momentum as function of mass for dimuon produced in proton interactions.

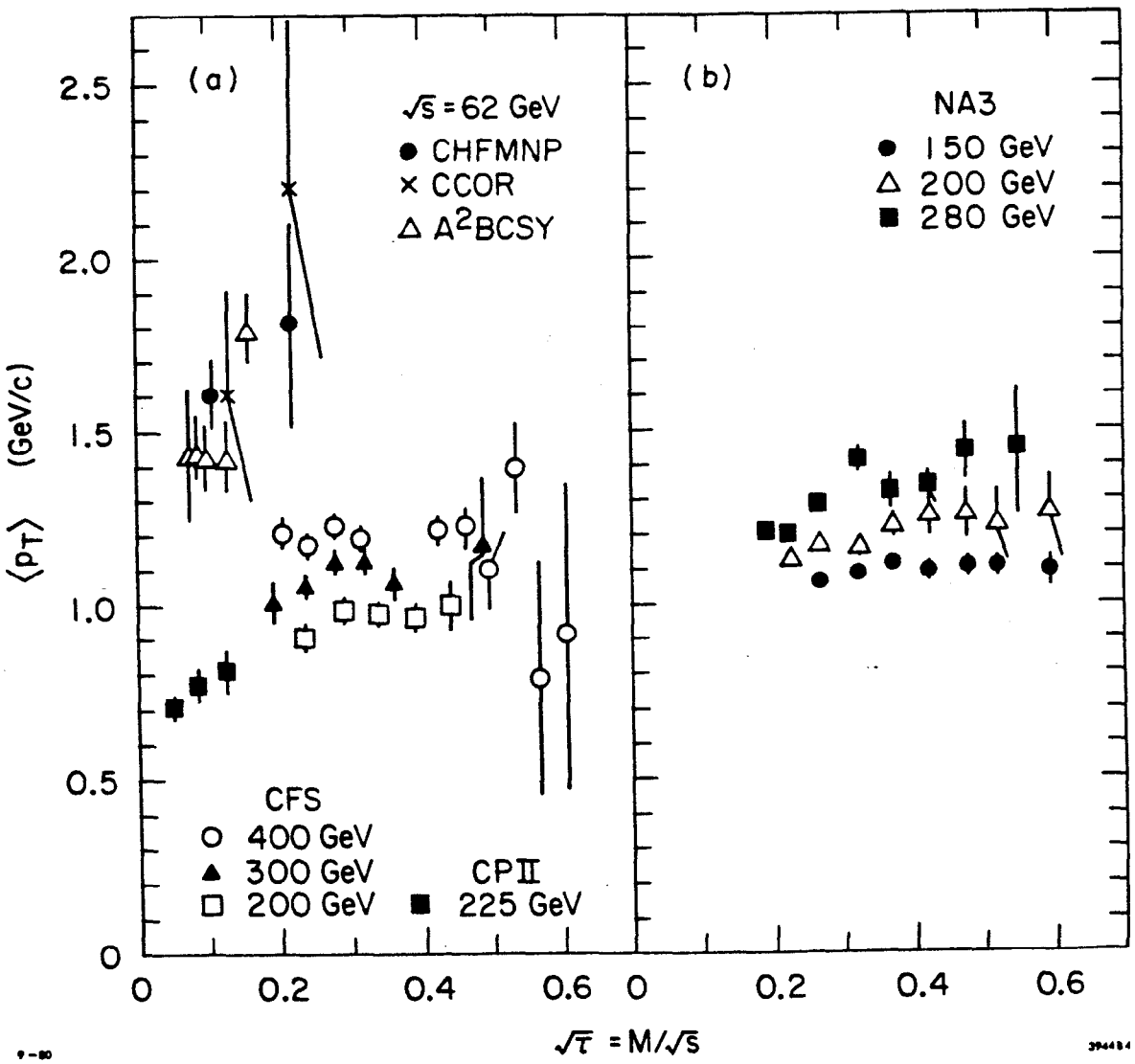

17. Average transverse momentum as function of $\sqrt{\tau}$ for dileptons produced in a) proton, b) pion interactions.

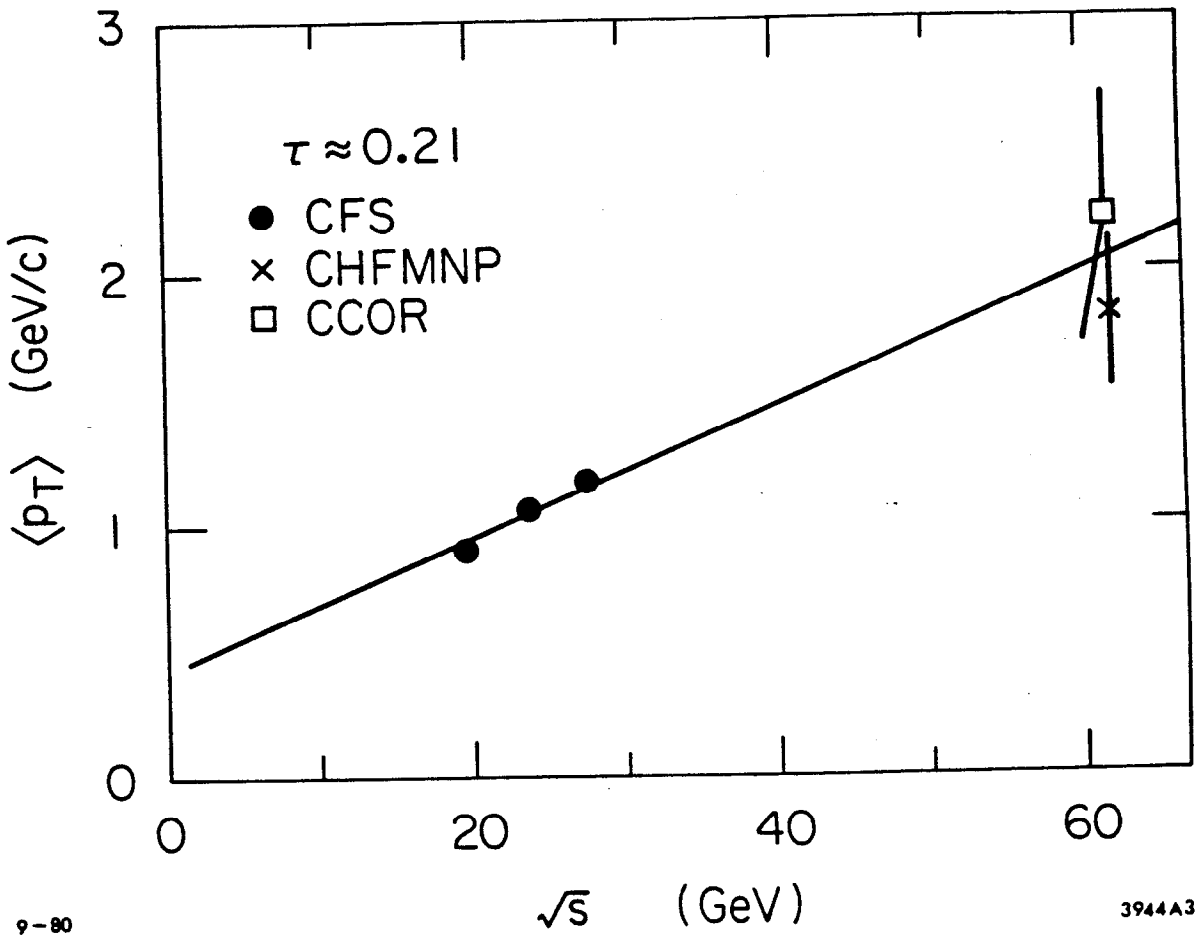

18. Energy dependence of the average transverse momentum.

performed by the NA3 Collaboration[42] resulted in the parametrisation similar to that for the proton case:

$$< p_T >_{\pi N} = (0.49 \pm 0.08) + (0.034 \pm 0.004)\sqrt{s} \quad .$$

At the same incoming momentum values of $< p_T >$ for the pion induced lepton pairs are, however, systematically higher than those for the proton produced dimuons. The Birmingham-CERN-Ecole Polytechnique group at the Omega spectrometer reported also strong x dependence of the $< p_T^2 >$ for the high mass muon pairs (fig. 19). Although for very high masses the effect may partly reflect the approach to the kinematic boundary, it persists for all masses. Also plotted on the fig. 19 are the measurements for the proton induced dimuons which do not show any significant x dependence.

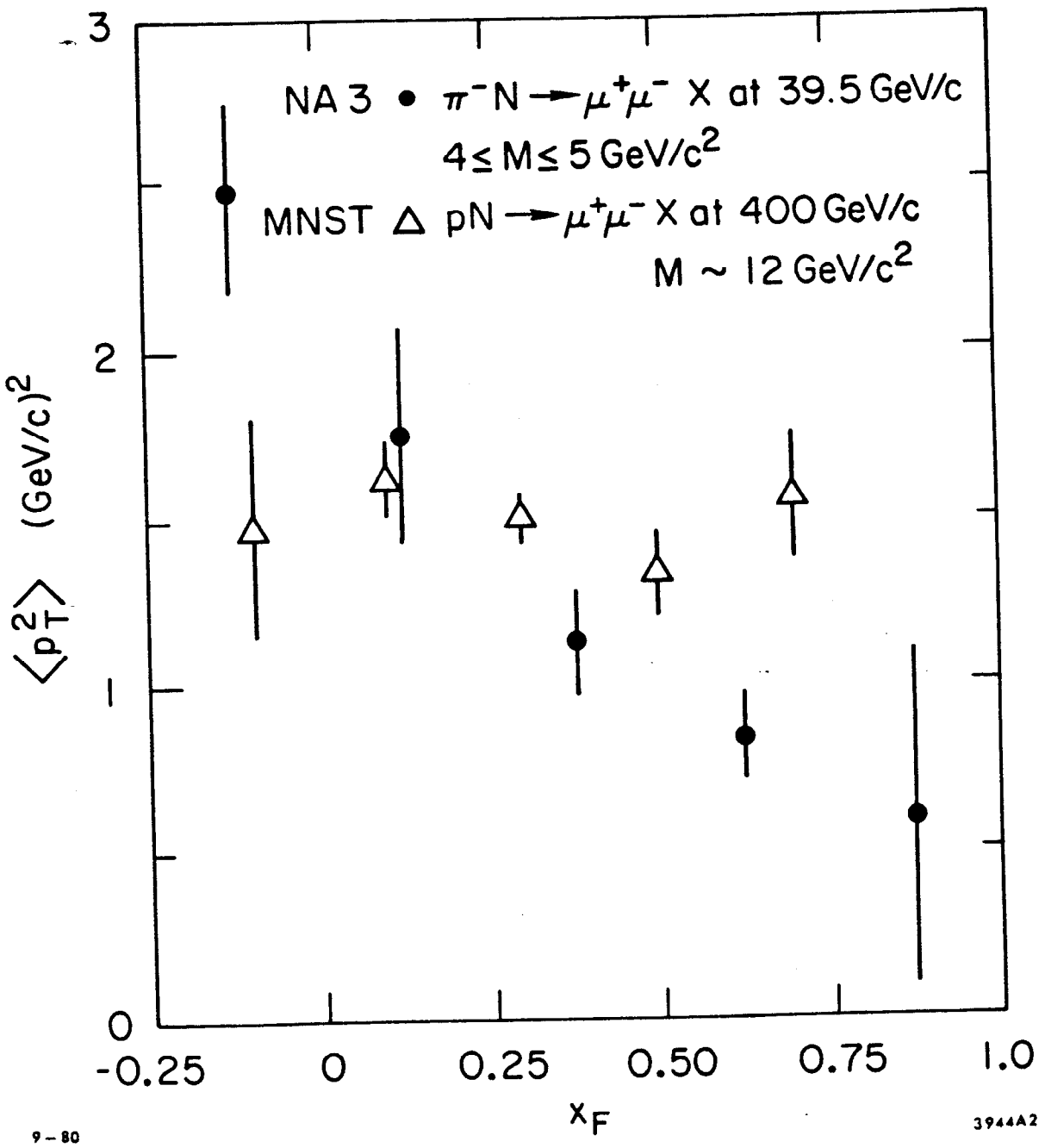

19. Average transverse momentum squared as function of x_F.

3.5 Longitudinal Momentum Distributions

In fig. 20 are presented the x_F distributions of dimuons measured by the Chicago-Illinois-Princeton Collaboration[45]. The data are parametrized as:

$$E \frac{d\sigma}{dx_F} = A (1 - x_F)^{\beta}$$

with the parameter β fitted in the range $0.2 \leq x_F \leq 1.0$. There are two obvious observations to be made:

i) the value of β is much smaller for the pion data than for the proton induced results, and

ii) there is a strong decrease of the value of β with increasing mass of the lepton pair.

Similar behavior was also seen in other experiments[41,52]. In the Drell-Yan picture both of these observations reflect the fact that the x distribution of the annihilating valence quarks in the pion is harder than that of the quarks in the proton.

In the case of the pN reactions, the asymmetry of the quark content of the beam and target systems may introduce small asymmetry around $x_F = 0$. For example, the isoscalar nuclear targets have equal number of protons and neutrons i.e., equal number of up and down quarks, while the incoming proton has two up and only one down valence quark. The weights given by the squares of the corresponding quark charges in the formula (10) introduce the asymmetry in the longitudinal momentum distribution. This effect has been indeeed observed in several experiments[40,45,50] (see e.g. fig. 21).

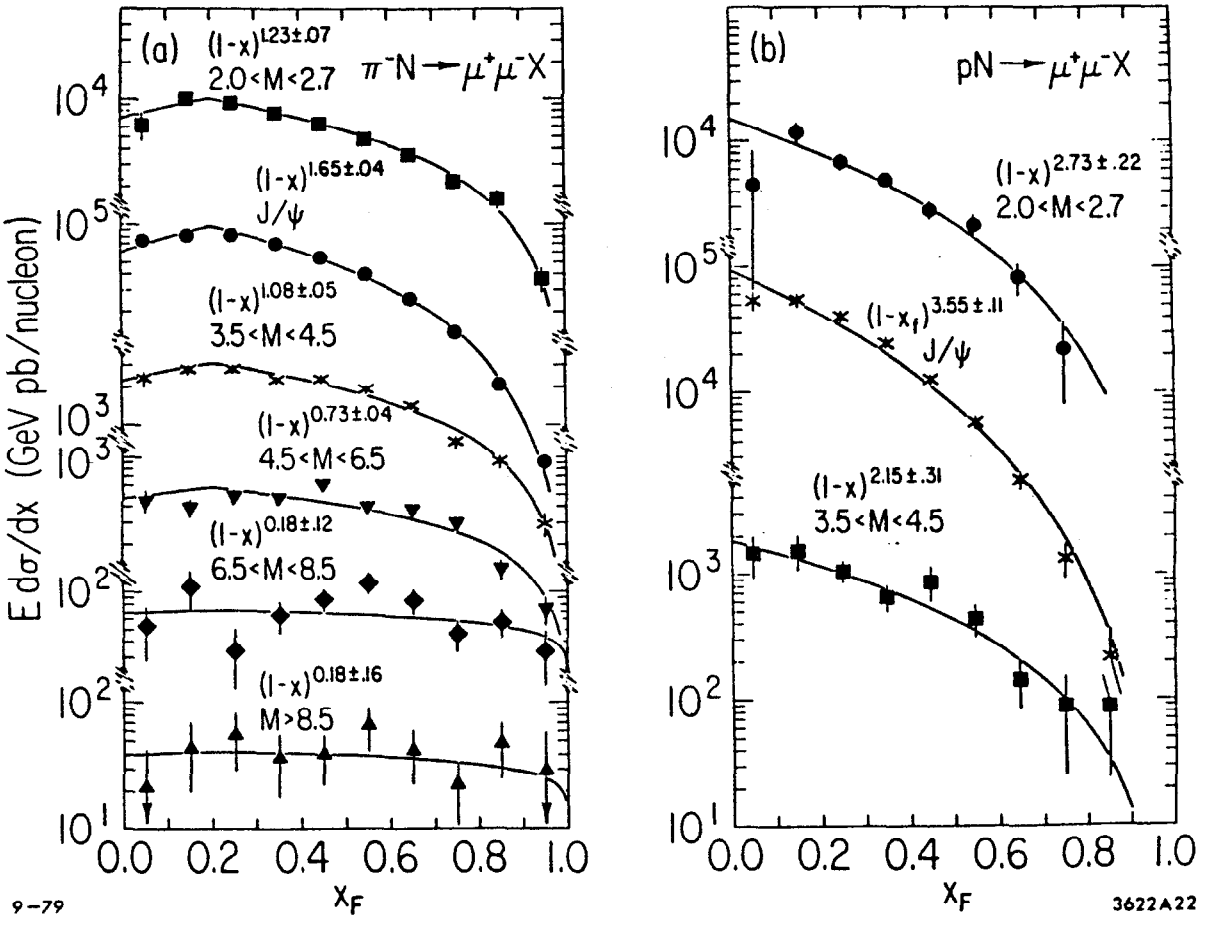

20. Invariant x_F distributions as function of the dimuon mass produced by: a) pions and b) protons.

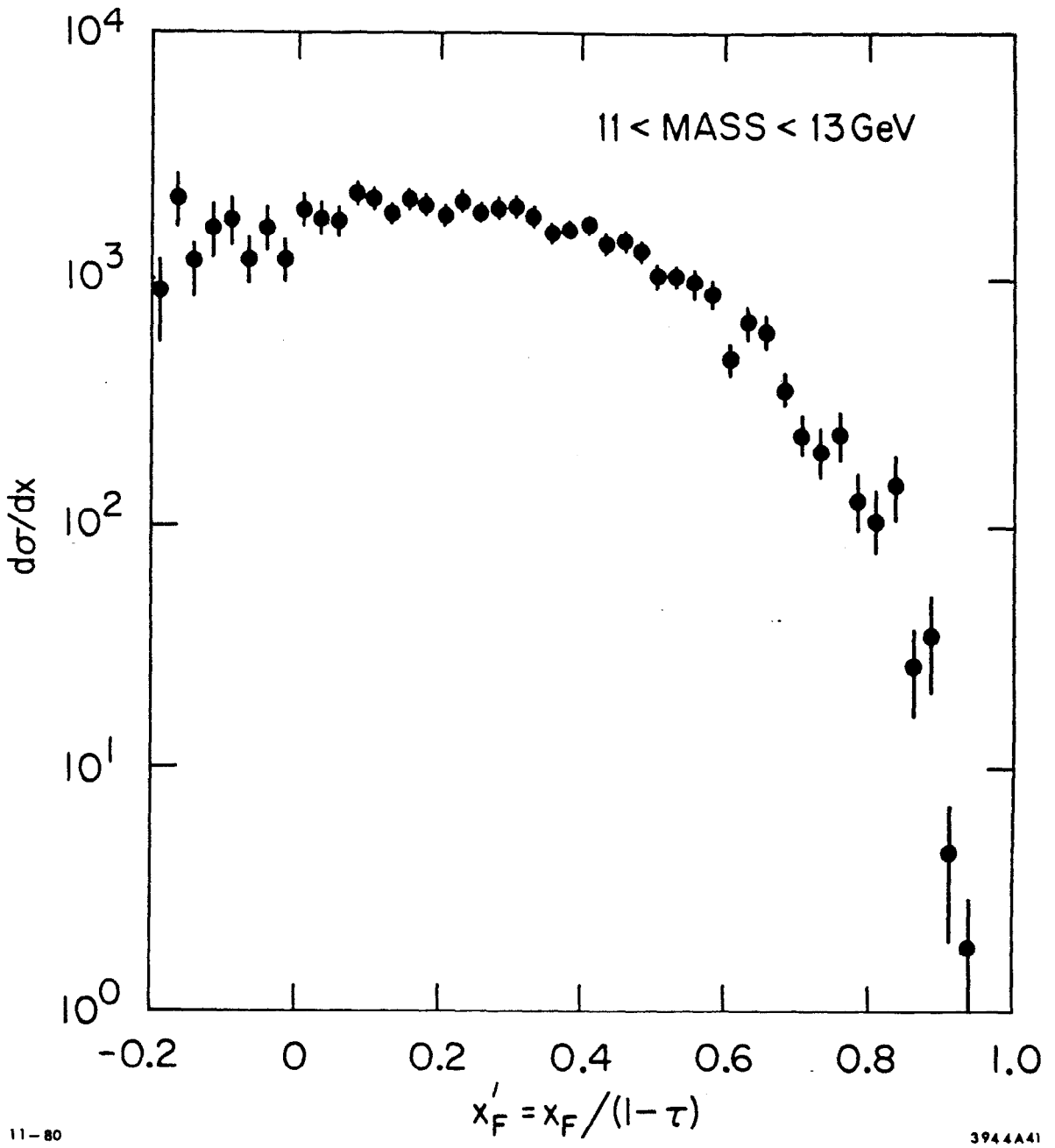

21. The cross section dependence of $x_F' = x_F/(1-\tau)$ for the $\mu^+\mu^-$ pairs produced by the 400 GeV/c protons on tungsten target[50].

4. The Drell-Yan Process in QCD

4.1 Perturbative Approach

The leading candidate for the theory of strong interactions is at present Quantum Chromodynamics (QCD) - a gauge field theory of interacting coloured quarks and gluons analogous in many respects to Quantum Electrodynamics. QCD has a peculiar property following from its renormalization group properties that the effective coupling constant at some momentum scale Q^2 decreases i.e.,

$\alpha_s(Q^2) \to 0$ as $Q^2 \to \infty$:

$$\alpha_s(Q^2) = \frac{12\pi}{(33 - 2n_f)\ \ln Q^2/\Lambda^2} \left[1 - O(1/\ln Q^2)^2 - \ldots\right] , \qquad (20)$$

where n_f is the number of flavours and Λ is a scale constant. This property, called an assymptotic freedom, allows for the perturbative approach to the QCD calculations at sufficiently large Q^2 values where α_s is small. In the Drell-Yan process Q^2 is usually identified with M^2, the mass squared of the virtual photon.

In the phenomenological QCD calculations in addition to basic parton model diagrams, like that of fig. 1, each order of perturbative approach introduces diagrams with emission of gluons. The first order diagrams in the strong coupling constant for the Drell-Yan process are shown in fig. 22. In the analogy to Quantum Electrodynamics they represent the "Compton" and "Annihilation" process respectively.

The subprocess variables, defined in fig. 22, are related to the overall c.m. variables through the following set of relations:

$$\begin{aligned} \hat{s} &= x_1 x_2 s \\ \hat{t} &= x_1 t + (1 - x_1)M^2 \\ \hat{u} &= x_2 u + (1 - x_2)M^2 \end{aligned} \qquad (21)$$

Here again the transverse momentum of the quarks and the masses involved had been neglected. Both the "Compton" and "Annihilation" cross sections had been calculated

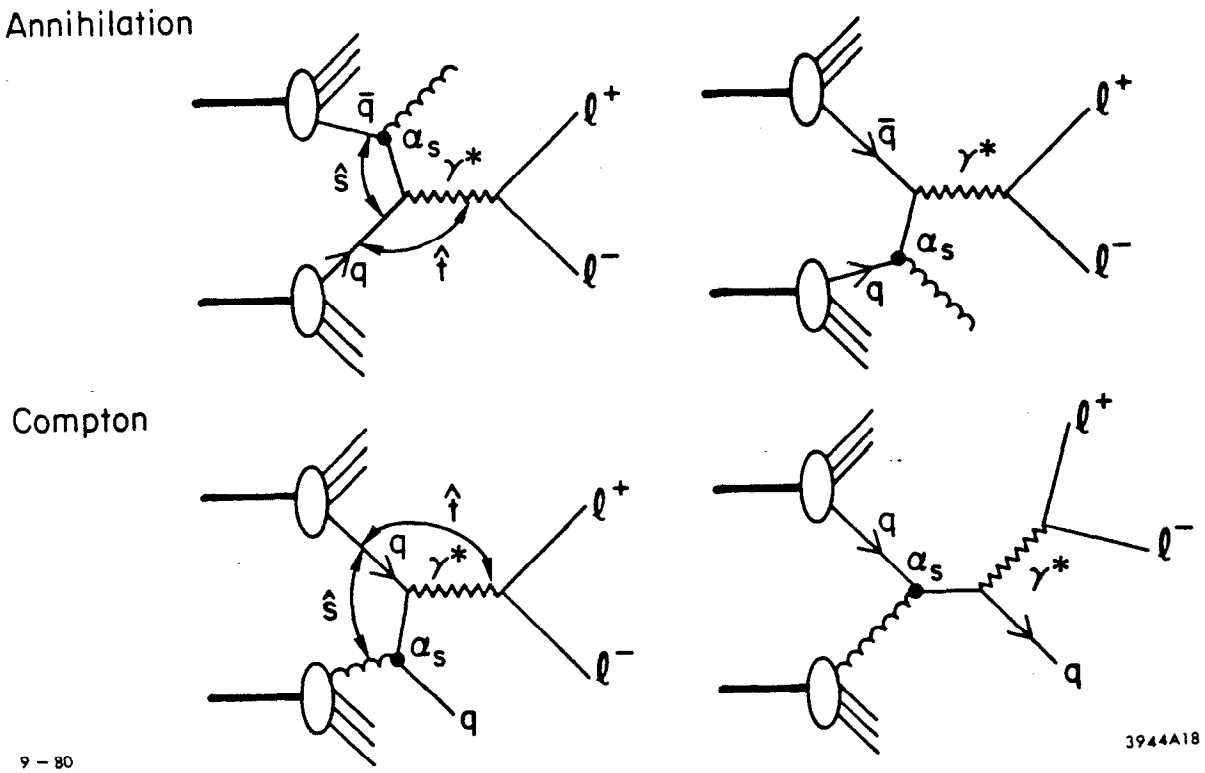

22. First order in α_s QCD diagrams contributing to the Drell-Yan process.

in the field of theory [71,74] and expressed in terms of the subprocess variables:

$$\frac{d^2\hat{\sigma}}{dM^2 d\hat{t}}\ (\text{Annihilation}) = \frac{8}{27}\,\alpha^2\alpha_s e_i^2\,\frac{2M^2\hat{s} + \hat{u}^2 + \hat{t}^2}{\hat{s}^2\hat{t}\hat{u}} \tag{22}$$

$$\frac{d^2\hat{\sigma}}{dM^2 d\hat{t}}\ (\text{Compton}) = \frac{1}{9}\,\alpha^2\alpha_s e_i^2\,\frac{2M^2\hat{u} + \hat{s}^2 + \hat{t}^2}{-\hat{s}^3\hat{u}} \tag{23}$$

The above cross sections are divergent for small values of $\hat{t}$ and $\hat{u}$, i.e., for the collinear emission of gluons and thus impossible to integrate over the internal subprocess variables. The problem is circumvented in practical calculations by the procedure proposed by Politzer [75] and Sachrajda [76] who found that in the leading log Q^2 approximation these divergencies can be factored out and absorbed into the incoming particle wave function. These procedure, called the factorisation theorem, has been later generalised [77] to all logs in perturbation theory. As the result the structure functions of the parent particles become Q^2 dependent (as illustrated in fig. 23) but again are expected to have the same pattern of scaling violations as those measured e.g. in deep inelastic lepton scattering. The parton model form of the resulting cross section is then replaced by

$$\frac{d\sigma}{dM^2} = \frac{4\pi\alpha^2}{9M^4}\ F(\tau, Q^2) \quad , \tag{24}$$

where function $F(\tau,Q^2)$ no longer scales.

$$F(\tau, Q^2) = \sum_i e_i^2 \int dx_1\, dx_2\, x_1 x_2\, \delta(\tau - x_1 x_2) * \\ * \left[G_{q_{i/A}}(x_1, Q^2)\ G_{\bar{q}_{i/B}}(x_2, Q^2) + (q_i \longleftrightarrow \bar{q}_i) \right] \quad . \tag{25}$$

Here again the summation goes over all quark flavors.

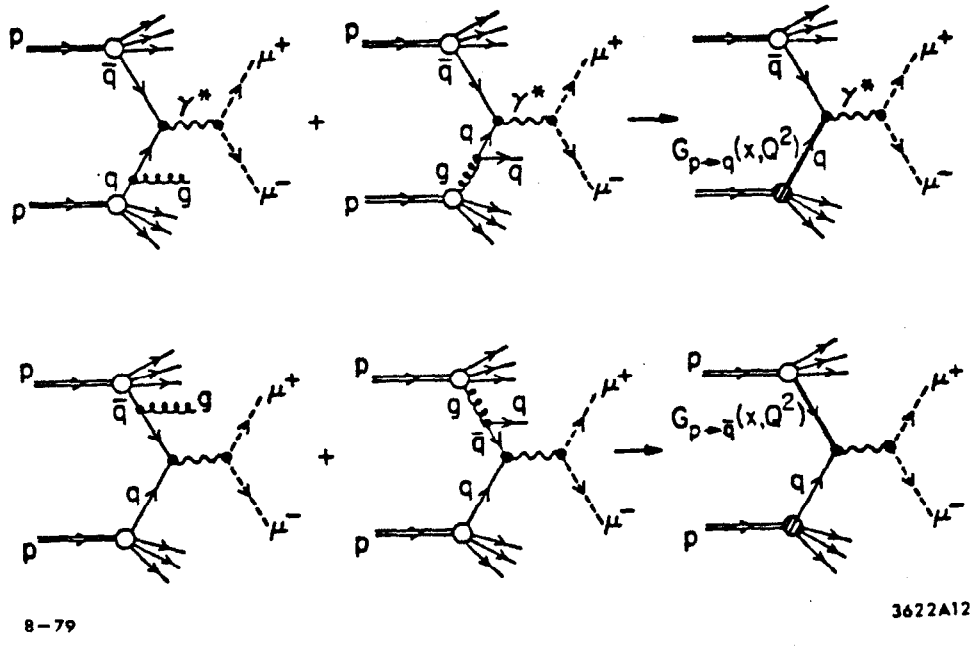

23. Illustration of the diagrams contributing to the "renormalization group improved" quark and antiquark distributions.

The approach described above has encountered several theoretical problems[78-80]:

1) There are also more complicated diagrams (e.g., "higher twists") which may contribute to the process and may also have similar divergencies in their cross section formulae. It is so far not proven that these divergencies may be treated in the same way as in the case of first order diagrams.

2) In order to fulfill the premise of the parton model that the quark structure functions should be the same in all processes, the time-like $Q^2 = M^2 > 0$ for the Drell-Yan process has to be identified with the space-like $Q^2 < 0$ in the deep inelastic lepton scattering

$$Q^2_{DY} = |Q^2_{DIS}|$$

This does create problems in calculating higher order corrections, where the non-leading terms, neglected in the first approximation, appear to have large contributions to the cross section. The large values of the contributions from second order terms have raised doubts whether the perturbative series is convergent. The hope is that only first few terms are important.

3) The identification of the large dimensional variable defining the scale of the calculations is usually $Q^2 = M^2$. However, in certain kinematical regions more than one variable may be large. This happens, for example, for the production of large mass pairs at large transverse momentum. The proper choice of the variable is in such case unclear.

Despite those theoretical problems, the procedure is remarkably simple and has been applied by many authors[81] to the phenomenology of the lepton

pair production. The calculations require as an input the individual quark structure functions, which have to be extracted from the deep inelastic lepton scattering data. Extra care has to be taken to account for the radiative corrections which are different in various processes. It is also important to keep in mind the fact that most of the quark structure functions are measured in the lepton scattering experiments in a small range of Q^2 well approximated by a constant value, while the dilepton data usually span rather large range of masses. Possible scaling violations may, therefore, introduce distortions of the calculated distributions. The effect of such first order scaling violation may be eliminated by following the standard prescription[82] of how to "evolve" the quark and gluon distributions from the measured to desired values of Q^2.

Although the nucleon structure function $\nu W2$ is quite well measured, its decomposition into the quark distributions is, so far, not very well known. Nevertheless, the application of the above procedure to the lepton pair mass spectra and their longitudinal distributions seems to provide an adequate description of the data, thus reproducing the success of the parton model. The transverse momentum distributions require, however, more complicated approach.

4.2 QCD Corrections to the Drell-Yan Process

There are several sources of the $O(\alpha_s)$ corrections which introduce the renormalisation[83-89] of the basic cross section formulae (24) and (25). Vertex corrections and soft gluon emission analogous to those discussed in previous section introduce large multiplicative factor of

$$1 + (\alpha_s/2\pi)(4/3)(1 + 4\pi^2/3) \quad . \tag{26}$$

This radiative correction is of comparable size to the contribution of the lowest order diagrams mainly due to the $\alpha\pi^2$ term originating from the continuation from the space-like to time-like Q^2. Such continuation is necessary when comparing deep inelastic scattering and the Drell-Yan process. For $\alpha \approx 0.33$ this correction factor is equal to ~ 2 thus rasing doubts whether higher order radiative corrections (so far uncalculated) can be neglected. The comparison with experimental data, discussed in the next section, indicates that the difference between the lower order calculations and the measurements is of the order of $2 \div 2.5$ i.e., of the size of the radiative correction factor (26). It provides, therefore, hope that higher order corrections will be small.

In addition to the radiative corrections also some other terms have already been calculated. The size of the contributions from the hard gluon bremsstrahlung diagrams was found[83,86] to depend on Q^2 and on the structure functions of quarks and gluons inside the colliding particles. In general they are small but in certain kinematic regions, they may have magnitude comparable to that of the lowest order terms.

Another type of the QCD corrections discussed extensively in the

literature are the so called "higher twist" diagrams[90]. These are corrections of the order of $0(m^2/Q^2)$ to the leading order calculations which take into account some of the possible correlations among the partons inside the incoming particles. They have been found to be possibly important[91] for the discussion of scaling violations in deep inelastic scattering processes. The "higher twist" diagrams for lepton pair production in πp collisions shown in fig. 24 may be important in estimating the quark structure functions near $x = 1$.

The overall cross section for the Drell-Yan process in perturbative QCD may be therefore written as:

$$\frac{d\sigma}{dM^2} = \frac{4\pi\alpha^2}{9M^4} F(\tau,Q^2)\left[1 + (\alpha_s/2\pi)(4/3)(1+4\pi^2/3)\right] +$$
$$+ \text{"}0(\alpha_s)\text{ hard gluon bremsstrahlung corrections"} + \qquad (27)$$
$$+ 0\ (\alpha_s)^2 + \ldots + \text{"higher twists"} + \ldots$$

In addition to all the perturbative terms mentioned above there are indications that also the non-perturbative effects due e.g. to confinement are needed for the description of the data. These are usually characterised as the "primordial" k_T--the transverse momentum of partons inside the parent hadrons--and will be discussed in more detail in chapter 5.3.

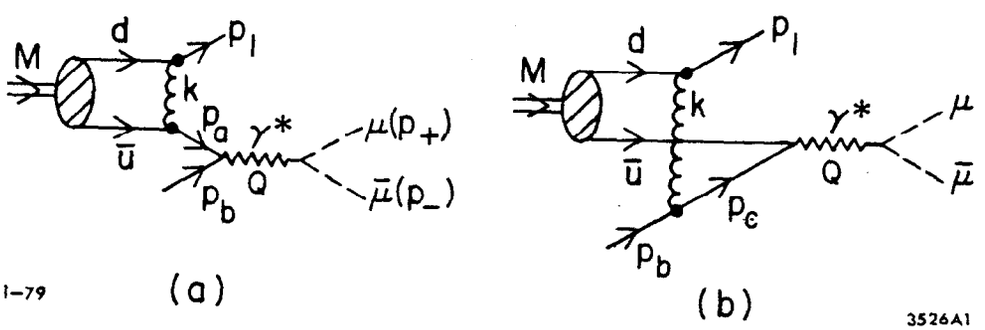

24. Diagrams for $Mq \to q\,\gamma^*$ used in calculations of higher twists by Berger and Brodsky (ref. 90).

5. QCD Phenomenology of the Dilepton Data

5.1 Scaling violations

As has been shown in sect. 3.3, the mass spectra of the lepton pairs show scaling within approximately 20% precision of the data. On the other hand, scaling violations seen[80] in deep inelastic scattering experiments indicate that also $M^3\, d\sigma/dM$ distributions of the dileptons should not scale. The two above statements are not necessarily in contradiction with each other. In case of proton interactions most of the experiments are performed at rapidity of the lepton pair y close to zero. The general form (24) may be differentiated with respect to rapidity to give:

$$s\frac{d^2\sigma}{d\sqrt{\tau}dy} = \frac{8\pi\alpha^2}{9\tau 3/2}\sum_i e_i^2\, G_{q_{i/A}}(x_1,M^2)\, G_{\bar{q}_{i/B}}(x_2,M^2) + (q_i \longleftrightarrow \bar{q}_i) \qquad (28)$$

At $y \approx 0$ the x_1 and x_2 values of the annihilating quarks are approximately equal to $\sqrt{\tau}$ (see eq. 5b). The pattern of the scale breaking of mass distribution should follow, therefore, that of the quark structure functions when substituting $\sqrt{\tau}$ for x. In deep inelastic scattering one observes[93] no scaling violations for $x \approx 0.2$, strong increase of the structure function with increasing energy for $x < 0.2$ and less dramatic decrease for $x > 0.2$. The data of fig. 12 agree with such behaviour.

The effect is better explained in Fig. 25 where the CFS Collaboration presented[40] the calculations of their cross sections for three different proton beam energies using the QCD parametrisation of nucleon structure function by Owens and Reya[94]. In the region covered by the CFS measurements, i.e. $0.15 < \sqrt{\tau} < 0.45$, the predicted QCD scale breaking is smaller than

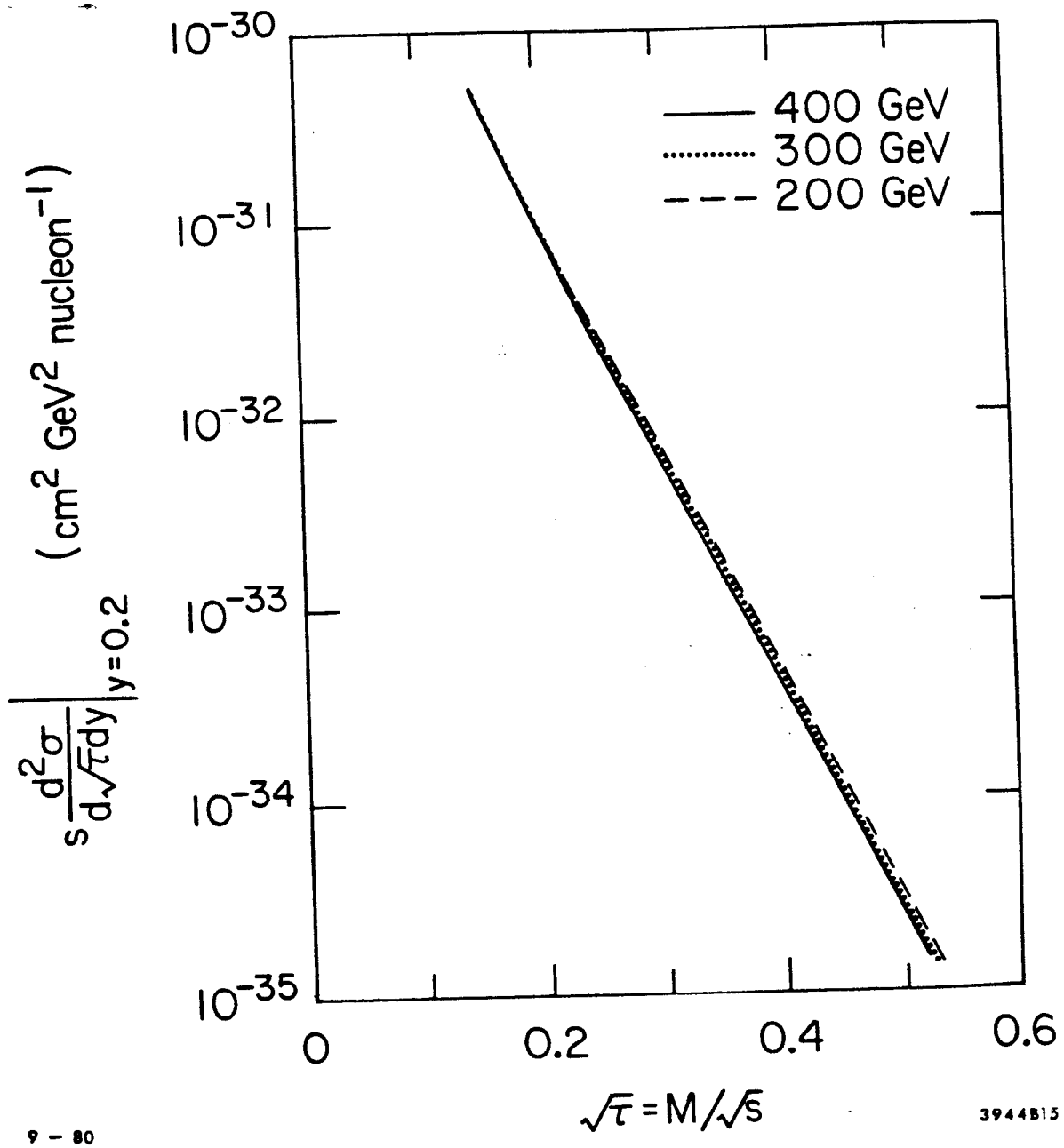

25. Cross section versus $\sqrt{\tau}$ at three different beam energies computed following a QCD calculation by Owens and Reya.

the uncertainty of the data. Unfortunately, the range of $\sqrt{\tau}$ values where scaling violations are expected to be strong is not yet covered by experiments spanning sufficient energy range. Similar comments apply also to the case of pion induced muon pair production.

5.2 Angular Distributions

In the simple quark parton model the two annihilating quarks travelling along the polar axis result, in the rest frame of the virtual photon, in the angular distribution of the form:

$$W(\theta^*) = 1 + \cos^2\theta^* \qquad (29)$$

There are several ways of defining the axes in the rest frame of the lepton pair. The usual choice is the Gottfried-Jackson frame, where θ^* is the angle between the beam and one of the leptons. This reference frame is well suited for testing of the Drell-Yan process when the direction of the quarks coincide with the direction of the beam. The transverse momentum of quarks inside the parent hadrons may, however, introduce additional smearing effects to the angular distributions, as the direction of the beam and of the annihilating quarks will no longer overlap. To deal with this problem Collins and Soper[95] have proposed a reference frame in which the z axis bisects the angle between the beam and reverse target momentum directions in the lepton rest system. Experimentally, the Collins-Soper frame is found to be very close to the Gottfried-Jackson reference system. In the π^-N interactions at 225 GeV/c the average angular difference between the two z axes was estimated[45] to be about 14^o.

The non-zero mass of the outgoing leptons introduces small corrections[10, 96] to the formula (29) due to the spin averaging and two-body decay phase space.

$$\left(1 - \frac{4m^2}{Q^2}\right)\left[\left(1 + \frac{4m^2}{Q^2}\right) + \left(1 - \frac{4m^2}{Q^2}\right)\cos^2\theta^*\right] , \qquad (30)$$

where m is the mass of the lepton and Q is the mass of the virtual photon.

The correction is negligible for the outgoing electrons and muons but may play an important role in the study of e.g., heavy leptons τ.

The general form of the angular distribution for the decay of the virtual photon into a lepton pair may be written[97] as:

$$W(\theta^*,\phi) = \frac{3}{8\pi}\left[\rho_{11}(1+\cos^2\theta^*) + (1-2\rho_{11})\sin^2\theta^* + \rho_{1-1}\sin^2\theta^*\cos 2\phi + 2\mathrm{Re}\rho_{10}\sin 2\theta^*\cos\phi\right], \quad (31)$$

where the density matrix elements ρ_{ij} depend on the choice of the reference frame and all the variables describing the virtual photon, i.e., Q^2, x_F, p_T, s. Integration over either polar or azimuthal angle gives:

$$W_1(\theta^*) \sim 1 + \alpha\cos^2\theta^* \quad (32)$$

$$W_2(\phi) \sim 1 + \beta\cos 2\phi \quad , \quad (33)$$

where both α and β may vary between -1 and +1.

Experimentally, the polar distributions of the lepton pairs were measured by various groups[41,45] and found to be well described by the formula (32) with the parameter α compatible with $a \approx 1$ (see fig. 26). So far, however, there is no information available for the azimuthal distributions.

The Quantum Chromodynamics calculations predict significant deviations from the purely transverse polarisation of the virtual photon, i.e., $\alpha < 1$. Two possible origins of these deviations have been discussed recently in the literature.

1. First order in α_s "Compton" subprocesses (fig. 22) in which a quark interacts with a spin 1 gluon, were shown to lead to a $\sin^2\theta^*$

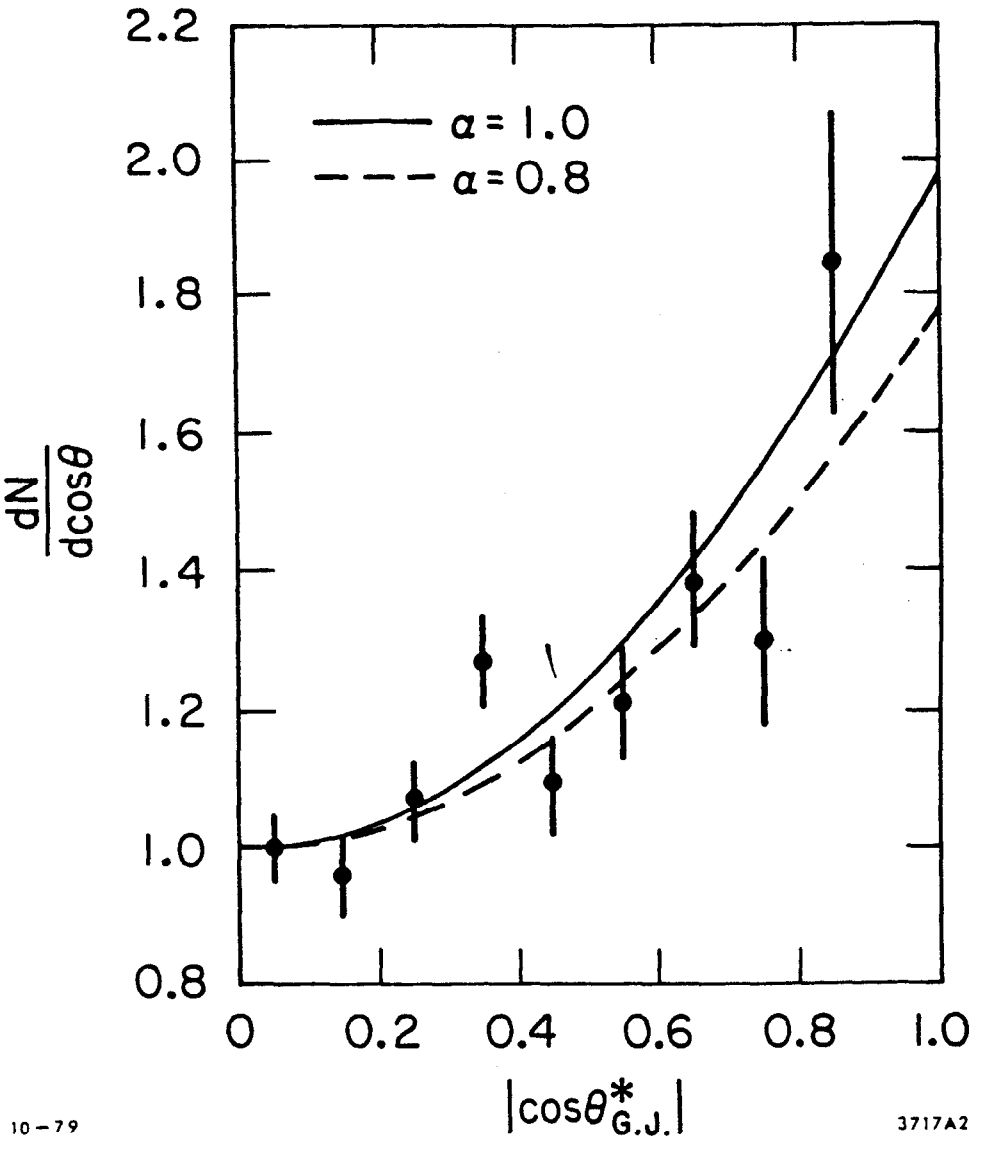

26. Distribution of cos θ^* for $\pi^- N \to \mu^+\mu^- X$ at 200 GeV/c with $4 < M < 6$ GeV and $p_T < 1$ GeV/c. The two curves correspond to the formula (32) description of the data.

behavior at large p_T of the lepton pair. A non-trivial azimuthal dependence is also expected, and the parameter β in the formula (33) is related[98] to α through:

$$\beta = \frac{1 - \alpha}{2(3+2\alpha)} \qquad (34)$$

The variation of α and β as function of x_F of the lepton pair is shown in fig. 27.

2. Another source was pointed out by Berger and Brodsky[90] who calculated the "higher twist" terms of fig. 24. These higher order effects result in the decay angular distribution varying strongly with Q^2 and x_F of the virtual photon:

$$d\sigma \sim (1-x)^2(1+\cos^2\theta^*) + \frac{4}{9}\,\frac{\langle k_T^2\rangle}{Q^2}\,\sin^2\theta^* + \frac{2}{3}\sqrt{\frac{4k_T^2}{Q^2}}\,(1-x)\sin^2\theta^*\cos\phi \ . \qquad (35)$$

At fixed mass the longitudinal polarization of the virtual photon increases as x approaches 1.

The theoretical work stimulated the experimentalists to study the angular distributions in more detail. The data of the Chicago-Illinois-Princeton collaboration[45] for the $\pi^- N \to \mu^+\mu^- X$ at 225 GeV/c are plotted in fig. 28 as function of x, of the annihilating valence quark of the pion. In each of the intervals the form (32) is a good representation of the data, but the parameter α shows strong x and p_T dependence plotted in fig. 29. Also shown in fig. 29 are the predictions due to the two QCD calculations described above. Though first order diagrams calculations predict some x dependence of the parameter α, they do not describe the available data in the region of x close to 1. This may be interpreted as the evidence that the "higher twist" effects contribute substantially to this kinematic region. The conclusive test of the "higher twists" crucially depends, however, on the observation of the

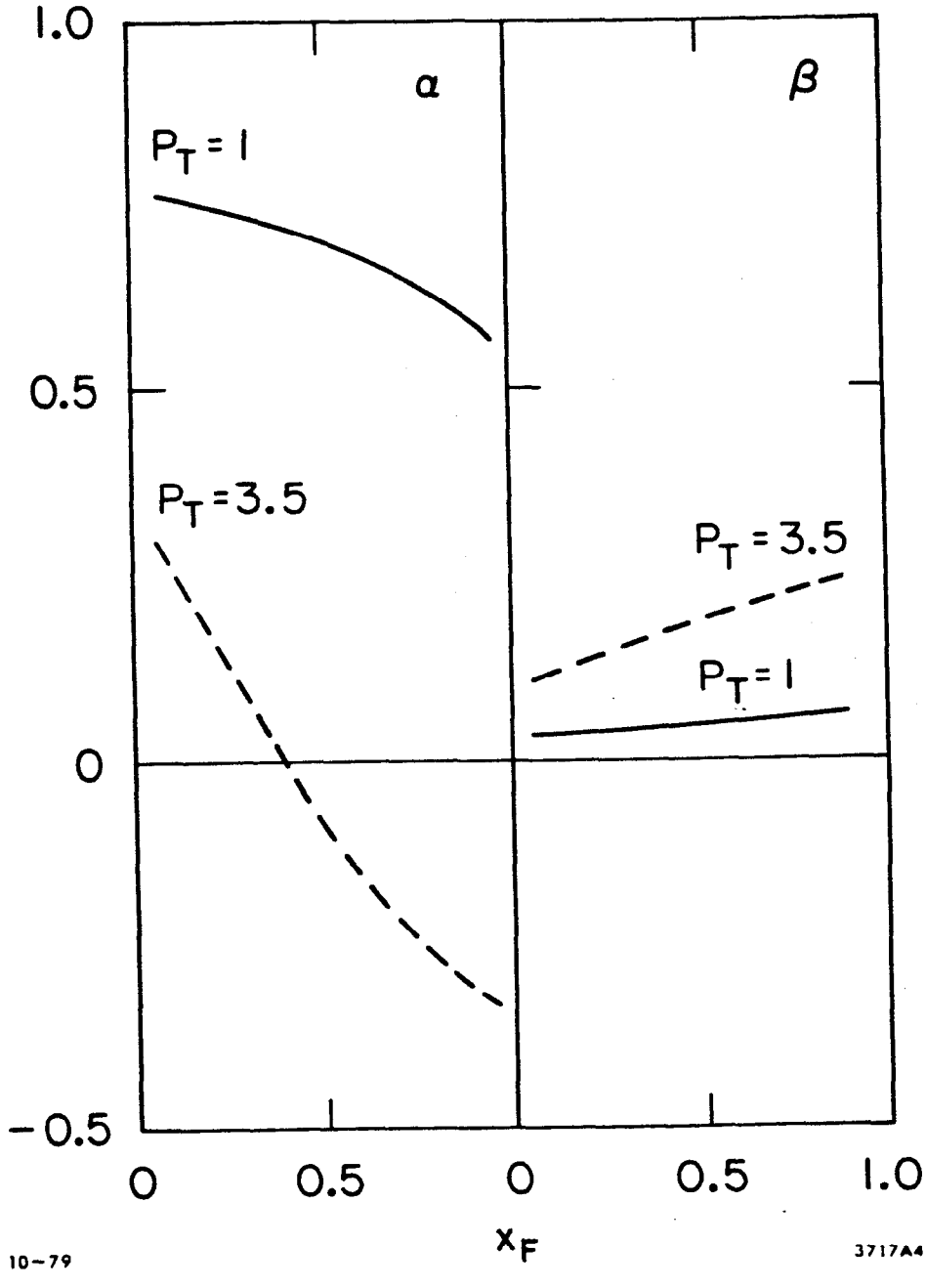

27. The Feynman x dependence of parameters α and β calculated in ref. (98).

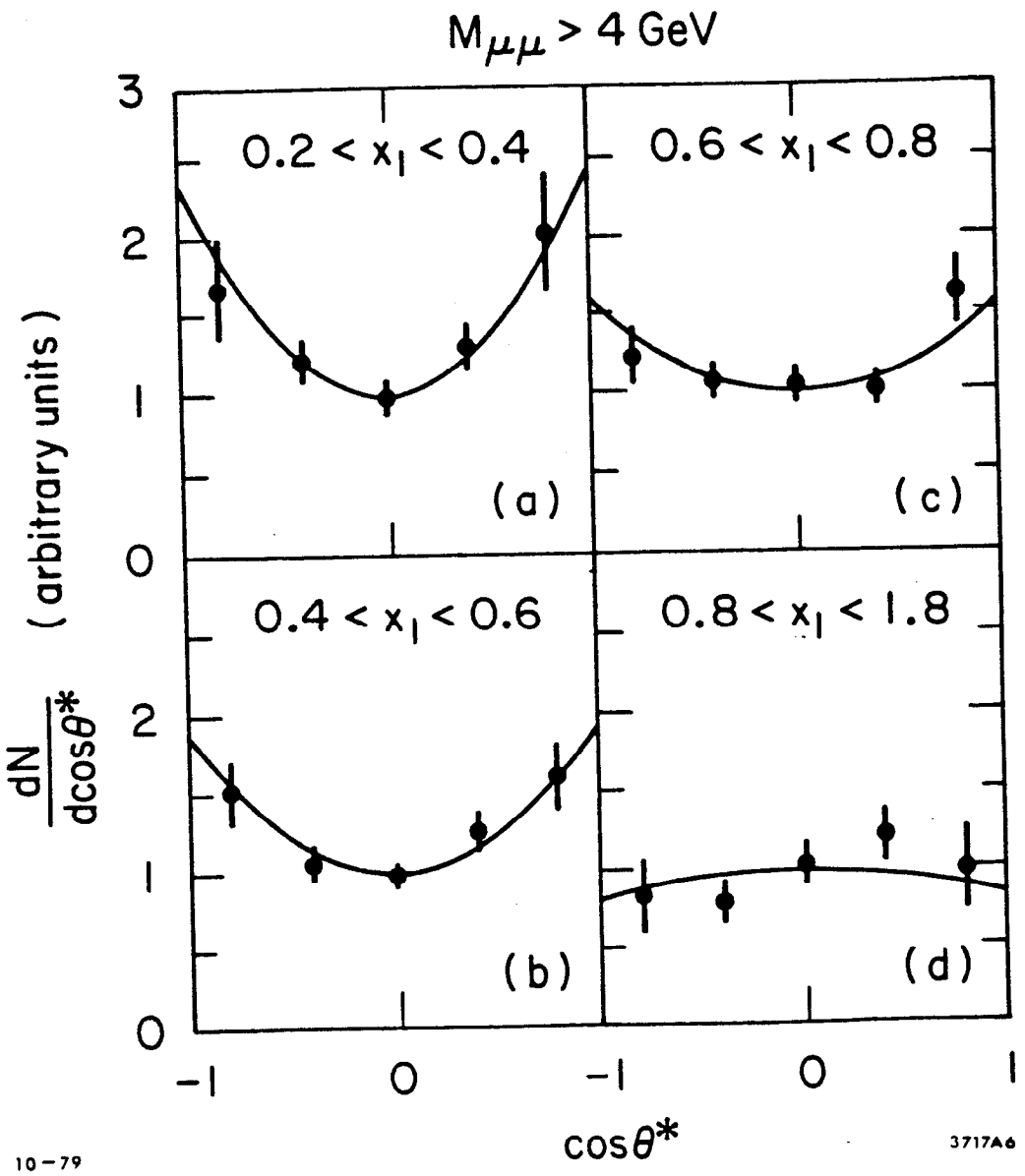

28. Angular distribution of dimuons for various intervals of the fractional momentum x of the pion antiquark.

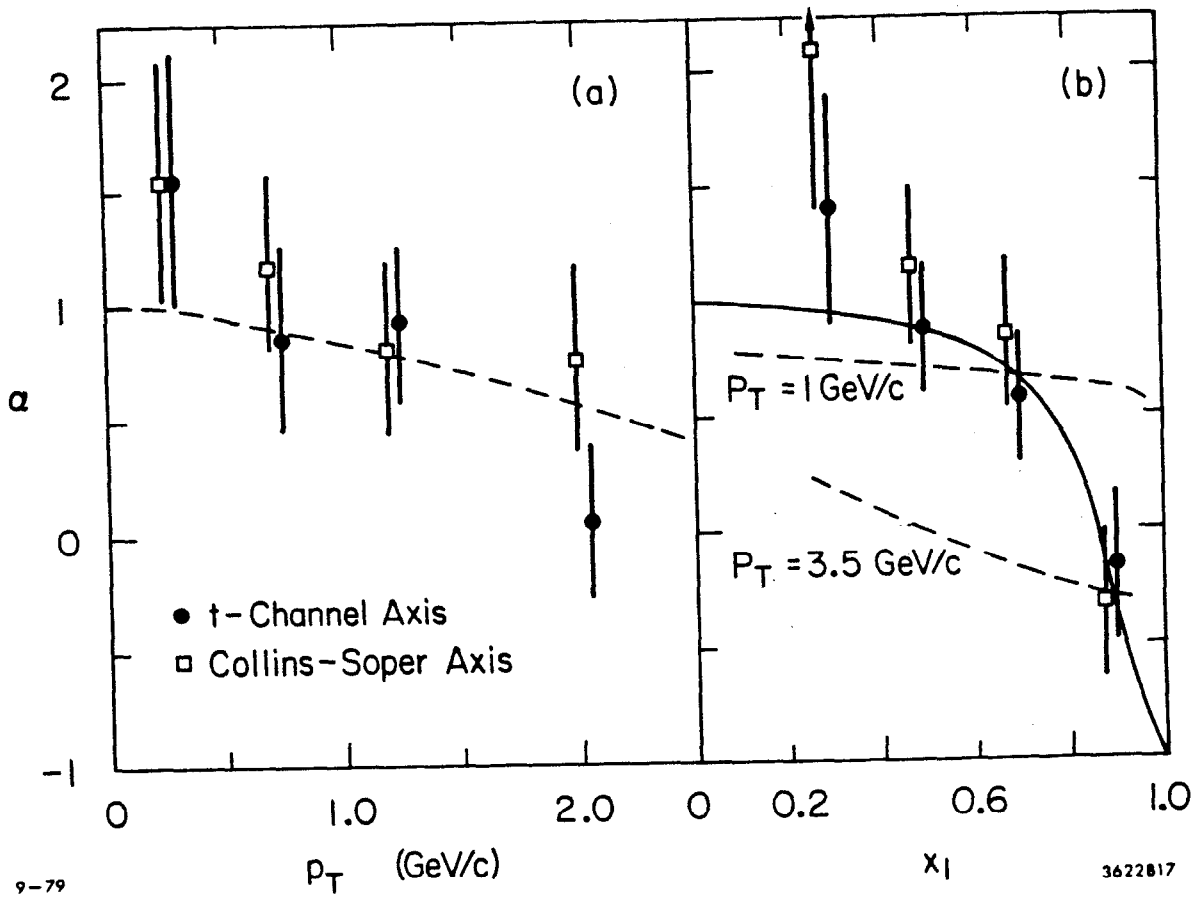

29. Dependence of the parameter α on: a) transverse momentum of dimuons, b) fractional momentum x of the pion antiquark. Data points are from the CIP Collaboration measurements of $\pi^- N \to \mu^+ \mu^- X$ at 225 GeV/c. The dashed lines are the prediction of first-order QCD "Compton" diagrams. Solid line is from the calculations of Berger and Brodsky.

$\frac{k_T}{Q^2}$ dependence of the formula (35). Such test, together with tests of other predicted[99] relations between various terms of the general expression (31) have to wait for higher statistics data.

It should also be noted that in the approximation taken by Berger and Brodsky one does not expect strong azimuthal dependence in the angular distributions integrated over θ^* ($\beta \approx 0$). Furthermore, the first order QCD diagrams contribute equally to the dimuons produced by the pion and proton beams, while the "higher twist" effects appear to be much reduced in the later case. Careful studies of both azimuthal and polar distributions may provide, therefore, a measurement of relative contribution of these two QCD effects.

5.3 Transverse Momentum Distributions in QCD

In the simple quark model for the Drell-Yan process the produced dileptons are expected to have very small transverse momentum. In the perturbative QCD the virtual photon acquires its transverse momentum through the emission or absorption of gluons. The first order in α_s diagrams of fig. 22 can be calculated according to formulae (22) and (23). Their contribution to the total p_T spectrum is shown[10] in fig. 30. In the region of small transverse momentum both "Annihilation" and "Compton" contributions diverge and one is forced to argue that other, e.g., non-perturbative phenomena, dominate there. Nevertheless, even above p_T = 1 GeV/c, the contribution of the first order diagrams is about factor of two smaller and has the curvature opposite to that of the data. This does not mean, however, that the QCD is necessarily failing to describe the Drell-Yan process. There are in the literature

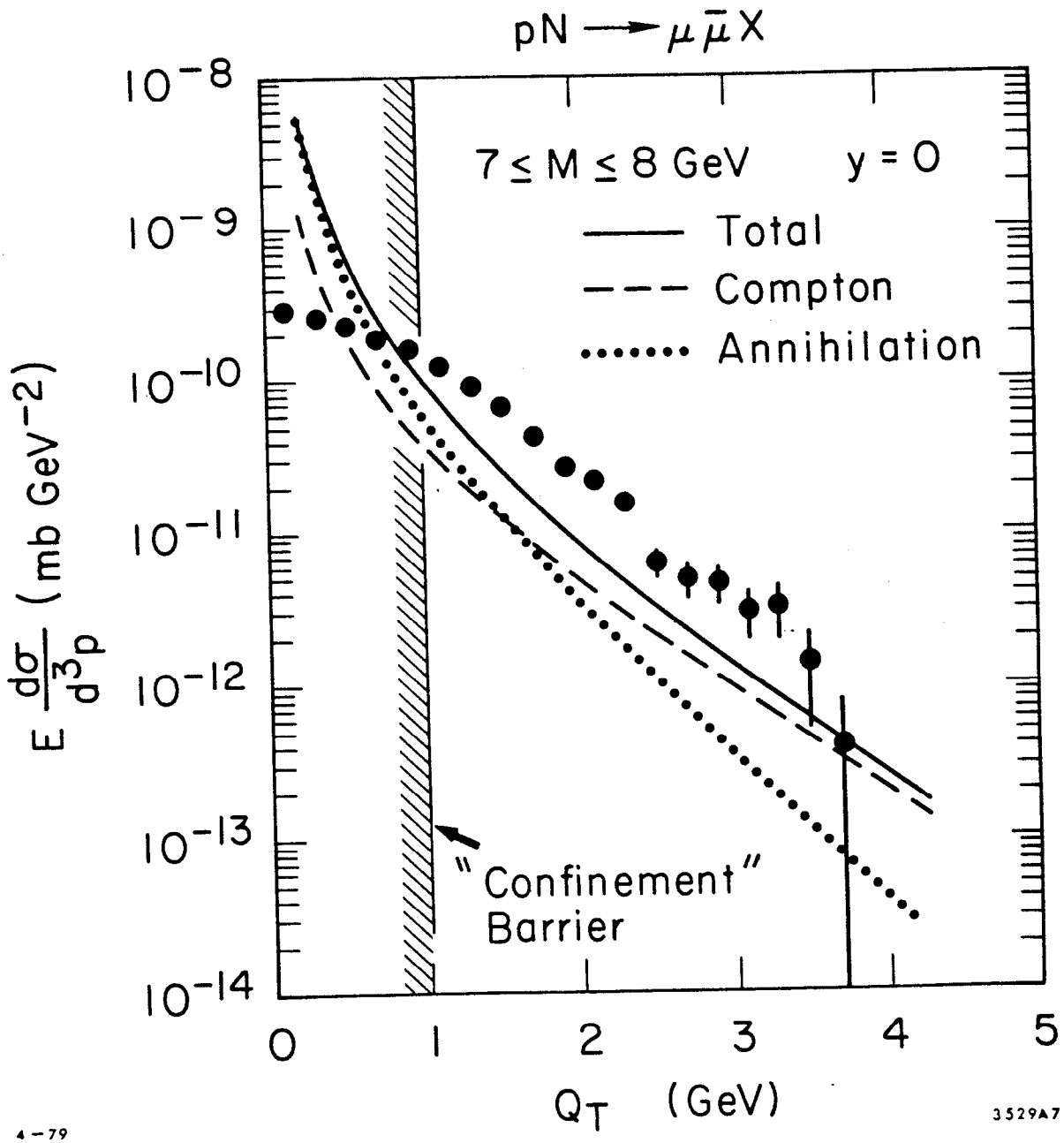

30. Comparison of the dimuon transverse momentum distribution measured by the CFS Collaboration with the cross section calculated from the first order QCD diagrams.

several ways of approaching this problem.

1. "Primordial" transverse momentum. It is proposed[92,100,101] that the intrinsic, non-perturbative, transverse momentum due to the quark confinement in the original hadron is, for some unspecified reason, large. The observed p_T of the lepton pair is then described by the incoherent sum of the primordial component and the contribution of the perturbative QCD. The confinement transverse momentum is in such approach parametrised usually as Gaussian with the average k_T varying from 0.6 to 1.5 GeV/c, depending on the analysis. The calculations fit the data[71,72,100] but require large values of $\langle k_T \rangle$. It should be stressed here, that most of the phenomenological analyses performed so far have used the leading logarithm approximation in their analysis of the data. It may be, that the large values of primordial k_T necessary for the description of the measurements are reflecting the fact that the non-leading terms and higher order effects have been usually neglected. Such possibility have been illustrated by recent calculations of Parisi and Petronzio[102] who have discussed the process of multiple gluon emission in Drell-Yan collisions. They argued that multiple bremsstrahlung of gluons may result in the lepton pairs with low transverse momentum since the k_T acquired at each individual gluon emission will cancel out in the stochastic sum. At the same time the effect of primordial k_T is washed out. The phenomenological application of such calculations, shown in fig. 31, succesfully describe the data of both CFS and CHFMNP Collaborations[103] with the value of the average intrinsic transverse momentum somewhat smaller than in the leading logarithm type of analyses.

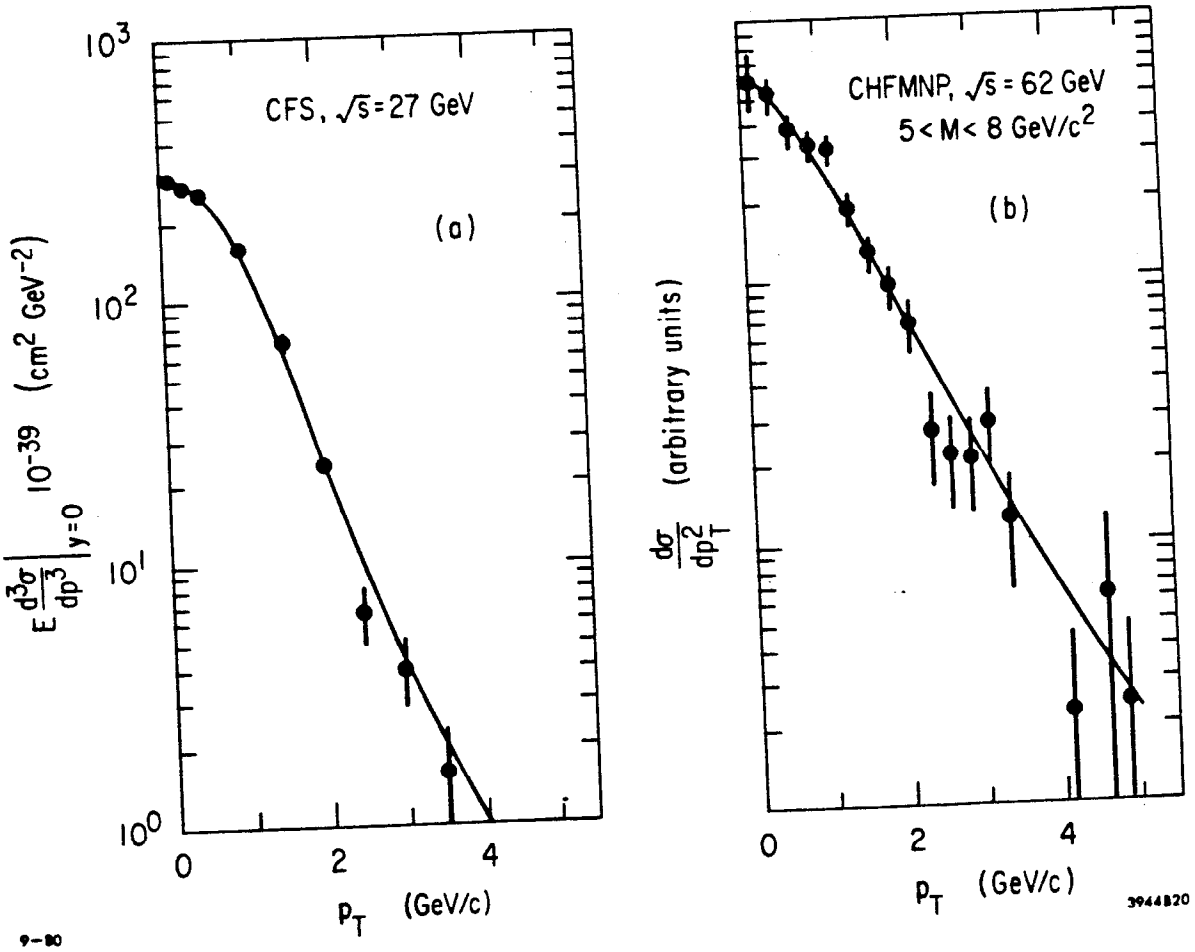

31. QCD calculations (ref. 102) of the p_T distributions of Drell-Yan pairs: a) at $\sqrt{s}$ = 27 GeV, and b) at $\sqrt{s}$ = 62 GeV compared with experimental data.

2. "Higher twist" effects. The Constitutent Interchange Model approach[104] is used to account for the neglected higher order terms in α_s. This approach stresses the quasi-bound structure of the incoming hadrons by emphasizing the meson-quark or diquark-quark subprocess contributing to the reaction. The model introduces effective coupling of mesons to quarks and unknown distribution of diquarks and mesons inside the hadrons, but it succesfully reproduces the behavior of the dilepton transverse momentum.

3. An interesting approach had been chosen by Dokshitser, Dyakonov and Troyan[80] and others[104] who have calculated the QCD terms to all orders in α_s in the leading log Q^2 approximation and also the next to leading terms. The solution has been obtained in the kinematical regions of $p_T^2 >> M^2$ and also for $p_T^2 < M^2$ when both p_T^2 and M^2 are large. The identification of the scale breaking variable Q^2 in the region of two large dimensional quantities (p_T^2 and M^2) is, however, unclear. So far there is no experimental data available for $p_T^2 > M^2$.

All the corrections discussed above do not change the general dependece of the moments of the transverse momentum distributions on the total c.m. energy squared s. In the leading log Q^2 approximation they are expected[71-73] to behave as:

$$< p_T > = a + b \sqrt{s} \qquad (36)$$

or

$$< p_T^2 > = a' + b' s \quad . \qquad (37)$$

Such behavior is indeed born out by the data (see fig. 18) and represents one of the strongest arguments in favor of the perturbative QCD

and the idea of gluons. It is worth noting, that the extrapolation of $\leq p_T >$ to high energy, using the parameters from sect. 3.4, i.e., for pN collisions

$$< p_T > \; = 0.44 + 0.026\sqrt{s} \quad ,$$

gives the value of average transverse momentum of about 21 GeV/c for $\sqrt{s}$ = 800 GeV. Thus, the Drell-Yan process may be expected to provide severe background in the search of the intermediate vector boson in the future colliding beams machines.

The values of the constants a or a' in the expressions (36) and (37) could be interpreted[105] as the measure of the intrinsic transverse momentum of quarks inside the parent hadrons provided that the higher order in α_s terms do not change the expectations. It should be stressed here that both the "primordial" transverse momentum approach and higher twist effects introduce strong dependence of $<p_T>$ on x_F of the lepton pair. Such dependence, i.e., rising of $< p_T >$ with increasing x, has not been observed in the available data (see fig. 19).

5.4 Normalization

Large values of the QCD corrections summed up in expression (27) require special care when discussing the normalization of the Drell-Yan process. Improving quality of experimental measurements and better understanding of the data allowed recently for the quantitative comparison with the Drell-Yan predictions following from the first order diagrams:

$$\frac{d\sigma}{dM} = \frac{8\pi\alpha^2}{9M^3} \sum_i e_i^2 \int dx_1 dx_2 \; \delta(\tau - x_1 x_2) \; * \qquad (38)$$

$$* \left[G_{q_{i/A}}(x_1,Q^2) \; G_{\bar{q}_{i/B}}(x_2,Q^2) + G_{\bar{q}_{i/A}}(x_1,Q^2) \; G_{q_{i/B}}(x_2,Q^2) \right]$$

The functions $G(x,Q^2)$ represent in this approach the effective structure functions of the projectile and target particles and are, in case of proton induced lepton pairs, the same as those measured in deep inelastic electron, muon and neutrino scattering. The equation (38) does not have, therefore, any free parameters and predicts the absolute value of the cross section for the reactions where the structure functions of both the target and the projectile are known. Such tests have been recently undertaken[41,42] by the NA3 Collaboration.

In the reaction

$$pN \rightarrow \mu^+\mu^- X$$

the Drell-Yan process is dominated by the annihilations of the valence quarks with the antiquarks in the sea, although the sea-sea contribution may also be present. In contrast valence-valence annihilations represent the bulk of the cross section for the $\bar{p}$ induced dimuons. All the corresponding terms of eq. (38) have been calculated[42] by the NA3 group using the quark structure functions measured by the CDHS Collaboration[106] in the ν and $\bar{\nu}$ scattering. The valence antiquarks in the antiproton were assumed to have the same distributions as the valence quarks in the proton and suitable corrections were taken for the neutron content of the platinium target. The resulting predictions, shown in fig. 32, were found to be a factor $K = 2.3 \pm 0.5$ lower than the measured data.

$$\frac{d\sigma}{dM} = K \left(\frac{d\sigma}{dM}\right)_{\text{Drell-Yan}} \qquad (39)$$

The results did not indicate any substantial mass or x dependence of the scale factor K.

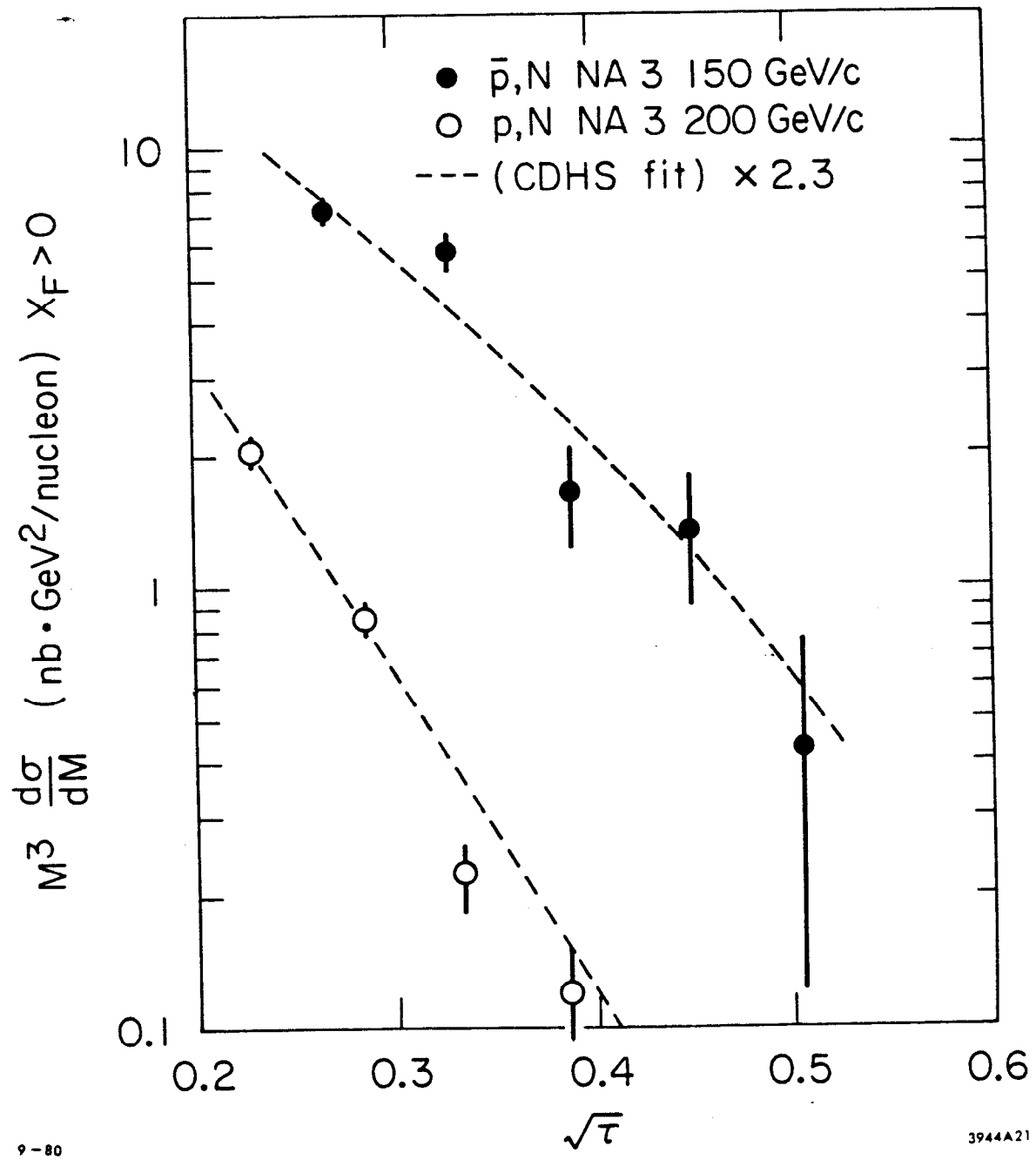

32. The comparison of the M dσ/dM of dimuons produced in pN and $\bar{p}$N interactions at x > 0 with the QCD type parametrization following the fit to the ν and $\bar{\nu}$ data.

Similar values of such scale factor were found also in analyses of the valence quarks structure functions and the sea quarks distributions of proton and pion in this and other experiments[40,42,49] and will be discussed in the next chapter. The discrepancy between the first order calculations and the measured cross sections seems thus to be well established. The numerical agreement of the value of the factor K with recently calculated next to leading order corrections[83,85,105] may be, nevertheless, accidental, since the size of even higher order terms has not been, as yet, estimated. One may also expect some kinematical variations of this difference, which are still hidden by the experimental errors.

6. Structure Functions and Quark Distributions

6.1 General Remarks

In the simple parton model the scaling function $F(\tau)$ depends only on the x distributions of the individual quarks. In order to reduce the number of unknowns one usually neglects heavy quark contributions and assumes SU(2) symmetry i.e.:

$$u_p(x) = d_n(x) = u(x)$$
$$u_n(x) = d_p(x) = d(x) \quad ,$$

where the subscripts p and n refer to the distributions of quark of a given flavor in proton or neutron, respectively. In case of proton interactions these steps leave six unknown fuctions: u(x), d(x), s(x), $\bar{u}(x)$, $\bar{d}(x)$ and $\bar{s}(x)$. The normalization of these functions is provided by the integrals: [1]

$$k_u = \int_0^1 u(x)dx,$$

$$k_d = \int_0^1 d(x)dx, \quad \text{etc.}$$

such that k_i is the fraction of the proton's momentum carried by quarks of flavor i. In the Drell-Yan process in pN collisions the antiquarks come only from the sea, while u and d quarks have both sea and valence components. It is therefore often useful to separate explicitly the quark structure function into the valence and sea parts:

$$u(x) = u_v(x) + u_s(x)$$
$$d(x) = d_v(x) + d_s(x) \qquad (40)$$

Taking into account the isospin invariance, the deep inelastic lepton scattering measurements provide the following equations;

$$\nu W_2^{ep}(x) = \frac{4}{9} x \left[u(x)+\bar{u}(x)\right] + \frac{1}{9} x \left[d(x)+\bar{d}(x)\right] + \frac{1}{9} x \left[s(x)+\bar{s}(x)\right]$$

$$
\begin{aligned}
\nu W_2^{en}(x) &= \frac{4}{9}\, x\left[d(x)+\bar{d}(x)\right] + \frac{1}{9}\left[u(x)+\bar{u}(x)\right] + \frac{1}{9}\, x\left[s(x)+\bar{s}(x)\right] \\
\nu W_2^{\nu p}(x) &= 2\, x\left[d(x)+\bar{u}(x)\right] \\
\nu W_2^{\bar{\nu} p}(x) &= 2\, x\left[u(x)+\bar{d}(x)\right] \qquad (41) \\
\nu W_3^{\nu p}(x) &= 2\, x\left[\bar{u}(x)-d(x)\right] \\
\nu W_3^{\bar{\nu} p}(x) &= 2\, x\left[\bar{d}(x)-u(x)\right] \quad .
\end{aligned}
$$

It is possible, in principle, to extract from these measurements the individual distributions and fully describe the Drell-Yan process.

The same arguments may be applied to the first order QCD calculations. Here, the quark distribution functions contain scale breaking dependence on Q^2: $u(x, Q^2)$, $d(x, Q^2)$...etc., and in order to satisfy the equation (24) they have to be determined at the $|Q^2| = M^2$ of the lepton pair. In practice there is not sufficient overlap of the available data on deep inelastic lepton scattering (DIS) in the region of x and Q^2 covered by the dilepton data, to allow for the direct test of the above method. Therefore, the procedure most commonly applied[92,100,101,107] consists of the following steps:

1. Use the DIS data to extract the parton distributions at low Q^2 and in the limited range of x where the measurements overlap sufficiently.
2. Assume the behavior of these distributions in the x region not covered by experiments.
3. Extrapolate these distributions to large values of Q^2 using the QCD evolution equation.

These steps are not uniquely defined and various analysis[94,108] lead to slightly different parametrization of the DIS data and various prescriptions fo

the Q^2 dependence of the quark and gluon distributions. The dilepton data available so far are concentrated in the region where scaling violations are expected to be small and, therefore, they are not sensitive to most of the variations in these procedures. It should be stressed, however, that the neglected higher order QCD corrections lead to significant discrepancies of the overall predicted normalization.

6.2 Extraction of the Proton Sea

A more direct approach has been taken by the Columbia-Fermilab-Stony Brook Collaboration[40], which used experimental measurements of deep inelastic muon and electron scattering to extract the sea quark distributions.

In addition to the muon pair data the input was provided by the Q^2 dependent fit to the Fermilab DIS results and the relation

$$\frac{\nu W_2^n}{\nu W_2^p} = 1.0 - 0.8x \qquad (42)$$

suggested by low Q^2 SLAC measurements. Eq. (42) was used to account for the neutron content of the nuclear target. The antiquark distributions were parametrized for all Q^2 values as:

$$\begin{aligned} \bar{d}(x) &= A(1-x)^N \\ \bar{u}(x) &= A(1-x)^{N+\beta} \\ \bar{s}(x) &= \left[\bar{u}(x)+\bar{d}(x)\right]/4 \quad . \end{aligned} \qquad (43)$$

The inequality of the $\bar{u}(x)$ and $\bar{d}(x)$ content of the proton sea has been suggested by Feynman and Field[109] as the result of the Pauli exclusion principle and different number of u and d valence quarks. The suppression of the strange sea was suggested[106] by neutrino scattering measurements. The results of the CFS fit to the dimuon data summarized in Table 5

support this suggestions.

The ratio of the νW_2 structure functions of neutron and proton (eq. (42)) assumed no Q^2 dependence. The CFS group had also used the QCD calculations[94] to estimate the expected Q^2 dependence of this ratio and obtained for the range appropriate for their experimental data

$$\frac{\nu W_2^n}{\nu W_2^p} = 0.807 - 0.535x \quad . \qquad (44)$$

The result of the fit to the data using eq. (44) as input is also shown in Table 5. The values of the parameters A, β, N are similar to those obtained without Q^2 dependence and support the inequality $\bar{u}(x) \neq \bar{d}(x)$. In both cases fits with parameter $\beta = 0$ resulted in substantialy greater value of χ^2.

TABLE 5

Nucleon sea parameters fitted to eq. (43)

	Without Q^2 correction	With Q^2 correction
A	0.548 ± 0.002	0.536 ± 0.016
β	3.48 ± 0.25	2.51 ± 0.39
N	7.62 ± 0.08	7.77 ± 0.11
χ^2/DF	211/156	208/155

The SU(3) violating asymmetry of antiquarks in the proton sea manifests itself also in the slope of the longitudinal momentum distributions of the lepton pairs near y = 0. For the CFS data shown in fig. 33 it is partially due to the inequality of the u and d valence quarks in the Cu target (40% proton and 60% neutron). The slopes at various values of τ are however, larger than the Drell-Yan model fit with symmetric sea quark distributions and favour a surplus of $\bar{d}$ quark over $\bar{u}$ quarks in the proton.

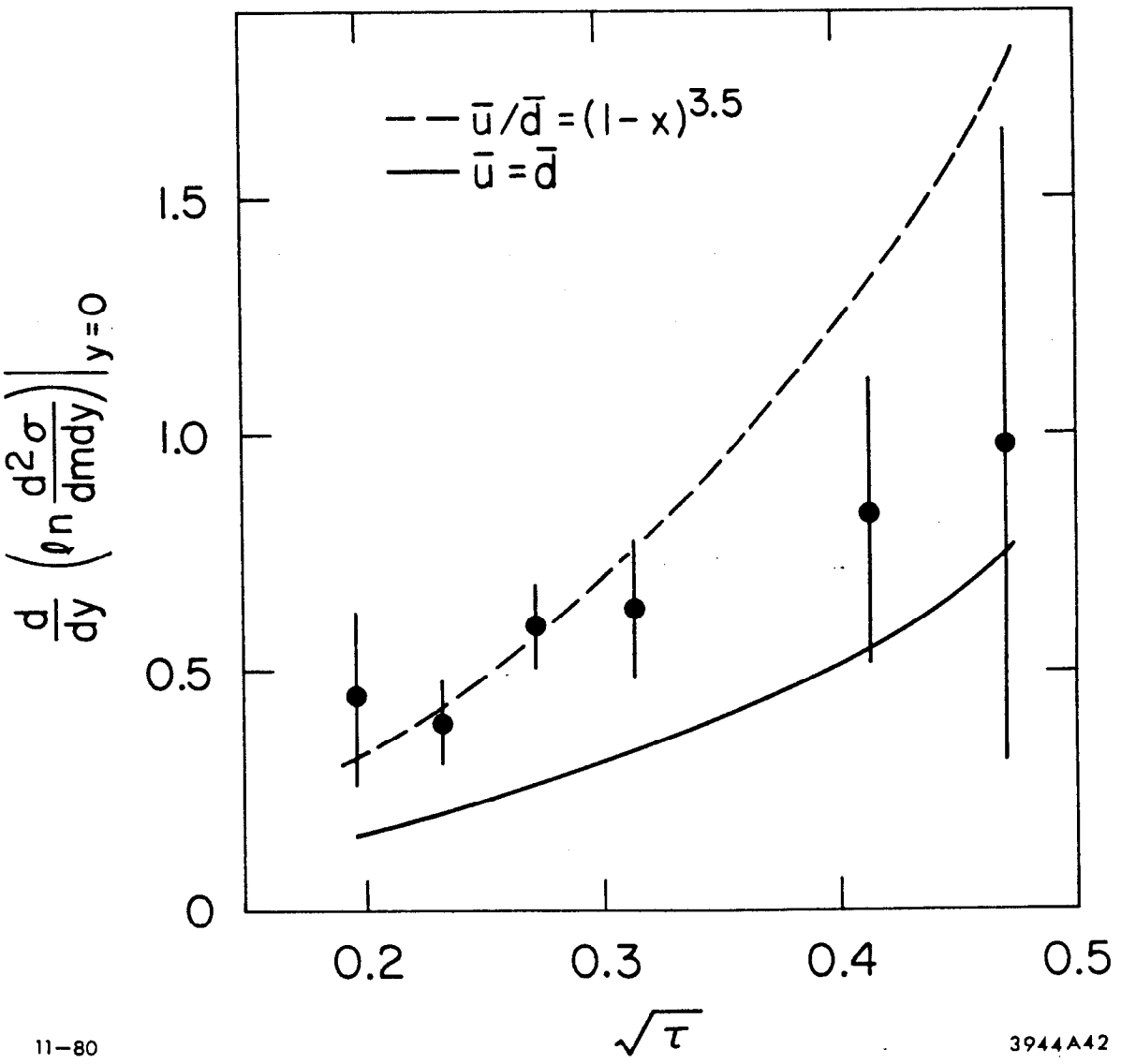

33. Slope of the rapidity distribution evaluated at y = 0. The solid line is the Drell-Yan model fit to the data with $\bar{u} = \bar{d}$ and the dashed line in the fit with $\bar{u} \neq \bar{d}$.

In addition to the above calculations the CFS group was able to test the sensitivity of the extracted sea quark distributions to the explicit inclusion of the first order QCD diagrams[72]. The intrinsic transverse Fermi motion of quarks inside the nucleon was parametrized as

$$f(k_T) = e^{-ak_T^2}$$

and the gluon distribution within the nucleon as

$$g(x) = B(1-x)^m \quad .$$

With the assumption of no Q^2 dependence of the parameters and the normalization of the gluon distribution

$$\int_0^1 g(x)dx=0.5 \quad ,$$

the fits used as input all the muon pair and DIS data. The resulting values of the parameters listed in Table 6 are again similar to those from Table 5. This indicates that the extracted sea distributions depend little on the method of analysis.

Table 6

A	0.56 ± 0.01	m	4.1 ± 0.2
β	2.6 ± 0.3	α_s	0.27 ± 0.01
N	8.1 ± 0.1	a	1.14 ± 0.02

Caution is needed, however, when comparing results of analysis of different data.

In fig. 34a is shown a comparison[40] of the quantity

$$\bar{q}(x)+\bar{s}(x) = \bar{u}(x)+\bar{d}(x)+2\bar{s}(x)$$

measured in inelastic neutrino scattering experiments at CERN and Fermilab

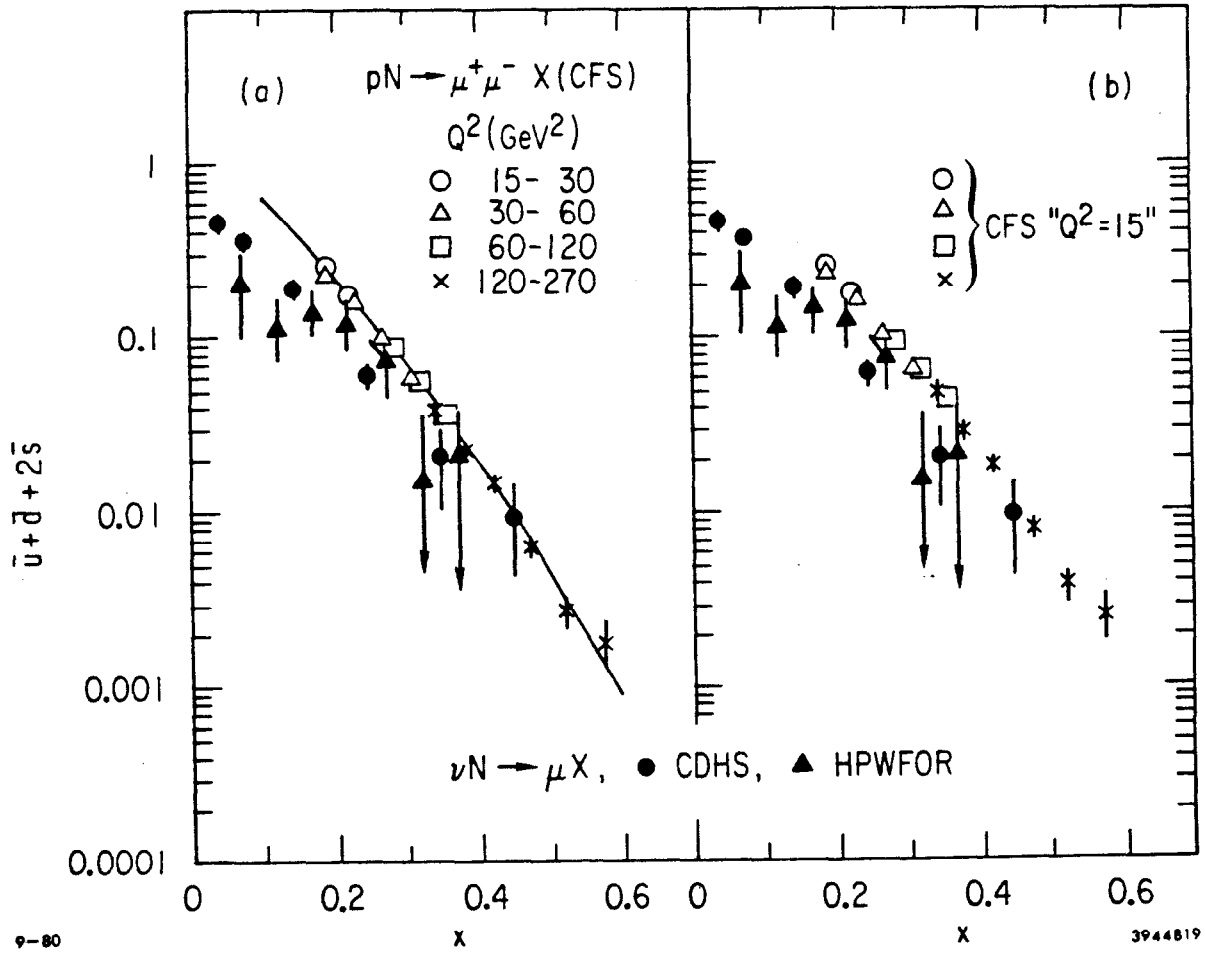

34. Comparison of the proton sea quark distributions measured in neutrino interactions with those obtained from dimuon data a) CDHS, HPWOFR and CFS data, solid line represents the fit described in Table 5. b) dimuon data evolved to Q^2 = 15 GeV^2.

with values obtained by the CFS group. The most striking feature of the graph is the difference, both in shape and in the absolute normalization, of the two sets of data. The neutrino scattering is measured at rather small Q^2 range with the average value $Q^2 \approx 15$ GeV^2, while the dimuon data span large range of masses. The scale breaking effects may, therefore, introduce substantial distortion of the shape of the distribution. As an example of the size of this effect the evolution equations were used[110] to estimate the values of the CFS points corresponding to $Q^2 = 15$ GeV^2. The new points, shown in fig. 34b have similar x dependence as the neutrino data. The CFS measurements remain, however, about factor of two higher. This provides another evidence for the discrepancy of the normalization of the lepton pairs measurements and the calculations of the leading QCD terms of the Drell-Yan model which use the DIS data.

6.3 Structure Functions of Unstable Particles

6.3.1 Pion

The measurements of the massive lepton pairs produced by the pion beams allow for the determination of the pion structure function. In the simple parton model the cross section for the Drell-Yan process can be differentiated with respect to x_1 and x_2 of the annihilating quarks:

$$\frac{d^2\sigma}{dx_1 dx_2} = \frac{4\pi\alpha^2}{9s} \sum_i \frac{ei^2}{x_1^2 x_2^2} \left[G_{q_{i/\pi}}(x_1)\, G_{\bar{q}_{i/N}}(x_2) + G_{\bar{q}_{i/\pi}}(x_1)\, G_{q_{i/N}}(x_2) \right], \quad (45$$

where the structure functions G have both valence and sea contributions. For a pion it follows from change conjugation and isospin invariance that the x distributions are the same for both valence quarks

$$f^{\pi}(x) = u_{v}^{\pi^+}(x) = \bar{d}_{v}^{\pi^+}(x) = \bar{u}_{v}^{\pi^-}(x) = d_{v}^{\pi^-}(x) \quad .$$

The normalization here is given by the number of valence quarks i.e.:

$$\int_0^1 \frac{f^{\pi}(x)}{x}\, dx = 1$$

Separating explicit valence and sea components of the pion and allowing for a normalization scale factor K (see section 5.4) the equation (45) may be rewritten as

$$\frac{d^2\sigma}{dx_1 dx_2} = K \frac{4\pi\alpha^2}{9sx_1^2x_2^2} \left(F^{\pi}(x_1)\, g^N(x_2) + S^{\pi}(x_1) \cdot h^N(s_2) \right) \qquad (46)$$

Functions $g^N(x_2)$ and $h^N(x_2)$ represent linear conbination of the u, d and sea components of the target nucleons. Equation (46) may be further simplified by neglecting the pion sea

$$M^2 \frac{d^2\sigma}{dx_1 dx_2} = K \frac{4\pi\alpha^2}{9x_1x_2} f^{\pi}(s_1) \left[\frac{4}{9} u^N(x_2) + \frac{1}{9} \bar{d}^N(x_2) \right] \qquad (47)$$

The measurements of the muon pair production in the large range of mass and x_F values allowed several groups to extract the pion structure functions using above set of equations. The simplest factorization method uses eq. (47). The data are binned into the (x_1, x_2) grid and for each of the N_1 bins of x_1 there is an unknown value of $f^{\pi}(x_1)$ and for each of the N2 bins of x_2--an unkonwn $g^N(x_2)$. The N1+N2 unknowns can be then extracted from the N1*N2 grid cells. The method neglects the contribution from the pion sea but this problem may be circumvented by the simultaneous analysis of the π^- and π^+ induced data [41]. Other two methods applied by the NA3 group consisted of

i) parametrization of the pion and nucleon structure functions in eq. (46) with functional forms suggested by Buras and Gaemers[108]

$$
\begin{aligned}
f^{\pi}(x) &= Ax^{\alpha}(1-x)^{\beta} \\
S^{\pi}(x) &= B\ (1-x)^{n} \\
u^{N}(x) &= A_u'\ x^{\alpha'}(1-x)^{\beta'} \\
d^{N}(x) &= A_d'\ x^{\alpha'}(1-x)^{\beta'+1} \\
S^{N}(x) &= B'(1-x)^{n'}
\end{aligned}
\qquad (48)
$$

ii) Direct use of the nucleon structure functions determined by e.g. neutrino scattering as input to eq. (46). This method allowes also for the determination of the normalization scale factor K.

The results of such analysis are illustrated in fig. 35. The distributions are arbitrarily normalized and show a general agreement. The shape of the pion structure function is much flatter than that of the proton. The values of the parameters fitted to eq. (48) by various groups are summarized in Table 7.

Table 7

	CIP	GOLIATH	OMEGA	NA3	
	225 GeV/c	150,175 GeV/c	40 GeV/c	200 GeV/c	150 GeV/c
A	0.90 ± 0.06	2.43 ± 0.30		0.75	0.55
α	0.5	0.5	0.44 ± 0.12	0.40 ± 0.15	0.40 ± 0.10
β	1.27 ± 0.06	1.57 ± 0.18	0.98 ± 0.15	1.07 ± 0.12	0.90 ± 0.10
B			0.36	0.32 ± 0.20	0.32
n			5	6.9 ± 2.9	6.9

Values without errors represent quantities imposed in the fits.

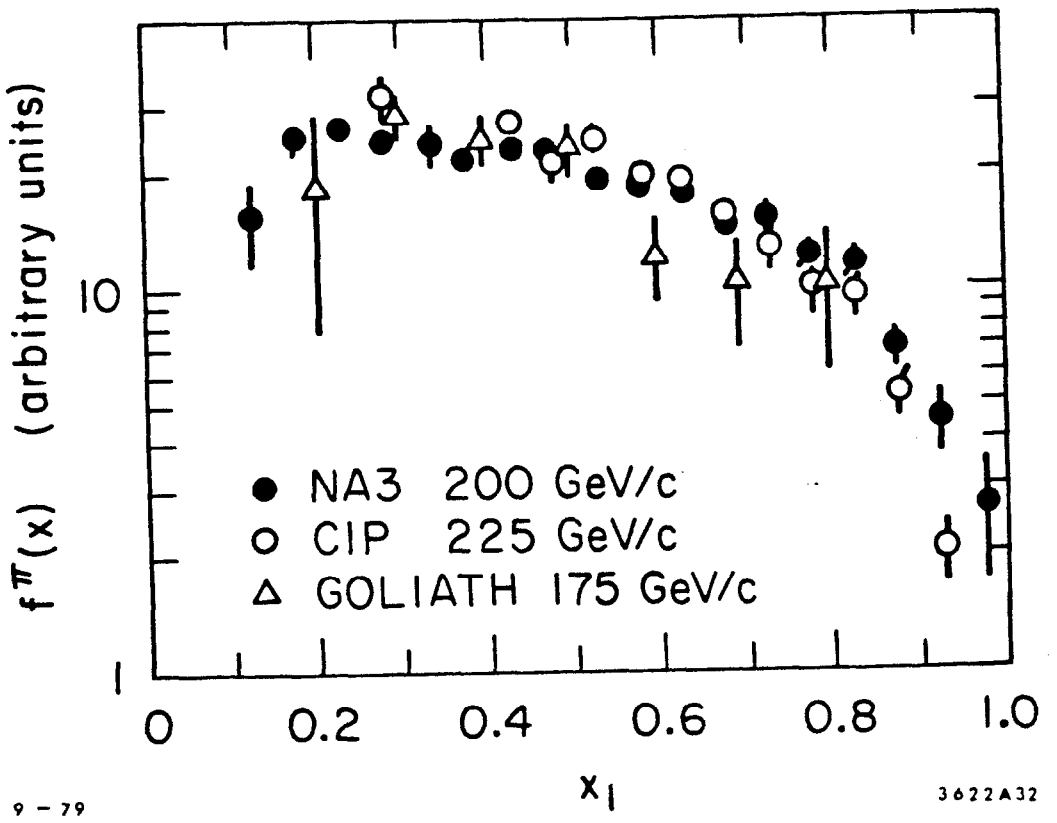

35. Pion structure function.

The integrals of the above parametrizations indicate that the pion sea quarks carry about (5 ÷ 10)% and valence quarks about (30 ÷ 40)% of the pion momentum.

The similarity of the results spanning the incoming momentum from 40 to 280 GeV may result, however, from large statistical and systematical errors of the analyses used by various groups. The comparison of the pion structure function obtained by the NA3 group at 150 and 200 GeV/c (see fig. 36) shows small energy dependence reminiscent of the scaling violations observed in the proton case. The expected effects are, however, small and the proper QCD type analysis which would include dimuon scaling violations of the nucleon structure function requires much higher statistic data. Nevertheless, even the simplified parton model approach indicates a normalization discrepancy between the Drell-Yan model calculations and experimental measurements. The scale factor K, discussed already in sect. 5.4 was measured to be 2.2 ÷ 2.4 for μ pairs production by pions. The fact that the experiment of Chicago-Illinois-Princeton group did not observe such effect may be related to the different nuclear target dependence used by this group.

The identification of this normalization scale factor K with the radiative corrections expected[85,86] in QCD is at the moment not clear. Recent calculations of the size of such corrections by Kubar et al.[105] for the dilepton production by pions showed ∿ 50% variation of expected factor K with x_1 and x_2 of annihilating quarks. Such x dependence of the scale factor may strongly distort the shape of the extracted pion structure function.

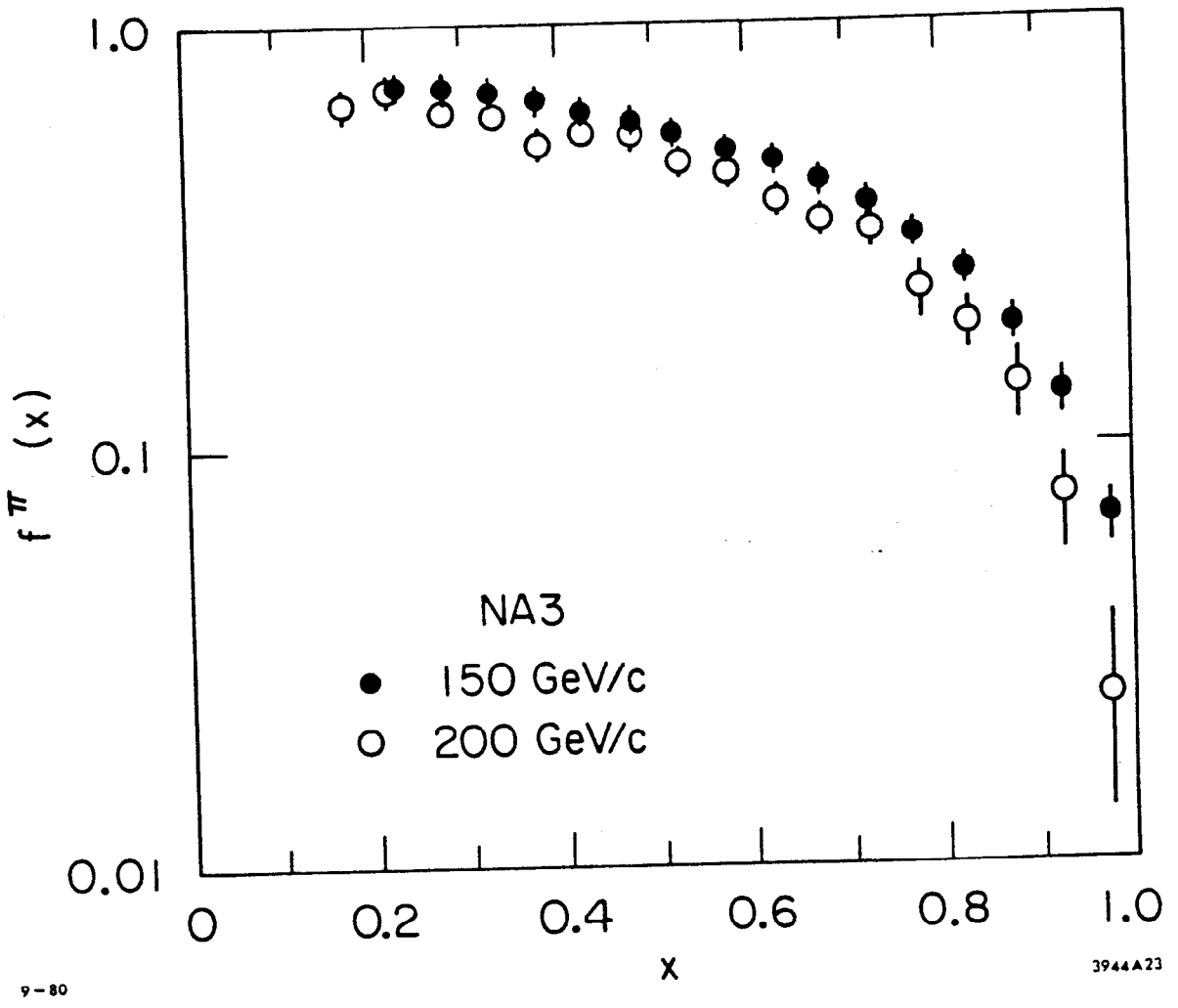

36. Pion structure functions extracted by the NA3 Collaboration from $\pi^- p$ interactions at 150 and 200 GeV.

6.3.2 Kaon

Similar procedure may be also applied to the lepton pairs produced by kaons. However, the available data on dileptons produced by kaon beams are rather scant and further simplifications of the analysis have to be introduced. The NA3 group had neglected the meson sea and determined[42] the kaon valence structure function relative to that of the pion. They have assumed identical scale factor K for the kaon and pion beams and expressed the ratio of the valence structure functions as the ratio of the experimental x distributions:

$$R(x_1) = \frac{L_\pi \left(\frac{dN}{dx_1}\right)_K}{L_K \left(\frac{dN}{dx_1}\right)_\pi} C(x_1) \quad , \qquad (49)$$

where L_π and L_K are the luminosities of the measurements and fuction $C(x_1)$ describes the integrals over the target variable x_2 involving the nucleon structure function. Further approximation neglects terms corresponding to the annihilation of the charge $^{-1}/3$ valence quark of the pion or kaon with the sea quarks of the target nucleon. This simplifies $C(x_1) = 1$ reducing eq. (49) to the ratio of the measured quantities. The results are presented in fig. 37. Although it appears that at large x the valence quark distribution in kaon decreases faster than corresponding one for the pion, one has to keep in mind that the approximations listed above may introduce large effects in certain kinematic regions. Theoretically, deviations from R=1 are expected in QCD due to the mass difference of strange and up quarks. The results of the nonrelativistic leading twist calculations[111] which assume the ratio of masses of strange and up quarks equal to 540/336 are shown in fig. 37 as the solid line. The good agreement with presented data points is probably fortuitous at the present precision of both calculations and experimental analysis.

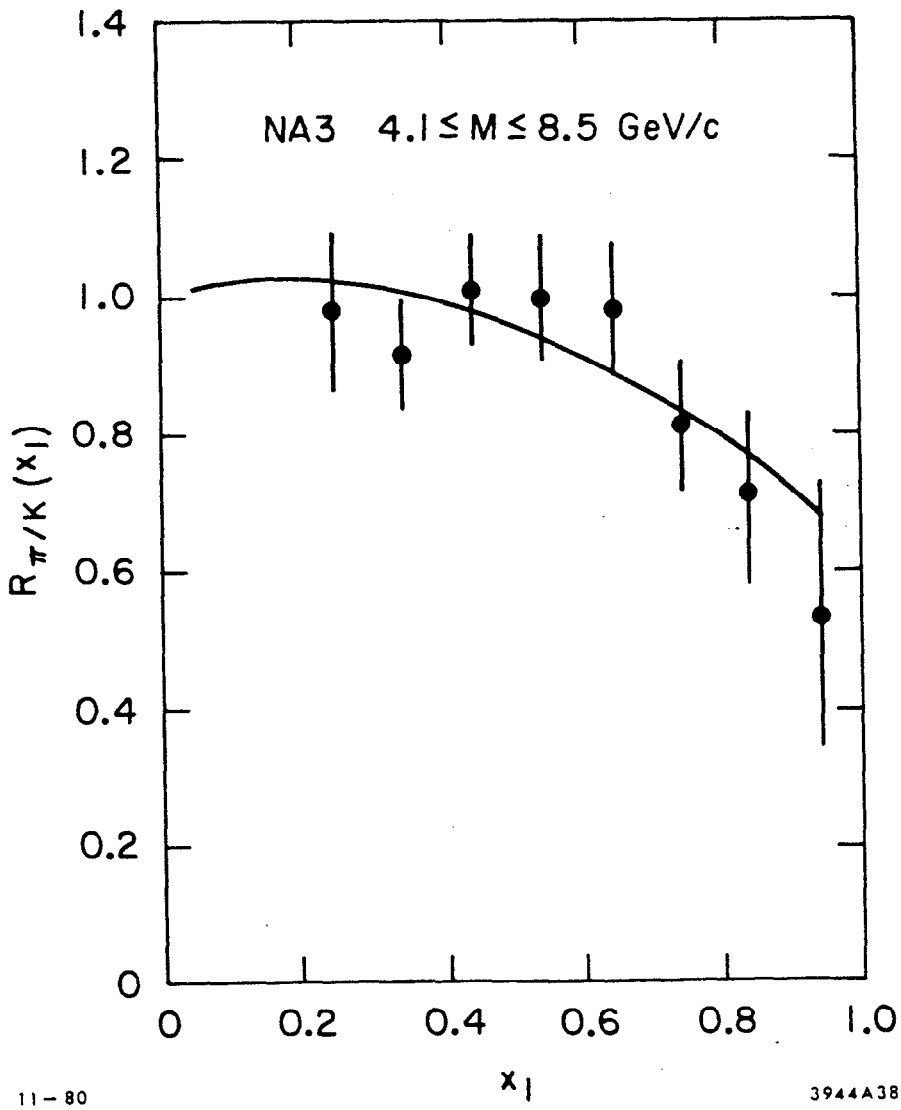

37. Ratio $R_1(x)$. Solid curve describes the calculations from ref. 111.

6.3.3 Antiproton

Simultaneous measurements of the dileptons produced in proton and antiproton interactions allow for the cleanest determination of the nucleon valence quarks distributions. Since the proton and antiproton structure fuctions are expected to be the same the difference between lepton pair production in $\bar{p}N$ and pN collisions arises from the asymmetry in the valence-valence annihilations only. All other contributions from the sea-valence and sea-sea annihilations cancel out in the subtraction. In the quark parton model the difference of the differential cross sections on the platinum target nucleon N (Z/A = 0.4) can be written explicitly[42] using the valence u and d quarks distributions:

$$\left.\frac{d^2\sigma}{dx_1 dx_2}\right|_{\bar{p}N} - \left.\frac{d^2\sigma}{dx_1 dx_2}\right|_{pN} = \frac{4\pi\alpha^2}{9sx_1^2x_2^2} \cdot \frac{1}{9}\left(\left[4u(x_1) + d(x_1)\right]\left[0.4u(x_2) + 0.6d(x_2)\right] + 0.2d(x_1)\left[u(x_2) - d(x_2)\right]\right) \tag{50}$$

The second term inside the bracket is very small (< 2%) and can be neglected. Therefore

$$\left.\frac{d^2\sigma}{dx_1 dx_2}\right|_{\bar{p}N-pN} = \frac{4\pi\alpha^2}{9sx_1^2x_2^2} \cdot \frac{1}{9} f(x_1)\, g(x_2) \tag{51}$$

where $f(x_1)$ and $g(x_2)$ are the valence structure functions of the antiproton and target nucleon respectively.

The NA3 Collaboration had again used[42] the technique described in previous sections, i.e. parametrized the quark x distributions according to set of equations (48) and determined the normalization scale factor K

to be K = 2.3 ± 0.4. The resulting $\bar{p}$ valence structure function is shown in fig. 38. For x > 0.4, it compares very well with the proton structure function obtained from the pN interactions alone. At lower x values the proton data clearly show the sea contribution. With the K factor taken into account both distributions are well described by the parametrizations of the valence and sea components which are compatible with the neutrino results and also CFS data described in Sect. 6.2.

It should be stressed here that although the present knowledge of $\bar{p}N \to \mu\mu X$ is still fragmentary, precise measurements of the difference described by eq. (50) will eventually provide best (i.e., least biassed) estimate of the scale factor K and its dependence on kinematical variables.

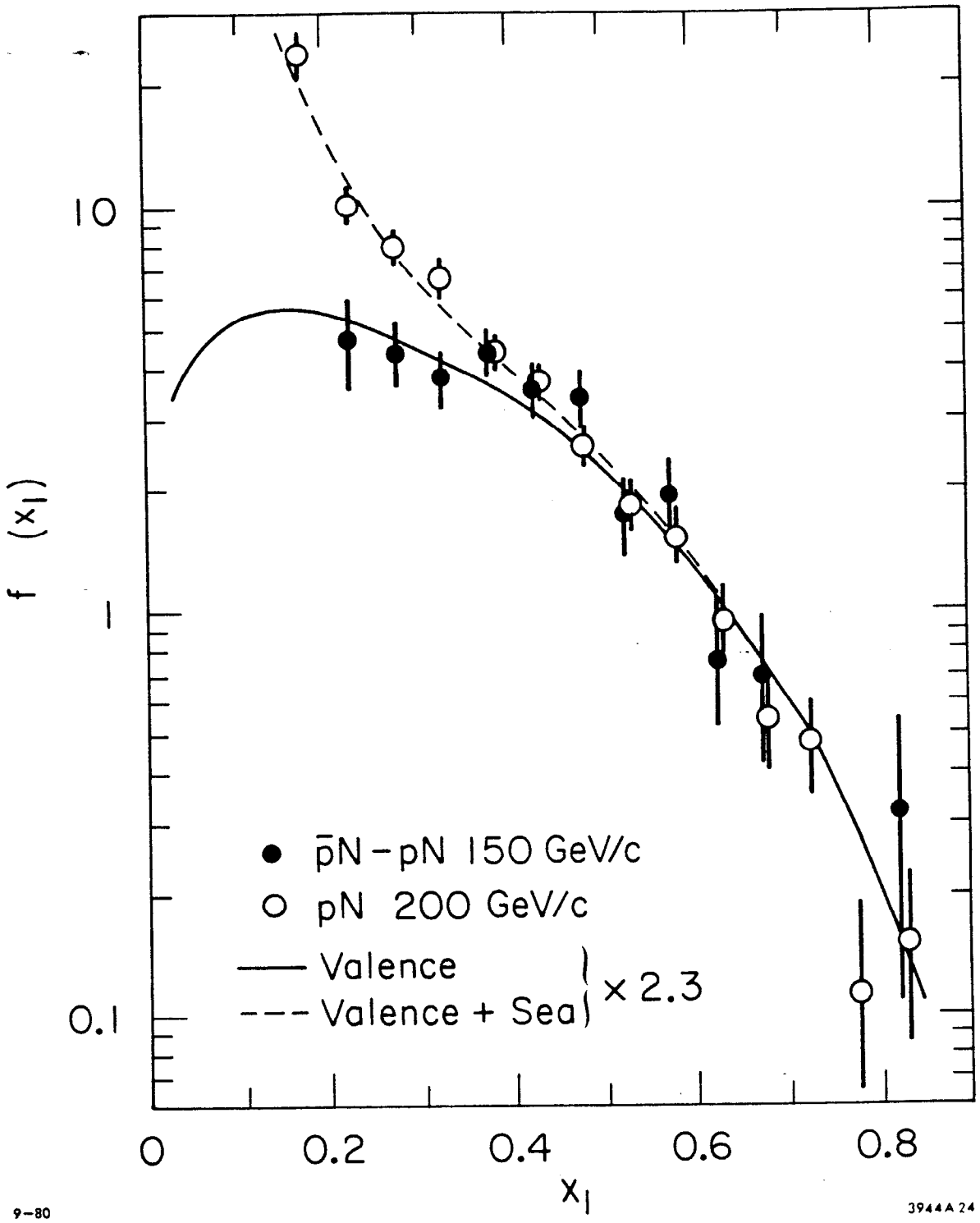

38. The $\bar{p}$ valence structure function compared with proton structure function obtained from the pN interactions.

7. Review of Low Mass Data

Although the cross section for the production of dileptons with mass $M \lesssim 1$ GeV is almost two orders of magnitude higher than for $M > 3$ GeV, the present knowledge and understanding of the low mass data is rather limited. This is mainly due to the severe background problems and the uncertainties of the inclusive cross sections and kinematic distributions of known resonances which contribute to the low mass e^+e^- or $\mu^+\mu^-$ spectra. Tables 3 and 4 list recent experiments addressing this problem.

In fig. 39 are shown typical $\mu^+\mu^-$ spectra measured[56] by the Chicago-Princeton Collaboration at 150 GeV/c. The distributions are similar in shape for the pion and proton induced reactions and their characteristic features, i.e., the prominent $\rho - \omega$ peak and the large enhancement between the threshold and $\sim$ 600 MeV, have been also observed in most of the other experiments with good mass resolution. The intensity of the dimuons was shown to decrease strongly with rising x and p_T of the pair. The parametrization describing the data of the BNL-Yale group[58] at 28 GeV/c:

$$\frac{d\sigma}{dx} = 40\ \mu b\ e^{-(10.0\pm0.3)x} \qquad (52)$$

is compatible with muon pair behavior at higher energies.

As was discussed in sect. 2.4 several known sources contribute to the low mass region. These are direct and Dalitz decays of ρ, ω and η resonances and the Bethe-Heitler process. The estimates of such contributions require as input the knowledge of the inclusive production cross sections and their branching ratios into the final states with e^+e^- and $\mu^+\mu^-$. In addition, since most of the experiments have

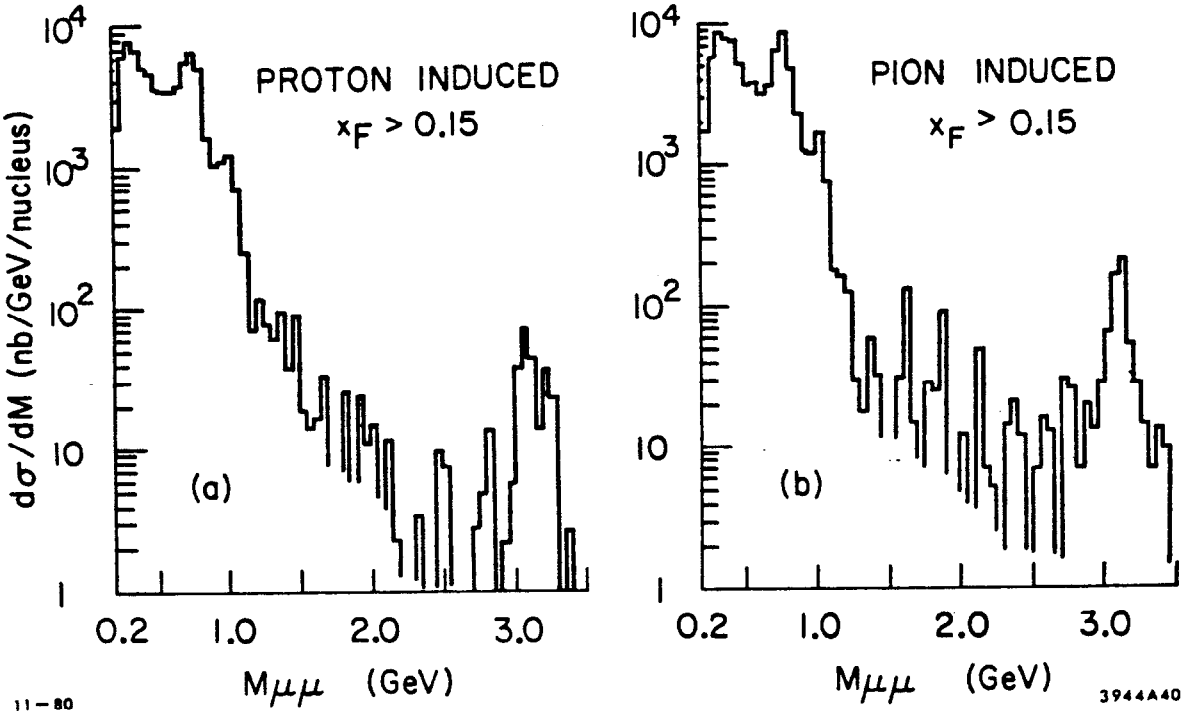

39. Effective mass spectrum of muon pairs produced in a) proton and b) pion interactions with beryllium target at 150 GeV/c.

limited acceptance, the knowledge of the inclusive kinematic distribution in x and p_T of these resonances is also needed. All of these above quantities are poorly known and the best guesses have a systematic error of up to 50%. Nevertheless in several analyses[56-60] such best estimates account for at most 40 to 50 % of the measured cross section below the mass $M \lesssim 700$ MeV, thus indicating an underlying dilepton continuum not explained by the known sources. As an example, in fig. 40 is shown the $\mu^+\mu^-$ spectrum measured in π^-N interactions at 225 GeV/c by the Chicago-Princeton group[56] together with the estimates of the η and ω contributions. Both CPII and BNL-Yale groups reported[56,58] changes of the shape of the mass distributions with x of the lepton pair. The inherently poor resolution of dimuon experiments made, however, detailed study of the low mass continuum difficult.

Until recently the low mass electron pair data were scarce and inconclusive. Two ISR experiments[62-64] measured the low mass e^+e^- pairs at large transverse momentum ($p_T > 2$ GeV/c). In each case the observed distribution was consistent with the contributions resulting from Dalitz decays of η and ω mesons and semileptonic decays of charmed particles. Several bubble chamber groups[67-69] have seen indications of the low mass continuum, but these experiments are limited by their low sensitivity. Better quality results are coming, however, from recent experiments[65,112]. The SLAC-Johns Hopkins-Caltech group measured[65] direct e^+e^- pair production at low values of x using the π^- beam at 16 GeV/c. At this energy the inclusive cross sections of the resonnaces and their x and p_T distributions

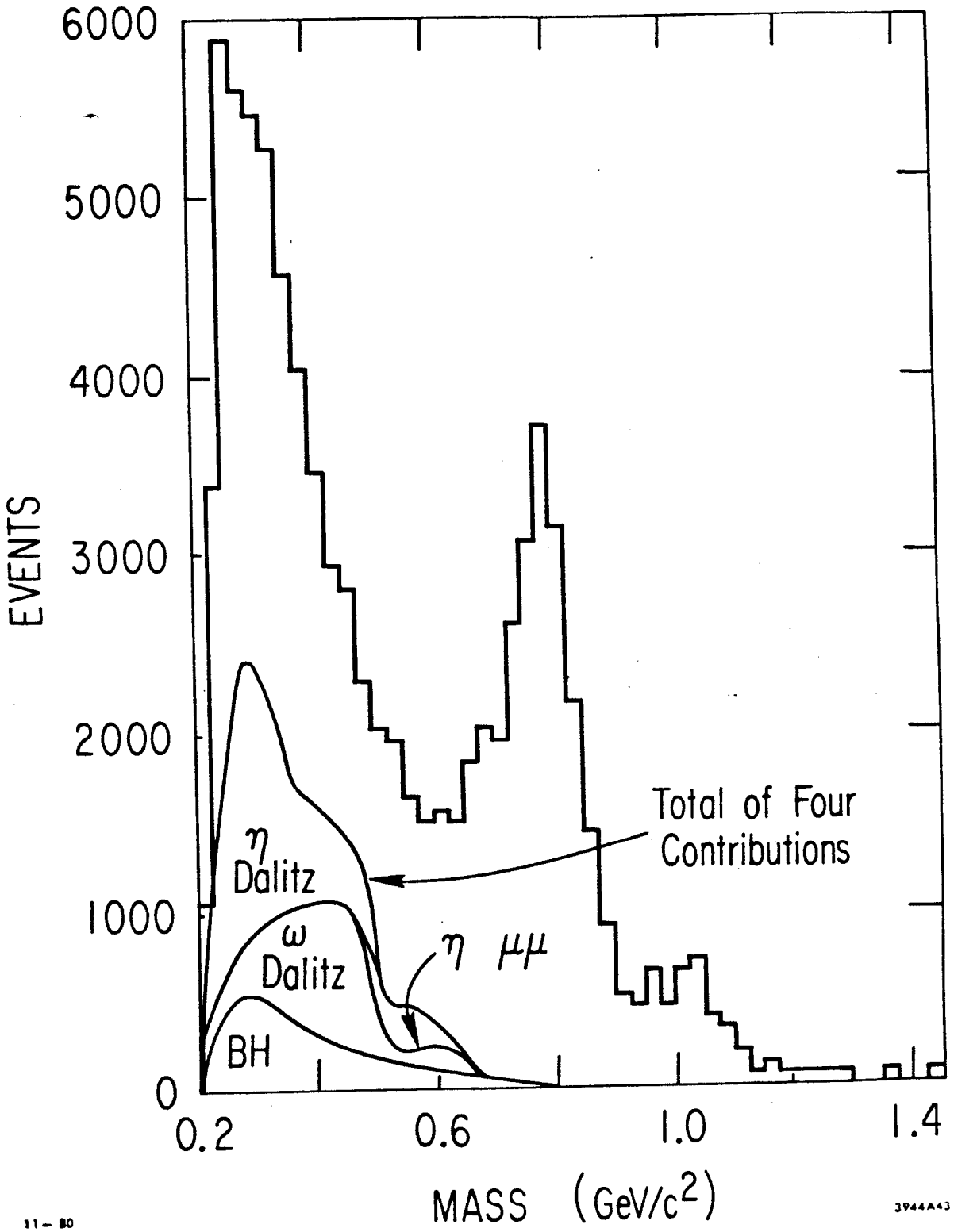

40. The $\mu^+\mu^-$ mass spectrum measured in 225 GeV/c π^-N interactions (histogram). Solid curves represent contributions from ω Dalitz decays, η direct and Dalitz decays and from the Bethe-Heitler process.

are relatively well known and it was possible to remove their contribution with good accuracy. The remaining e^+e^- spectrum (see fig. 41) provided clear evidence for the low mass continuum which was compatible with M^{-1} dependence and exhibited very step x and p_T^2 behavior. Similar preliminary results have been also reported[112] by the BNL-Pennsylvania-Stony Brook Collaboration.

In a complementary experiment the SLAC-Vanderbilt-Santa Cruz-MIT group has measured[55] $\mu^+\mu^-$ pair production in πp interactions also at 16 GeV/c. This experiment spanned the region of large x_F and also found the evidence for the low mass dilepton continuum. Recent analysis[113] combined the results of the two 16 GeV/c πp experiments providing the coverage of almost full range of x_F. After subtraction of the contributions of known sources and correction for the different mass thresholds of $\mu^+\mu^+$ and e^+e^- pairs, the combined x_F distribution of the continuum, shown in fig. 42, is well described by single exponential functions:

$$\frac{d\sigma}{dx_F} = (7.86 \pm .02)\ e^{-(6.3 + 0.1)x} \quad . \qquad (53)$$

The steep x_F and p_T behaviour of the continuum, together with the phase space suppression factor introduced by the dimuon mass threshold may account for the differences in the e/π and μ/π ratios observed[9] in the single particle experiments.

The origin of the low mass continuum remains so far unclear. The relatively high cross section observed at low energies (e.g., $\sim$ 2.5 μb in 16 GeV/c πp collisions) excludes the explanations in terms of copious charm production or conventional Drell-Yan model. The Bjorken-Weisberg mechanism[20] discussed in sect. 2.4.3 may

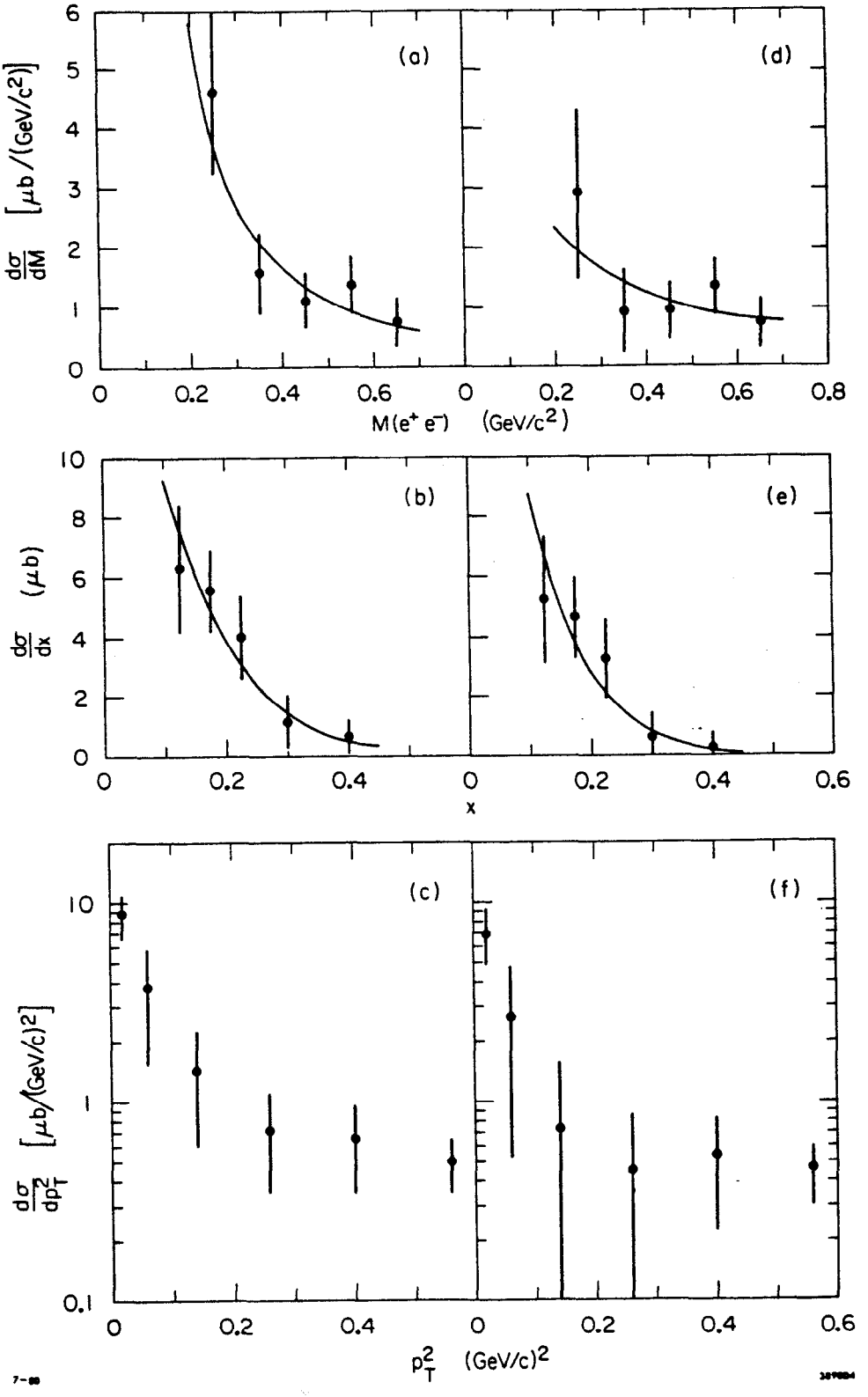

41. The acceptance corrected mass, x and p_T^2 distributions for the e^+e^- continuum produced in 16 GeV/c π^-p interactions[65]:

(a) - (c) before and (d) - (f) after subtraction of the η and

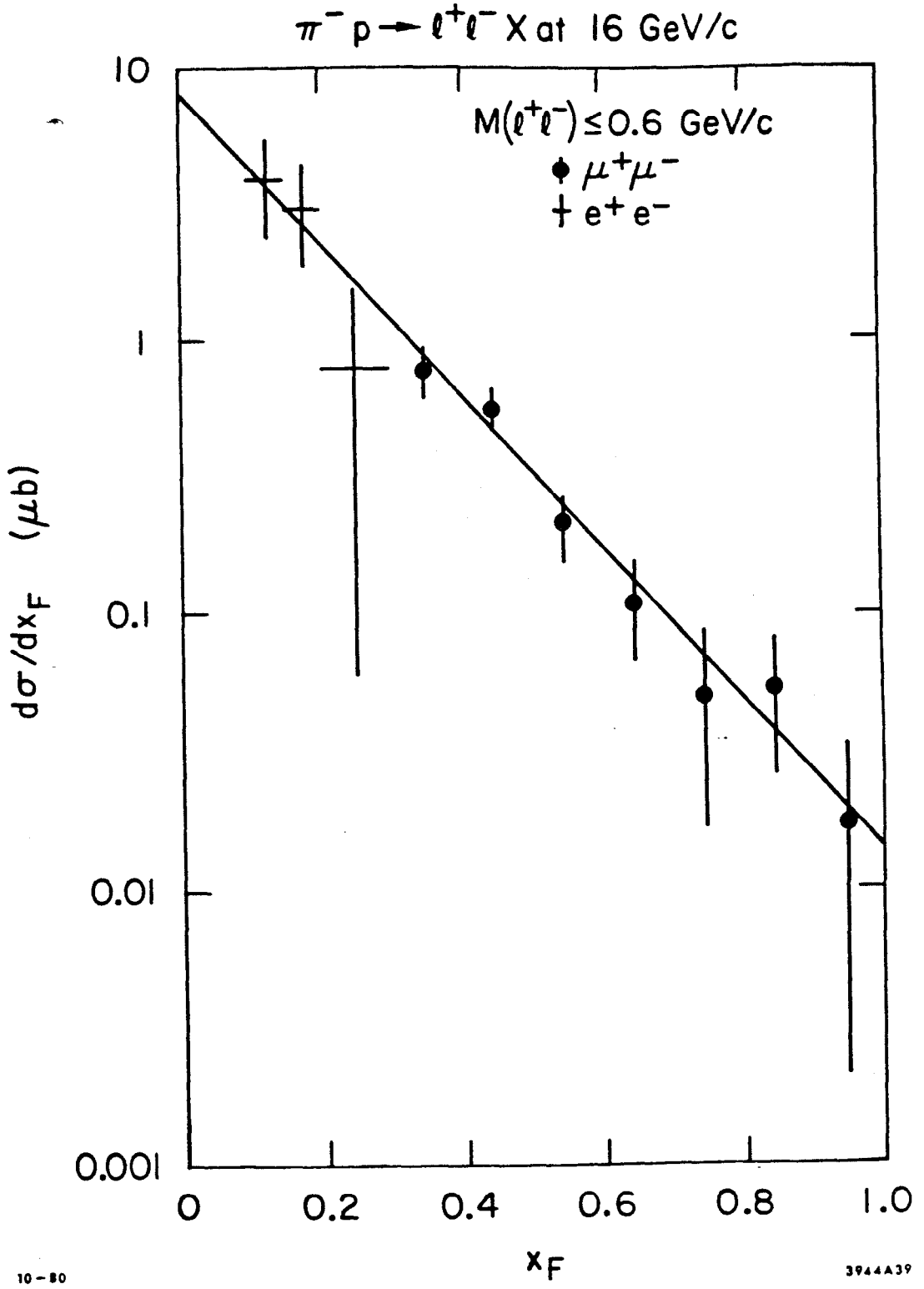

42. The x distribution of the low mass dilepton continuum produced in 16 GeV/c π^-p interactions. The e^+e^- data have been corrected for the difference of the dielectron and dimuon mass thresholds. The solid line represent the fit to the formula (53).

provide sufficient enhancement of the Drell-Yan process to account for the magnitude of the observed cross section. The detailed calculations describing x_F and p_T distributions of the low mass lepton pairs have not as yet been performed.

Another possibility pointed out recently[113] is the Dalitz like decay of the non-resonant $J^P = 0^-$ partial wave produced in hadron collision. This picture was suggested by the similarity of the kinematic distributions of the low mass continuum to the corresponding spectra from the π^o Dalitz decays. Such mechanism correctly describes observed properties of the continuum and furthermore, contributes also to the direct production of photons in hadron interactions. The present knowledge of the data is still fragmentary and their precision does not allow for the disproval or firm establishment of this mechanism as the source of the low mass dileptons. It remains, however, an attractive possibility.

8. Outlook

Massive lepton pairs production plays at present a dual role. On one hand it is one of the most sensitive testing grounds of the QCD phenomenology allowing for the detailed comparison of the theoretical calculations with experimental data. On the other hand, in the framework of the parton model or Quantum Chromodynamics, it makes possible to study the structure functions of unstable hadrons: pions, kaons and antiprotons. The importance of higher order QCD corrections in the description of the Drell-Yan process has been already established on the basis of existing data. The new experiments at CERN and in Fermilab are expected to provide accurate measurements allowing for detailed studies of the character of these corrections. Presently running experiments will also allow for better determination of π, k and $\bar{p}$ structure functions in the analyses independent of the deep inelastic lepton scattering results.

New, high energy machines under construction in CERN, Fermilab and Brookhaven will increase the accesible range of dilepton masses. The Drell-Yan process is expected there to produce the neutral intermediate vector boson Z^o and pairs of charged intermediate vector bosons W^+W^-. The leptonic decays of these particles may provide clean experimental signatures for their detection.

The interest in the studies of the low mass lepton pair production is at the moment rather small. The improving quality of the experiments measuring direct photon production will require, however, in the near future better understanding of the origin of the low mass continuum, since the two processes may be related.

ACKNOWLEDGEMENTS

I would like to thank D. Antreasyan, W. Dunwoodie, G. Fox S. Gupta and W. Innes for their critical comments and many clarifying discussions.

REFERENCES

1. J. Christenson et al., Phys. Rev. Letters 25(1970)1523 and Phys. Rev. D8(1973)201
2. S. D. Drell and T. M. Yan, Phys. Rev. Letters 25(1970)316 and Ann. Phys. 66(1971)578.
3. J. J. Aubert et al., Nucl. Phys. B89(1975)1.
4. S. W. Herb et al., Phys. Rev. Letters 39(1977)252.
5. R. P. Feynman, Phys. Rev. Letters 23(1969)1415 and "Photon-Hadron Interactions" (Benjamin, Reading, Mass., 1972).
6. J. D. Bjorken, Phys. Rev. 148(1966)1467., Phys. Rev. 179(1969)1547.
7. S. M. Berman, J. D. Bjorken and J. B. Kogut, Phys. Rev. D4(1971)3388.
8. L. M. Lederman, Physics Reports 26(1976)149.
9. N. S. Craigie, Physics Reports 47(1978)1.
10. E. L. Berger, Proceedings of the 3rd International Conference at Vanderbilt University on New Results in High Energy Physics, 1978, and Invited talk at the Orbis Scientiae 1979, Coral Gables, Florida.
11. F. Vanucci, Contribution to the Karlsruhe Summer Institute, Karlsruhe 1978.
12. R. Stroynowski, Lectures at the SLAC Summer Institute on Particle Physics, 1979, SLAC-PUB-2402.
13. M. Glück, talk presented at the Workshop on Lepton-Pair production in Hadron-Hadron Collisions, Bielefeld 1978.
14. I. H. Dunbar, Phys. Rev. Letters 41(1978)210.
15. C. H. Lai and C. Quigg, FNAL Report No. FN-296(1976), T. Miyazaki and E. Takasugi, Phys. Rev. D8(1973)2051.
16. N. M. Kroll and W. Wada, Phys. Rev. 98(1955)1355.
17. Yu. B. Bushnin et al., Phys. Letters 79B(1978)147, R. I. Dzhelyadin et al., Phys. Letters 84B(1979)143.

18. For a review, see e.g. A. Bodek, Invited talk at the Annual Meeting of the APS Division of Particles and Fields, Montreal 1979. University of Rochester Report UR-730(1979).

19. K. Kajantie, Review talk at the European Conference on Particle Physics, Budapest 1977.

20. J. D. Bjorken and H. Weisberg, Phys. Rev. D13(1976)1405.

21. V. Cérny, P. Lichard and J. Pišut, Phys. Letters 70B(1977)61 and Acta Phys. Pol. B9(1978)901.

22. C. T. Sachrajda and R. Blankenbecler, Phys. Rev. D12(1975)3624.

23. T. Goldman, M. Duong-van and R. Blankenbecler, Phys. Rev. D20(1979)619.

24. R. Cassell et al., "Dimiuon production in 15.5 GeV/c πp interactions and the observation of a low mass continuum", SLAC-PUB-2409(1979).

25. R. N. Cahn, Phys. Rev. Letters 29(1972)1481 and Phys. Rev. D7(1973)247.

26. N. S. Craigie and D. Schildknecht, Nucl. Phys. B118(1977)311.

27. R. Ruckl, Phys. Letters 64B(1976)39.

28. G. R. Farrar and S. C. Frautschi, Phys. Rev. Letters 36(1976)1017.

29. S. Berman, D. Levy and T. Neff, Phys. Rev. Letters 23(1972)1363.

30. N. S. Craigie and H. N. Thompson, Nucl. Phys. B141(1978)121.

31. A.L.S. Angelis et al., CERN-EP/79-112 and COO-2232A-82.

32. J. H. Cobb et al, Phys. Letters 72B(1977)273.

33. C. Korkoumelis et al. Phys. Letters 91B(1980)475.

34. D. Antreasyan et al., Paper presented by V. Becker at the EPS International Conference on High Energy Physics, Geneva 1979, CERN-EP/79-116 and G. Bellettini, Review talk at the Second International Symposium on Hadron Structure and Multiparticle Production, Kazimierz, 1979.

35. D. Antreasyan et al., Phys. Rev. Letters 45(1980)863.

36. D. C. Hom et al., Phys. Rev. Letters 36(1976)1236.

37. D. C. Hom et al., Phys. Rev. Letters 37(1976)1374.

38. D. M. Kaplan et al., Phys. Rev. Letters 40(1977)435.

39. J. K. Yoh et al., Phys. Rev. Letters 41(1978)684.

40. A. S. Ito et al., "Measurements of the continuum of dimuons produced in high-energy proton-nucleus collisions," FERMILAB-Pub-80/19-EXP(1980).

41. J. Badier et al., Contributions to the EPS International Conference on High Energy Physics, Geneva 1979, CERN reports EP 79-67 and EP 79-68.

42. J. Badier et al., Phys. Letters 89B(1979)145 and contributions to the XXth International Conference on High Energy Physics, Madison 1980; CERN/EP 80-147 EP80-148 and EP80-150.

43. L. Kluberg et al., Phys. Rev. Letters 37(1976)1451.

44. D. Antreasyan et al., Phys. Rev. Letters 39(1977)906.

45. K. J. Anderson et al., Phys. Rev. Letters 42(1979)944 and Phys. Rev. Letters 43(1979)1219.

46. G. E. Hogan et al., Phys. Rev. Letters 42(1979)948.

47. C. B. Newman et al., Phys. Rev. Letters 42(1979)351.

48. M. Abolins et al., Phys. Letters 82B(1979)145.

49. R. Barate et al., Phys. Rev. Letters 43(1979)1541.

50. Michigan-Northeastern-Seattle-Tufts Collaboration, paper submitted to the 19th International Conference on High Energy Physics, Tokyo, 1978 and University of Michigan preprint UM HE 80-23.

51. J. Alspector et al., Phys. Letters 81B(1979)397.

52. C. Reece et al., Phys. Letters 85B(1979)427.

53. D. McCal et al., Phys. Letters 85B(1979)432.

54. K. Bunnell et al., Phys. Rev. Letters 40(1978)136.

55. R. Cassell et al., SLAC preprint SLAC-PUB-2408(1979).

56. K. J. Anderson et al., Phys. Rev. Letters 36(1976)237, 37(1976)799
G. G. Henry, Ph D. Thesis, University of Chicago (1978).

57. J. G. Branson et al., Phys. Rev. Letters 38(1977) 457; 38(1977)580; 38(1977)1331 and 38(1977)1334.

58. W. M. Morse et al., Phys. Rev. D18(1978)3145.

59. D. M. Grannan et al., Phys. Rev. D18(1978)3150.

60. M. J. Corden et al., Phys. Letters 76B(1978)226 and CERN preprint CERN EP/80-152(1980).

61. M. Faessler et al., Phys. Rev. D17(1978)689.

62. A. G. Clark et al., Nucl. Phys. B142(1978)29.

63. A. Chilingarov et al., Nucl. Phys. B151(1979)29.

64. J. H. Cobb et al., Phys. Letters 78B(1978)519.

65. R. Stroynowski et al., Paper submitted to the XXth International Conference on High Energy Physics, Madison, Wisconsin, 1980, and SLAC-Pub-2571.

66. S. Naito et al., Contribution to the INS Symposium on Particle Physics, Tokyo 1979, reviewed by S. Mikamo, KEK-PREPRINT-79-27(1980).

67. R. Barloutaud et al., Rutherford Laboratory preprint RL-80-003(1980).

68. J. Ballam et al., Phys. Rev. Letters 41(1978)1207.

69. See e.g. S. Mikamo, KEK-PREPRINT-79-27(1980).

70. Yu. M. Antipov et al., Phys. Letters 76B(1978)235.

71. G. Altarelli, G. Parisi and R. Petronzio, Phys. Letters 76B(1978)351 and Phys. Letters 76B(1978)356.

72. K. Kajantie and R. Raitio, Nucl. Phys. B139(1978)72.

73. H. Fritzsch and P. Minkowski, Phys. Letters 73B(1978)80.

74. V. N. Baier and V. A. Khoze, JETP(Sov. Phys.)21(1965)629.

75. H. D. Politzer, Nucl. Phys. B129(1977)301.

76. C. T. Sachrajda, Phys. Letters 73B(1978)185.

77. R. K. Ellis et al., Phys. Letters 78B(1978)281 and Nucl. Phys. B152(1979)285. S. Gupta and A. H. Mueller, Phys. Rev. D20 (1979) 118.

78, Yu. L. Dokshitser, K. I. Dyakonov and S. I. Troyan, Phys. Reports 58 (1980) 269.

79. S. J. Brodsky, Proceedings of the SLAC Summer Institute on Particle Physics, 1979. SLAC-Report 224, A. Mosher Editor.

80. For the review see J. Ellis, Proceedings of the 9th International Symposium on Lepton and Photon Interactions, Batavia, Illinois, 1979.

81. E. Reya, DESY report 79/88(1979).

82. G. Altarelli and G. Parisi, Nucl. Phys. B126(1977)298.

83. G. Altarelli, R. K. Ellis and G. Martinelli, Nucl. Phys. B143(1978)521 and Nucl. Phys. B146(1978)544.

84. A. P. Coutogouris and J. Kripfganz, Phys. Rev. D19(1979)2207.

85. J. Kubar-Andre and F. E. Paige, Phys. Rev. D19(1978)221.

86. G. Altarelli, R. K. Ellis and G. Martinelli, Nucl. Phys. B157(1979)461.

87. J. Abad and B. Humpert, Phys. Letters 78B(1978)627 and Phys. Letters 80B(1979)433.

88. B. Humpert and W. L. van Neerven, Phys. Letters 84B(1979)327 and Phys. Letters 85B(1979)293.

89. K. Harada, T. Kaneko and N. Sakai, Nucl. Phys. B155(1979)169.

90. E. Berger and S. J. Brodsky, Phys. Rev. Letters 42(1979)440.

91. L. F. Abbott and R. M. Barnett, Annals Phys. 125(1980)276.

92. R. P. Feynman, R. D. Field and G. C. Fox, Phys. Rev. D18(1978) 3320.

93. W. B. Atwood, Proceedings of SLAC Summer Institute on Particle Physics 1979, SLAC Report 224, A. Mosher Editor.

94. J. F. Owens and E. Reya, Phys. Rev. D17(1978)3003.

95. J. C. Collins and D. E. Soper, Phys. Rev. D16(1977)2219.

96. R. J. Oakes, Nuovo Cimento 44(1966)440.

97. K. Gottfried and J. D. Jackson, Nuovo Cimento 33(1964)309.

98. K. Kajantie, J. Lindfors and R. Raitio, Phys. Letters 74B(1978)384 and Nucl. Phys. B144(1978)422.

99. C. S.Lam and W. K. Tung, Phys. Rev. D21 (1980) 2712.

100. F. Halzen and D. Scott, Phys. Rev. D18(1978)3378 and Phys. Rev. D19(1979)216.

101. R. D. Field, Proceedings of the 19th International Conference on High Energy Physics, Tokyo 1978.

102. G. Parisi and R. Petronzio, Nucl. Phys. B154(1979)427.

103. D. Antreasyan, private communication.

104. S. D. Ellis and W. J. Stirling, Washington University preprint RLO-1388-821(1980).

105. J. Kubar et al., University of Nice preprint N TH 80/8 (1980).

106. J. G. H. de Groot et al., Zeit. Phys. C1(1979)143.

107. M. Gluck and E. Reya, Nucl. Phys. B130 (1977) and Nucl. Phys. B145(1978)24.

108. A. J. Buras and K. J. F. Gaemers, Nucl. Phys. B132(1978)249.

109. R. P. Feynman and R. D. Field, Phys. Rev. D15(1977)2590.

110. I am grateful to R. M Barnett for calculating the Q^2 dependence of the sea quarks.

111. F. Martin, Contribution of the XV Rencontre de Moriond. Les Arc, 1980 CERN preprint TH2845

112. G. Abshire et al., Contribution to XX International Conference on High Energy Physics, Madison, Wisconsin (1980).

113. SLAC-Johns Hopkins-Caltech Collaboration, W. M. Dunwoodie et al., in preparation.